Production of Sustainable Aviation Fuel through Biomass

Moaaz Shehab

PRODUCTION OF SUSTAINABLE AVIATION FUEL THROUGH BIOMASS

EXPERIMENTAL AND SIMULATION APPROACH

DISSERTATION

to obtain
the degree of doctor at the University of Twente,
on the authority of the rector magnificus,
prof. dr. ir. A. Veldkamp,
on account of the decision of the Doctorate Board
to be publicly defended
on Tuesday – 07 May 2024 at 12.45 hours

by

Moaaz Gamal Ahmed Mohamed Shehab

born on the 1st of October, 1992
in Menia, Egypt

This dissertation has been approved by:

Supervisors

prof. dr. ir. E. Zondervan
prof. dr. ing. M.B. Franke

The research described in this thesis was carried out at the German National Institute of Metrology and the Laboratory of Process Systems Engineering in Sustainable Process Technology group of the Faculty of Science and Technology, the University of Twente, the Netherlands.

Cover design: Moaaz Shehab
Printed by: Gildeprint
Lay-out: Moaaz Shehab
ISBN (print): 978-90-365-6078-8
ISBN (digital): 978-90-365-6079-5
URL: https://doi.org/10.3990/1.9789036560795

Graduation Committee:

Chair / secretary:	Prof. dr. J.L. Herek (Jennifer)
Supervisors:	Prof. dr. ir. E. Zondervan (Edwin) Universiteit Twente, TNW, Sustainable Process Technology
	Prof. dr. ing. M.B. Franke (Meik) Universiteit Twente, TNW, Sustainable Process Technology
Committee Members:	Prof. dr. ir. A. Nijmeijr (Arian) Universiteit Twente, TNW, Inorganic Membranes
	Prof. dr. ir. S.R.A. Kersten (Sascha) Universiteit Twente, TNW, Sustainable Process Technology
	Prof. dr. G.J. Kramer (Gert) Universiteit Utrecht
	Prof. dr. rer. nat. R. Fernandes (Ravi) Technische Universität Braunschweig Physikalisch-Technische Bundesanstalt (PTB)
	Dr. K. Moshammer (Kai) Physikalisch-Technische Bundesanstalt (PTB)

Summary

In this thesis, special attention is given to the influence of biomass characteristics and their uncertainties on the production of sustainable aviation fuel (SAF). As SAF mandates are being introduced to reach net-zero carbon emissions in the aviation sector, reliance on biomass feedstocks is growing; however, it comes with challenges and obstacles. Many pathways and configurations are being developed and scaled up to reach their full commercial potential. Resolving the challenges associated with biomass characterization will pave the way to the successful use of biomass in SAF production. Therefore, this thesis has two phases: an experimental and a simulation phase.

Firstly, the experimental phase aims to improve the measurements of the biomass characteristics in the laboratory by performing a key comparison of the measurement techniques between different metrological institutes in the EU. The overarching goal of this phase was to lower the measurement uncertainty by improving repeatability and reproducibility. Eventually, new modifications to the ISO standards will be proposed. The improvement in the measurement accuracy directly impacts the values of purchasing and taxing biomass, as aspects like the energy and moisture content play a significant role in setting these values. Moreover, these improvements are expected to enhance biorefinery processes' design, performance, and yield.

The second phase focuses on the impact of different types of biomass, their heterogeneity, and uncertainty on the production of SAF. Therefore, the various pathways of SAF production were comprehensively analyzed while considering technical and non-technical aspects to determine the most promising routes for producing SAF from biomass. Moreover, the analysis assessed the EU's biomass potential for SAF, focusing on its ability to meet proposed EU mandates for SAF uptake in the short and long term. After this analysis, several steady-state models for the Fischer Tropsch and Methanol to Jet were simulated in Aspen Plus commercial software. These models aimed to determine the influence of the experimentally determined biomass characteristics and their uncertainties on SAF production. Moreover, the models were used to determine the optimal and cost-effective pathway for SAF production through biomass. Different approaches, configurations, and tools were employed to achieve this objective, such as process simulation, sensitivity analysis, Monte Carlo simulation, and techno-economic analysis.

Samenvatting

In dit proefschrift wordt speciale aandacht geschonken aan de invloed van biomassakarakteristieken en hun onzekerheden op de productie van duurzame vliegtuigbrandstof (Sustainable Aviation Fuels, SAF). Aangezien SAF-wetten worden ingevoerd om net-zero koolstofdioxide emissies in de luchtvaartsector te bereiken, groeit de afhankelijkheid van biomassa als grondstof; dit brengt echter uitdagingen en obstakels met zich mee. Veel routes en configuraties worden ontwikkeld en opgeschaald om hun volledige commerciële potentieel te bereiken.

Het oplossen van de uitdagingen die samenhangen met de karakterisering van biomassa zal de weg effenen naar het succesvolle gebruik van biomassa in de productie van SAF. Daarom heeft dit proefschrift twee componenten: een experimentele en een simulatie component. Ten eerste heeft de experimentele fase tot doel de metingen van de biomassakarakteristieken in het laboratorium te verbeteren door een sleutelvergelijking van de meettechnieken uit te voeren tussen verschillende metrologische instituten in de EU. Het overkoepelende doel van deze fase is om de meetonzekerheid te verlagen door de herhaalbaarheid en reproduceerbaarheid te verbeteren. Uiteindelijk zullen er nieuwe aanpassingen aan de ISO-standaarden worden voorgesteld. De verbetering van de meetnauwkeurigheid heeft direct invloed op de waarden van de aankoop en belasting van biomassa, aangezien aspecten zoals de energie- en vochtigheid een belangrijke rol spelen bij het bepalen van de waarde. Bovendien wordt verwacht dat deze verbeteringen de ontwerp-, prestatie- en opbrengstprocessen van bio raffinaderijen zullen verbeteren.

De tweede fase richt zich op de impact van verschillende soorten biomassa, hun heterogeniteit en onzekerheid op de productie van SAF. Daarom zijn de verschillende trajecten van SAF-productie uitgebreid geanalyseerd, waarbij technische en niet-technische aspecten zijn overwogen om de veelbelovende routes voor de productie van SAF uit biomassa te bepalen. Bovendien is de analyse gebruikt om het biomassa-potentieel van de EU voor SAF te bepalen, met de nadruk op haar vermogen om te voldoen aan de voorgestelde EU-verplichtingen voor SAF-adoptie op korte en lange termijn. Na deze analyse werden verschillende stationaire modellen voor Fischer Tropsch en Methanol to Jet gesimuleerd in de commerciële simulatie software Aspen Plus. Deze modellen zijn gebruikt om de invloed van de experimenteel bepaalde biomassakarakteristieken en hun onzekerheden op de productie van SAF te bepalen. Bovendien zijn de modellen gebruikt om de optimale- en kosteneffectieve route voor SAF-productie via

biomassa te bepalen. Verschillende benaderingen, configuraties en tools werden gebruikt om dit doel te bereiken, zoals procesmodellering, gevoeligheidsanalyse, Monte Carlo-simulatie en techno-economische analyse.

Acknowledgment

In the Name of Allah, the Most Beneficent, the Most Merciful

This thesis marks the end of a long journey where I faced numerous challenges and obstacles but Alhamdulillah Rabb Al Alameen, I have finally managed to reach the finish line. I encountered during this journey so many wonderful friends and colleagues whom without them this work would have never been completed.

Firstly, I would like to sincerely thank my first promotor Edwin who was not just a supervisor, but also a friend and a companion during this journey. You have been always supportive of my decisions, treating me like a family member more than just a student under your supervision. It was amazing to be able to talk with you about everything whether scientifically, politically or socially. It was also inspiring to see that we share some similar passions. Definitely without your guidance and supervision, I would have not been able to finish this thesis. I could not have dreamed of a better supervisor. I also would like to thank my second promoter Prof. Meik for his support and valuable insights that have tremendously improved the quality of my work.

I would like to express my deepest appreciation and gratitude to Kai, my supervisor and mentor at PTB with whom I have worked closely for the last 5 years. I am so grateful for your unwavering support, encouragement and for always pushing me to achieve more. I truly appreciated that you have given me the full confidence to explore different ideas and implement them. To Ravi, I am indebted to you for your amazing flexibility, continuous motivation and for facilitating the way for me to excel.

To my friend Mahmoud Maged, there are no words capable of reflecting how grateful I am. I am certain that without your assistance and the long calls we had, I would have had a terrible time during my thesis. Thanks for your support, patience and kindness, it meant the world to me. I truly wish you all the best in your life with your wife and family.

I was fortunate enough to share an office with a dear friend and colleague Ajoy, thank you for always being there throughout the journey, for your suggestions, and for listening to my complaints all the time. My friend Ahmed Hashad, thanks for standing by my side, sharing your knowledge, and being like an older brother to me. Thanks for the many beautiful memories we had at PTB and beyond. To Diego at Imperial College London, many thanks for your assistance and patience, your support paved the way for me to successfully finalize this thesis. Thanks to my SPT colleagues at Twente University namely Albertus and Romolo for their willingness to honor me at my defense and to be my paranymphs despite their busy schedule. I am also grateful to my SPT colleagues Tufail Ahmed and Hilbert Keestra for their help and for sharing their work with me.

To my family, the main source of my strength who never left my side despite being physically thousands of kilometers away, my love and prayers to you in each and everyday. Thank you for your unwavering love and support, this thesis is definitely dedicated for you.

My dear Ina, you shared the burden of this journey with me. Thanks for being there and helping me during the rough times. Your assistance and encouragement during this journey made my years in Braunschweig bearable. Thank you for being always there whenever I needed you and for the whole Ruhnau family and Detlef for helping me settle and adapt in Braunschweig. I also would like to extend my gratitude to my dear friend Denis for being always willing to help at any time and regardless of the required effort. Thanks for being in my life.

Lastly, I would like to thank everyone who was part of my journey at PTB especially my colleagues in both groups 3.32 and 3.34, Dr. Stefan Sage, and my dear friend Xiaoyu He, as well as the BIOFMET project partners. My special gratitude to the PTB football team for making my time there enjoyable, especially Peter Widera and Dirk Gatzemeier. Everyone of my supervisors, family, friends, and colleagues have participated in my personal and academic growth and for that, I will always be grateful.

"الحمـــــد لله رب العالمـــين"

Table of Contents

CHAPTER 1

Chapter 1. Introduction

1.1 Background

Averting the planet from the detrimental effects of exceeding the critical 1.5°C threshold for global climate change necessitates a concerted effort to lower emissions using whatever technology or feedstocks are available. The aviation industry, in particular, stands out as a significant contributor to greenhouse gas (GHG) emissions, accounting for an estimated 2–3% of global carbon dioxide (CO_2) output [1,2]. While this may appear as a modest proportion, aviation emissions are projected to surge alongside the growing accessibility of air travel. Therefore, significant emission reductions are essential across all sectors, including aviation [3]. In 2009, the air transport industry pledged to slash its net carbon emissions to half of 2005 levels by 2050 [4,5]. Achieving this ambitious goal demands implementing measures such as employing more fuel-efficient aircraft, exploring hydrogen and electric propulsion options, and developing sustainable aviation fuels.

Sustainable aviation fuel (SAF) emerges as an alternative liquid hydrocarbon possessing physicochemical properties similar to conventional jet fuel (kerosene), specifically suitable for operation in existing aircraft. The advantage of using SAF lies in its considerably reduced carbon footprint, offering significant reductions in greenhouse gas emissions ranging from 50% to 80% compared to fossil fuel-based jet fuel, depending upon the feedstock and the production process [6]. SAF can be produced via renewables, waste gases, and biomass. Biomass is considered one of the most promising feedstocks for decarbonizing the aviation sector due to its availability and the presence of established technologies to utilize it. These different conversion pathways can convert biomass into a fuel that serves as a substitute for conventional jet fuel or blended with it [7].

1.2 Biomass categories and utilization

Biomass is classified into different types and varies in importance and suitability for use as a feedstock for producing SAF. Biomass, a renewable and versatile energy source, encompasses a wide array of organic materials derived from plants and animals, as shown in figure 1.1.

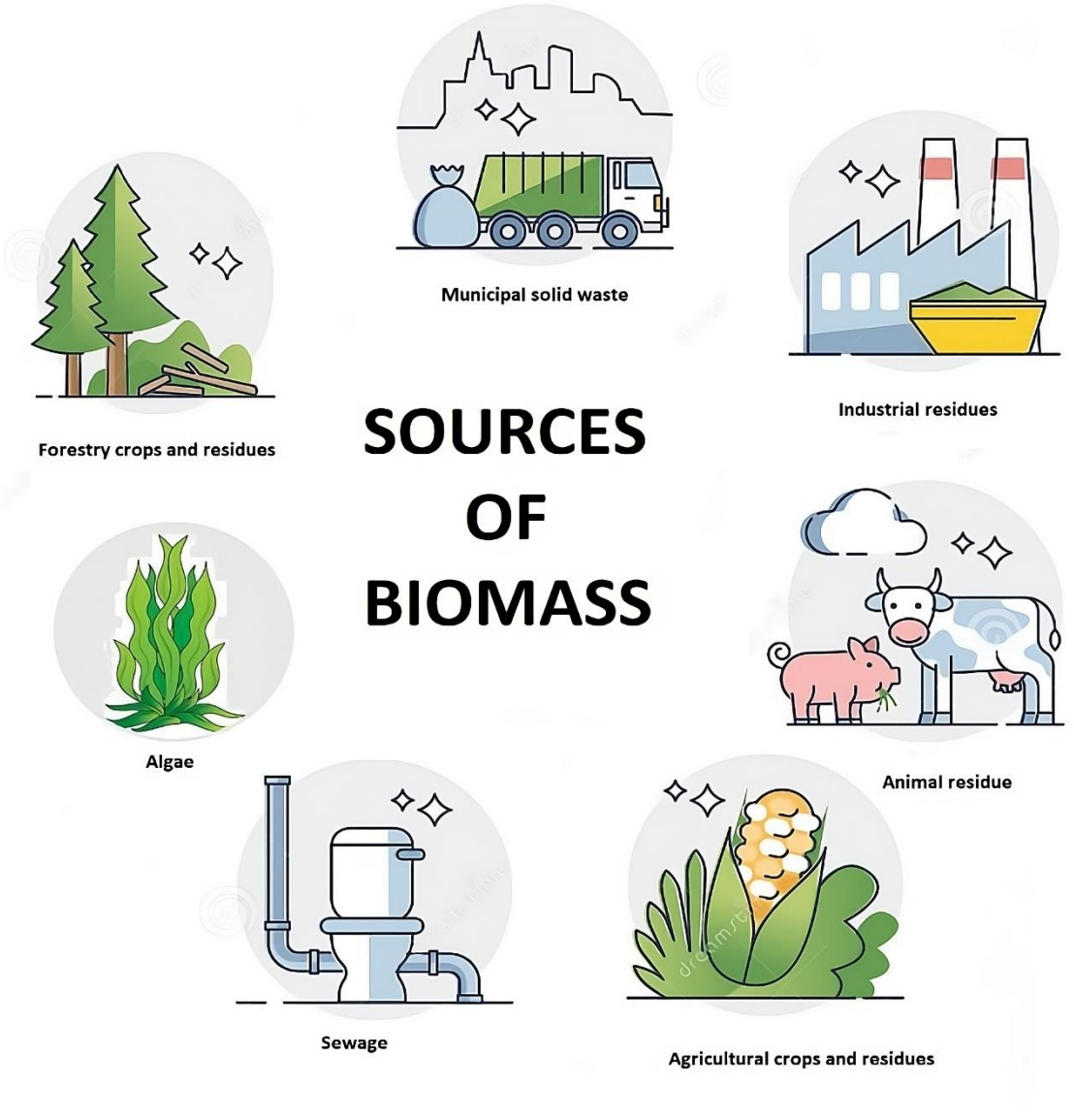

Figure 1.1. *Different biomass sources [8].*

The biomass materials are categorized into main groups: agricultural residues, forestry residues, dedicated energy crops, algae, and organic waste. Agricultural residues include crop residues such as corn stover and wheat straw, while forestry residues involve by-products from logging operations. Dedicated energy crops, such as switchgrass and miscanthus, are grown explicitly for bioenergy purposes. On the other hand, organic waste includes municipal solid waste and animal manure. These different types of biomass could be utilized in various ways, including generating energy through direct combustion for heat and power, conversion to biofuels like

biodiesel and SAF, or biogas production. Using biomass not only provides a sustainable alternative to fossil fuels but also contributes to waste reduction and environmental sustainability.

1.3 What is metrology, and why is it important?

To successfully utilize biomass feedstocks, they must be tested to determine their quality and suitability for use in different applications. Here, the metrological concepts of repeatability and reproducibility play a major role in ensuring measurement accuracy, precision, and quality. Therefore, it is essential to clarify what metrology is and why it is important. Answering these questions paves the way to understand this thesis's scope better. Figure 1.2 shows the Great Pyramid of Giza, which unlocks the answers to these questions.

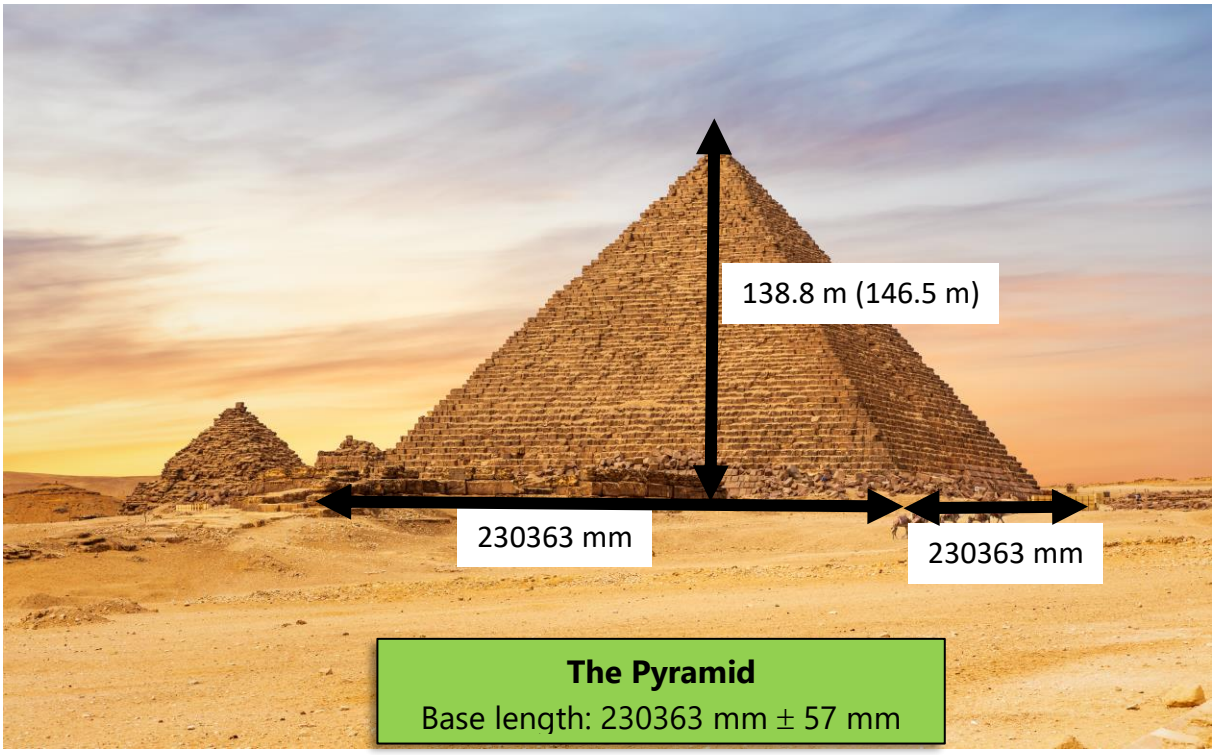

Figure 1.2. *Dimensions of the great pyramid of Giza [9].*

Figure 1.2 shows the detailed dimensions of the Great Pyramid of Giza, where the bases have the exact measurements of around 230.3 meters [10]. Designing a structure with the same dimensions is not an achievement nowadays. Still, when we consider the fact that the pyramids were established over 5000 years ago, it becomes a remarkable achievement as it is the only great wonder of the ancient world that still stands. Therefore, is it logical to question how this structure came to pass without well-founded metrology, quality manuals, and standards? Thus, to design the Great Pyramid, the ancient Egyptians had to establish a proper methodology to

ensure the pyramid would have the exact dimensions as planned. This was done through several steps as follows:

Defining a unit of length: since there was no tap measure to be used, the Egyptians had to establish their own unit of measurement. The cubit served as Ancient Egypt's primary unit of measurement, and there were two variations of the cubit: the short and royal cubit. The short cubit was defined as the distance from the pharaoh's elbow to the tip of their middle finger, while the royal cubit was measured from the elbow to the middle fingertip, in addition to a palm, as shown in figure 1.3. The pharaoh's hands will be the primary unit of measurement and reference, known in modern terminology as the primary standard.

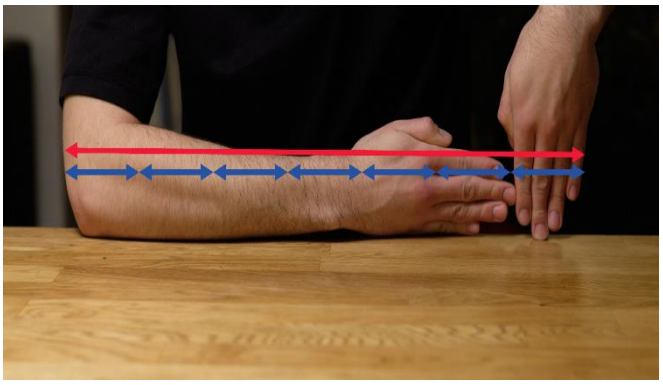

Figure 1.3. *Representation of the pharaoh's hand to form the unit of length [9]*

Creating a copy: using the pharaoh's measurements, a cast made out of iron or copper was used to create a copy that matched precisely the pharaoh's hands, as presented in figure 1.4.

Figure 1.4. *An example of the unit of length used in Ancient Egypt [11].*

Reproducing the unit: A unit of length was established, and a copy of it was created. However, it is expected that the pharaoh would not always be available, and it is illogical to need his hands for every calibration process. Therefore, massive production of these rulers (cubits) was needed to distribute them to the workers. However, these rulers had to be calibrated using the secondary standard to ensure that they would have the same dimensions. Ensuring the rulers were

calibrated, they became automatically traceable to the primary standard. In this case, it refers to the pharaoh's hands.

Thanks to this methodology, the pyramids had perfect dimensions with a very low level of uncertainty of 57 mm, around 0.02%. This uncertainty represents the deviation between the measurement of the pyramids' bases, which shows highly repeatable data (pyramid base). These concepts of primary standards, calibration, uncertainty, and traceability are the pillars of the science of metrology (measurements) to ensure precise characterization of any material or feedstock. Nowadays, the most common metrological standard is the SI standard, which defines the unit of measurement for different properties. When it comes to biomass, not every physical property is traceable to a primary standard when measured, which creates deviations between measurements. This causes multiple challenges, as discussed in the next section.

1.4 Challenges associated with biomass characterization and utilization in process design

Lignocellulosic woody biomass is the most commonly used feedstock in power and heat plants as well as in biorefineries to produce sustainable fuels like biodiesel or SAF. However, when purchasing such feedstocks, there is a potential for a financial loss that the biomass supplier or the end user will endure. This financial loss comes from biomass being purchased or taxed based on its physical characteristics, which have high uncertainty in measurements. The uncertainty during biomass characterization, especially for energy and moisture content, can reach up to 5%, which is the basis for determining the cost. Therefore, these measurements must be improved and performed correctly to guarantee repeatable and reproducible values and ensure fair biomass pricing. A 5% uncertainty is shocking when compared to the Great Pyramid of Giza, considering how old the pyramids are; even so, those cannot be directly compared as they have different units of measurement. Yet, it indicates how difficult it is to characterize the biomass properly. Therefore, there was a need for a detailed study to analyze the risks associated with determining the energy and moisture contents of biomass.

Moreover, an uncertainty analysis was required to determine the potential sources of improvements to lower the uncertainty and provide a unified practice to quantify it. On the other hand, the physical characteristics are not only essential to determine the biomass cost but also crucial during the process design phase. These physical properties represent the main building block and input for the design process. However, there are not enough studies to analyze how the uncertainty of the measurements of the physical characteristics of biomass affects the

process design, yield, and performance. Moreover, no historical data is available to evaluate the influence of different biomass types and configurations on the production of SAF and its uncertainty since these sustainable processes do not operate on a large commercial scale. Here is where the coupling between the science of metrology and process system engineering is crucial to address these issues.

1.5 Role of process system engineering

Thriving in today's competitive landscape requires biomass to SAF processes to be effectively designed and operated to obtain optimal efficiency and maximum yield. PSE methodologies offer new innovative integrated solutions to address the technical barriers. Moreover, PSE enables a systematic refinement of operational parameters, ensuring high efficiency, resource utilization, and economic viability [8]. On the other hand, integrating metrology with PSE techniques provides new answers to ensure the reliability of data obtained from the models and offers valuable insights about the potential risks and deviations expected in the process. Therefore, this potential of coupling the tools of metrology with PSE led to the objectives of this thesis.

1.6 Thesis objectives

The thesis has the following objectives:

Improving the experimental practices of biomass characterization by proposing an improved metrological framework to lower the uncertainty and enhance the measurement's repeatability and reproducibility. The focus is on biomass energy and moisture content as they are the key parameters to determine biomass's purchasing cost and taxes. Improving these experimental practices would aid fair biomass pricing without causing financial loss to either the biomass provider or the end user. Furthermore, lowering these uncertainties would directly be reflected in the accuracy of efficiency estimation, equipment sizing, and the sustainability of the process. This is made possible by accurately quantifying the error margin in the process, enabled by the availability of precise input data to the model/process (biomass characteristics).

Validating biomass availability in the EU and it’s potential as a promising feedstock for SAF production in the short and long term. Moreover, the existing technologies will be evaluated to determine the optimum SAF pathways. Eventually, analyzing the EU’s capability of meeting their SAF uptake targets by 2030 and 2050, relying on bio-based feedstocks while analyzing the technical and policy barriers.

Analyzing the influence of biomass characteristics and their uncertainties on SAF yield and cost by performing process simulation for two different SAF pathways, Fischer Tropsch and Methanol to Jet. The simulations cover various scenarios and configurations while combining different methodological tools from a palette encompassing process simulation and heat integration, Monte Carlo simulation, techno-economic analysis including direct and indirect cost evaluation, and uncertainty assessment. The overarching goal is to determine the most cost-effective biomass to SAF route.

1.7 Thesis outline

The thesis covers the experimental measurements of biomass characteristics, their uncertainties, and how these data play a role in process design and performance. The thesis contains the following chapters:

Chapter 1 introduces the decarbonization of the aviation sector and how it is connected to the science of metrology.

Chapter 2 is the first technical chapter, which focuses on analyzing different types of woody biomass to improve the accuracy of the measurements of their physical characteristics. The content of this chapter was collected within the framework of the BIOFMET project, where a key comparison between three different metrology institutes, the German, Turkish, and Romanian institutes, was performed. The comparison focused on improving the measurements and setting new experimental procedures. Moreover, the uncertainty sources were quantified to provide a reliable uncertainty budget, mainly for the energy content of biomass. In this Chapter, experimental tools such as bomb calorimeter, Ion chromatography, and elemental analysis (CHNSO) were utilized.

Chapter 3 contains extensive market research in which the potential of using biomass as feedstock for SAF production is analyzed. The chapter starts by validating the availability of biomass based on publicly available data. Moreover, a comprehensive analysis of the different ASTM D7566-approved pathways to produce SAF was performed. The analysis compared technical and policy aspects, where elements such as technology, fuel readiness, and life cycle assessment were evaluated, as well as the possible geopolitical implications of adapting different SAF technologies in the EU. Ultimately, the most promising SAF pathways were identified. In addition, it provided recommendations to ensure the EU's capability to meet its SAF targets in 2030 and 2050.

Chapter 4 provides the groundwork for the subsequent chapters (5 and 6), where various tools such as process simulation, heat integration, Monte Carlo simulation, and techno-economic analysis are discussed.

Chapters 5 and 6 provide a detailed process simulation of the process of Fischer Tropsch and Methanol to Jet, using Aspen Plus, respectively. The processes couple the results obtained from chapter 2 for biomass characterization. The biomass characteristics served as the model input since Aspen's library has no formula for biomass. The model was optimized using sensitivity analysis and heat integration, followed by Monte Carlo simulation to assess the influence of biomass characteristics and their uncertainties on SAF yield. Eventually, the study was concluded by a techno-economic analysis and uncertainty assessment to analyze the different scenarios and configurations to determine the most economical route. Lastly, conclusions and outlook were presented in chapter 7.

The core chapters of the thesis are summarized in table 1.1

Table 1.1. *Overview of the core chapters of the thesis.*

Title	Chapter 2: Enhanced Procedure for Biomass Characterization and Uncertainty Determination	Chapter 3: Evaluating the Viability of EU's Sustainable Aviation Fuel Targets Through Biomass	Chapters 5 and 6: Biomass to SAF – Fischer Tropsch pathway / Biomass to SAF – Methanol to Jet
Scope	Key comparison to improve the experimental practices and establish a methodology to quantify the uncertainty of biomass characteristics	Quantifying biomass availability and comparing the ASTM-approved SAF pathways to determine their potential	Process simulation of biomass and power to SAF upgraded via Fischer Tropsch and Methanol to Jet pathways
Method	Bomb calorimeter, Ion chromatography, and elemental analysis	Quantification analysis and policy assessment	Process simulation using Aspen Plus. Monte Carlo simulation and techno-economic analysis
Overview	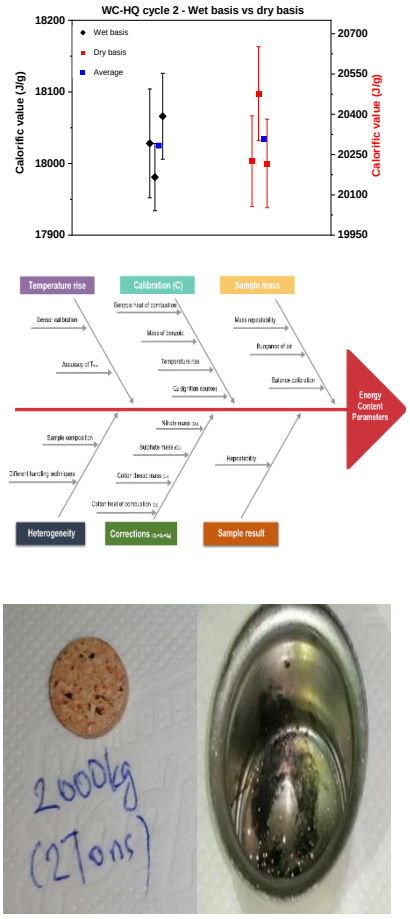		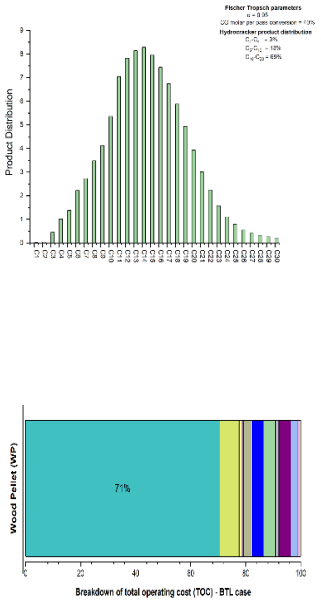

CHAPTER 2

Chapter 2. Enhanced Procedures for Biomass Characterization and Uncertainty Determination

2.1 Overview

The incorporation of biomass in both combined heat and power (CHP) systems and biorefinery plants stands out as a highly promising strategy for advancing the transition to green energy. Wood chips and wood pellets emerge as two of the most widely employed biomass sources for fuel in this context. To simulate and determine the efficiency of CHP or biorefinery plants, it is crucial to accurately determine the calorific value, moisture content, and elemental analysis (CHNSO) of these biofuels. Therefore, with the increased shift towards a biobased economy, the biomass cost and its physical properties must be precisely determined.

Current standards often fall short, lacking sufficient details on the challenges posed by biomass heterogeneity and variations in experimental practices. Issues such as data scattering, poor repeatability, and the lack of uncertainty budget commonly manifest when measuring calorific value and moisture content. In response to these challenges, an interlaboratory comparison involving three national metrology institutes employing bomb calorimetry has been conducted for the calorific value measurements. This comparison has proven instrumental in identifying the root causes behind the poor reproducibility observed in woody biomass samples/feedstocks. Additionally, the biomass composition was determined through elemental analysis, including assessing its uncertainty. This step is crucial when simulating biorefinery plants, such as those for sustainable aviation fuel production, or when elemental analysis is utilized as an alternative method to calculate energy content. The outcomes of this comparison have paved the way for an improved and detailed experimental methodology, enhancing repeatability and reproducibility.

Based On:

Shehab, M.; Stratulat, C.; Ozcan, K.; Boztepe, A.; Isleyen, A.; Zondervan, E.; Moshammer, K. A Comprehensive Analysis of the Risks Associated with the Determination of Biofuels' Calorific Value by Bomb Calorimetry. *Energies* 2022, *15*, 2771. https://doi.org/10.3390/en15082771

Shehab, M., Stratulat, C., Ozcan, K., Boztepe, A., Coskun, F., Senturk, F., Isleyen, A., Zondervan, E., & Moshammer, K. (2022). Improved Metrological Methodology to Address the Challenges Associated with the Determination of Biofuels Calorific Value by Bomb Calorimeter. *Chemical engineering transactions*, *92*, 433-438. https://doi.org/10.3303/CET2292073

2.2 Introduction

The release of greenhouse gas emissions represents a major world threat as it causes the rise of the earth's temperature. This is mainly due to the excessive utilization of fossil fuels, which releases CO_2 into the atmosphere when combusted. Here, biomass plays an essential role as an alternative energy source by providing relatively green energy compared to fossil fuels. Moreover, it is becoming one of the most important commercial products for heating supply [12]. Therefore, their quality has become an object of increased interest. All the different stages of wood chips and wood pellets production are crucial for efficient combustion, e.g., tree felling, storage, transport, pretreatment, and sample preparation [13,14].

With the high demand for biomass utilization, strict quality control criteria must be provided to guarantee accurate characterization of the physical properties of the biomass feedstock. In particular, the calorific value and the moisture content are the most essential factors in selecting biomass material for usage [15]. The calorific value is also considered one of the main properties responsible for evaluating the efficiency of thermal processes, such as in CHP plants and biorefinery. Thermal efficiency is defined as how much fuel is converted into the desired energy services. Moreover, it describes the economic and the environmental terms of any particular process [16]. Therefore, if the calorific value of the biomass is not measured precisely within a small margin of error, there is a risk of making false decisions by perceiving one process as more favorable than the other.

Furthermore, the biomass characteristics such as the dry calorific value and moisture content are essential elements to determine the purchasing cost of biomass [17]. Moreover, when heat production taxes are calculated based on the energy content of the fuel, this would have significant financial consequences. Therefore, a financial loss may be expected if the biomass characteristics are inaccurately measured. This loss would eventually impact the biomass provider or the end-user. The wider the scattering between the measurements, the more the probability of a financial loss and vice versa.

To resolve the issue of the inconsistency between the measurements, three metrological institutes from three different European countries have assembled to specify the best measurement strategy. These institutes are Physikalisch-Technische Bundesanstalt (PTB) from Germany, where this thesis is performed, the National Metrology Institute from Turkey (TUBITAK UME), and Biroul Roman de Metrologie (BRML) from Romania. The partners agreed to perform an interlaboratory comparison on a metrological level to measure the calorific value using calorimetric techniques. The calorific value of a substance, whether food or fuel, is

the amount of heat energy released when it is completely burned. It is measured in kilojoules per kilogram (kJ/kg) or calories per gram (Cal/g), depending on the country's unit system. On the other hand, the word calorimetry refers to the measurements of heat quantities, and it is used to determine the heat of a reaction through experiments. The calorimeter (bomb calorimeter) is a device that consists of a sealed metal vessel (bomb), typically made of stainless steel or aluminum, filled with oxygen, and placed inside a metal bucket filled with water. An insulating jacket surrounds this vessel to prevent heat loss or gain from the surrounding atmosphere. The combustion of the sample releases heat, which is then measured by the rise in water temperature inside the vessel. Different types of calorimetry could be used to determine the calorific value. Two of the most common ones are [18]:

1- Adiabatic calorimetry: ensures that no heat transfer occurs between the calorimeter and its surrounding environment (jacket). The jacket surrounding the calorimeter is constantly monitored and adjusted using heaters, coolers, and circulators to maintain an identical temperature between the calorimeter and its surroundings, creating an adiabatic environment.
2- Isoperibol calorimetry: in this type of calorimetry, the jacket temperature is kept constant at a specific temperature. When the combustion takes place in the closed vessel (Bomb), the temperature of the water in the bucket increases and is recorded. This information is used to calculate the temperature rise and the calorific value.

Typically, the isoperibol bomb calorimetry is the most dominant approach in industrial and academic laboratories [19]. The measurements of the calorific value of biofuels via bomb calorimeter tend to show poor results in inter-comparisons between different laboratories. Furthermore, the uncertainty of the calorific value measurements in the industry varies between 2-5 %. This high value can affect the calculations of plants' thermal efficiencies and the biomass cost. It deserves to be mentioned that the uncertainty range was determined after an online survey performed within this thesis's scope. The survey received answers from 66 participants, including biofuel producers, power plants, and research facilities, and has been published on the BIOFMET project website [20].

There are several standards for determining the calorific value of biofuels, i.e., ISO 18125:2017, ASTM D240-19, and DIN 51900-2. However, the available standards do not provide enough information regarding each aspect of the experiment. Adding the fact that the standards are general and neither take into consideration the different nature of different biomass materials nor the mistakes that can occur by different operators and handling techniques. Therefore, to

improve the measurements and minimize the uncertainty, the challenges associated with the material's nature, the experimental practice, and the limitations of the standards must be overcome.

Wood chips and wood pellets are the most common types of biomass used as solid raw fuels, as cited in the literature [21]**.** This information was further validated thanks to results obtained from the online survey [22]. Therefore, this study focuses on both of these materials. Sample criteria such as the optimum sieve size, sample mass, the applied pellet pressure to form the test pellets, and equilibrium moisture content were studied to provide an improved technical practice. The aim of providing such practice is to improve the repeatability and reproducibility of the measurements. Repeatability (or retest reliability) is commonly used to describe the deviation between successive measurements of the same sample under the same conditions. These conditions are, e.g., same operator, institute, room condition, instrument, and technical procedure within a short period of time [23,24]. However, reproducibility is another component of the precision of the measurements. It refers to the ability to obtain the same results but performed under completely different conditions, including the location and the operator [25,26]. The main objective is to improve the repeatability, which will decrease the margin of error between each measurement while minimizing the reproducibility difference between the institutes. The reproducibility difference refers to the maximum value in any given results of a comparison minus the minimum value from the same comparison. Minimizing the reproducibility will eventually help provide an accurate estimation of biomass cost since the possibility of scattering would be reduced.

Moreover, a detailed uncertainty is computed by defining all the uncertainty sources that influence the calorific value. On the other hand, the elemental analysis, carbon (C), hydrogen (H), nitrogen (N), sulfur (S), and oxygen (O), of biomass is also analyzed to determine its uncertainty and level of accuracy since it is considered an essential pillar when simulating bioprocesses using software like Aspen Plus. Furthermore, it can be an alternative method to estimate the energy content without using a bomb calorimeter. The final overarching objective of this chapter is to support the energy transition into a neutral CO_2 energy alternative where the biobased economy has a crucial role in securing the future of the energy supply.

2.3 Analysis of biomass characteristics – Energy and moisture content

The project partners agreed to conduct two distinct test cycles to accomplish the objectives. These cycles assessed and compared the repeatability and reproducibility obtained across different institutes. In the initial cycle (Cycle 1), the samples' measurements were executed following ISO 18125:2017 [27]. Certain aspects of the experiment lacked values in the standard, such as the crucible weight, precise oxygen pressure, and sources of uncertainty. Each institute, therefore, adhered to its own practices and handling procedures for these aspects. After the assessment of cycle 1 results, a new technical protocol was formulated to enhance measurement precision. The second cycle (Cycle 2) was then conducted following the newly established experimental protocol.

2.3.1 Materials

The identical samples, consisting of three types of woody biomass—wood chips of high quality (WC-HQ), wood chips of industrial quality (WC-IQ), and wood pellets (WP)—were utilized in both test cycles. The project coordinator from the Danish Technological Institute (DTI) in Denmark supplied these samples, which were subjected to a moisture content reduction treatment, bringing them to approximately 15%. The samples were delivered to the institutes in air-tight bags, with each package containing approximately 1 kg of the respective sample.

2.3.2 Sample preparation

The samples, with a diameter of approximately 50 mm, were deemed unsuitable for combustion in a bomb calorimeter [28]. Sample preparation in each institute adhered to ISO 14780 guidelines for solid biofuels, aiming to reduce the mass of the original batch into a uniformly smaller sample portion while maintaining the original composition [29]. The initial step involved sample grinding to achieve a sieve size of 1 mm, rendering the sample suitable for combustion. Subsequently, sample division occurred by segregating the ground sample into different batches, creating a representative and homogenized portion. It is important to note that at this stage, the moisture content of the newly produced portion no longer represents the moisture of the original batch.

In the case of Cycle 2, TUBITAK UME once again followed ISO 14780 to grind 500 g from the original batches of the samples to 1 mm using Fritsch Pulverisettle 19 (2800–3400 rpm).

These newly produced samples by TUBITAK were then shipped to each institute for measurement.

2.3.3 Experimental setup and methodology

In both cycles, subsequent to the production of the test portion, the samples underwent analysis on a wet basis (as predetermined basis). Each institute conducted 8 to 10 measurements for each sample to determine the calorific value. The ISO 18134:03 was followed to determine the moisture content of biofuels via the oven-dry method [30]. This standard prescribes that the sample's moisture should be measured a minimum of 2 times using a sample mass not less than 1 g. The sample is then subjected to an oven at 105 °C for up to 3 hours. The measured moisture value is subsequently employed to calculate the dry basis calorific value.

Both measurement cycles utilized the respective isoperibol bomb calorimeter available at each institute to measure the calorific value. The experimental procedure remains consistent when an isoperibol bomb calorimeter is employed. In this procedure, the calorimeter requires calibration to determine the heat capacity of the system. Heat capacity is defined as the amount of heat needed to raise the temperature of the calorimeter's components by 1°C, measured in J/°C [31]. During calibration and the actual determination of the calorific value of the samples, all operational parameters are kept constant to avoid recalibrating the system.

Calorimeter calibration typically involves using a mass of reference material, such as benzoic acid, traceable to the SI system. The mass of the benzoic acid, when combusted, should cause a temperature rise equivalent to that expected by the sample mass (in g). The calorimetric experiment includes charging a known mass of the sample into a closed vessel called the bomb. The bomb is filled with oxygen at approximately 30 bar [32]. The charged bomb is then placed inside a water-filled bucket where a thermometer records the temperature. The bucket containing the bomb (the system) is surrounded by water tubes at a fixed temperature, commonly called the jacket. The jacket ensures a constant heat transfer between the system and the surroundings. As combustion initiates, the water temperature rises due to heat transfer from the bomb to the water, and this temperature rise is recorded.

Following combustion, the bomb is rinsed with distilled water to collect the liquid resulting from the combustion. This liquid is then diluted and analyzed for nitrate and sulfate anions, depending on the method used. The presence of their corresponding acids, HNO_3 and H_2SO_4, is indicated by the nitrate and sulfate anions in the liquid. These acids impact the final calorific value by introducing additional energy into the system. Consequently, the calorific value requires correction post-combustion. The process of determining these acids for correcting the

calorific value is referred to as thermochemical correction [33]. This correction can be performed using either titration or ion chromatography, depending on the available instrument in each laboratory, as detailed in table 2.1.

Table 2.1 *Instruments used by each project partner for the calorific value determination.*

Institute	Calorimeter type	Method for thermochemical corrections
PTB	Parr- isoperibol oxygen bomb calorimeter	Ion chromatography – Metrohm IC 761
BRML	Parr-isoperibol oxygen bomb calorimeter	Titration using barium hydroxide and hydrochloric acid
TUBITAK	Leco-isoperibol oxygen bomb calorimeter	Assumed based on ISO 18125:2017 + Ion chromatography Dionex ICS3000

2.3.4 Calorific value calculations

Eq. (2.1) shows the calculation of the heat capacity of the bomb calorimeter as given in the ISO 18125:2017 [27].

$$\varepsilon_n = \frac{m_{ba} \times q_{v,ba} + Q_{fuse} + Q_z + Q_N}{\theta} \tag{2.1}$$

where ε_n represents the heat capacity of the system, m_{ba} is the mass (in g) of benzoic acid, $q_{V,ba}$ is the certified gross calorific value (in J/g) for the benzoic acid, θ is the temperature rise in K or any arbitrary unit. Q_{fuse} is the contribution from the fuse combustion, Q_z is the contribution from the ignition aid, and Q_N is the contribution from the formation of nitric acid (all in unit J). The determination of the calorific value on a wet basis is according to the Regnault Pfaundler as shown in eq. (2.2) [27].

$$H_w = \frac{\varepsilon_n \times \theta - (Q_{fuse} + Q_z + Q_N + Q_s)}{m_1} \tag{2.2}$$

where H_w is the gross calorific value of the fuel on a wet basis in J/g, m_1 is the sample mass in g, and Qs is the contribution from the formation of sulfuric acid in J.

From the obtained calorific value on a wet basis, the value on a dry basis can be calculated as shown in the following equation:

$$H_d = H_w \, x \, \frac{100}{100 - M} \tag{2.3}$$

Where H_d is the gross calorific value on a dry basis, and M is the moisture content in percentage.

According to eq. (2.3), the sample's moisture content needs to be measured. Therefore, the sample moisture was determined as described above to calculate the results on a dry basis to avoid any moisture variation that might happen to the samples because of the continuous change in the environmental conditions [34].

2.4 Results and discussion

This section covers the results of cycle 1 samples, followed by mapping the root cause analysis of any source of error, and concludes with further investigation to provide an improved technical procedure. A similar structure is followed in cycle 2.

2.4.1 Results of cycle 1

In the first cycle, the samples of high-quality wood chips, industrial-quality wood chips, and wood pellets underwent testing on a wet basis and were analyzed in the respective bomb calorimeters as per ISO 18125:2017. Subsequent to determining the calorific value on a wet basis, the values were recalculated by adjusting for each sample's moisture content to estimate the dry energy content. The comparative results are illustrated in figure 2.1.

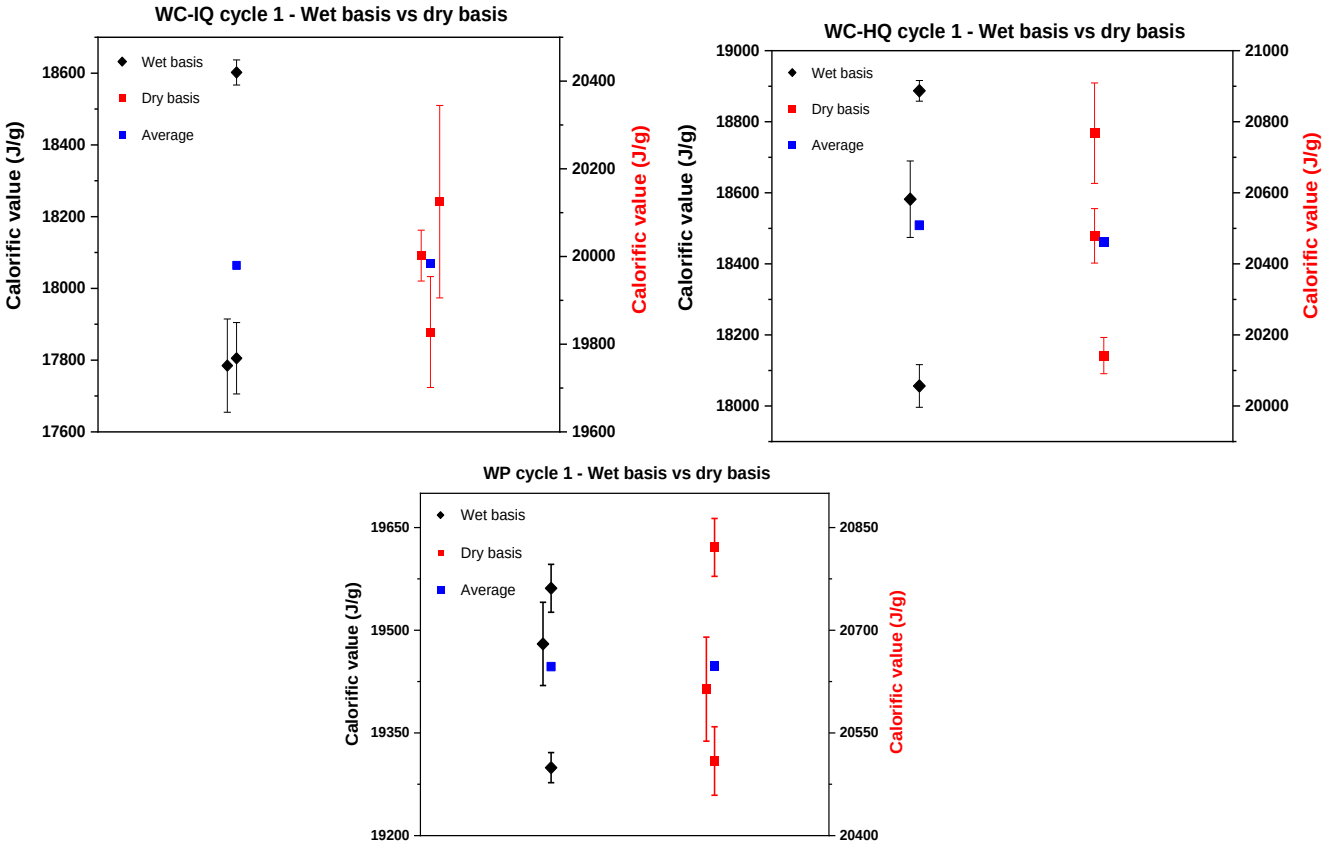

Figure 2.1. *Comparison of the calorific values between the wet basis and dry basis in cycle 1 for different types of biomass.*

Each data point in figure 2.1 represents the average of the results obtained from each institute. A noticeable dispersion is evident across all samples, with reproducibility differences on a wet basis measuring 800, 800, and 300 J for wood chips of industrial quality, high quality, and wood pellets, respectively. The literature indicates that wood chips exhibit heterogeneity, making it challenging to consistently reproduce results in the laboratory [35]. The substantial contrast in reproducibility between wood chips and wood pellets may stem from the fact that wood pellets are produced in a compacted pellet form and are blended with oils or starch to enhance moisture stability [36]. Consequently, they exhibit minimal reactivity to changes in the surrounding environment, resulting in a high probability of reproducing results for wood pellets.

Upon a side-by-side comparison of the dry basis with the wet basis, it can be deduced that the results for wood chips have improved, and the reproducibility difference has decreased. However, the values still deviate by approximately 300, 600, and 312 J for wood chips of industrial quality (WC-IQ), wood chips of high quality (WC-HQ), and wood pellets (WP), respectively. According to the ISO standard, the maximum allowable limit for reproducibility differences is 400 J for wood chips and 300 J for wood pellets. From this perspective, WC-HQ and WP would have been rejected for exceeding the ISO limit. A comprehensive root cause analysis was conducted to identify all potential sources of error or deviation in the measurements to systematically analyze the reasons for these discrepancies.

2.4.2 General root cause analysis – Cycle 1

Figure 2.2 depicts the root analysis of cycle 1 where it highlights the factors that cause deviations in the measurements. Each of these factors is later investigated to provide recommendations to limit the influence of each factor on the final calorific value.

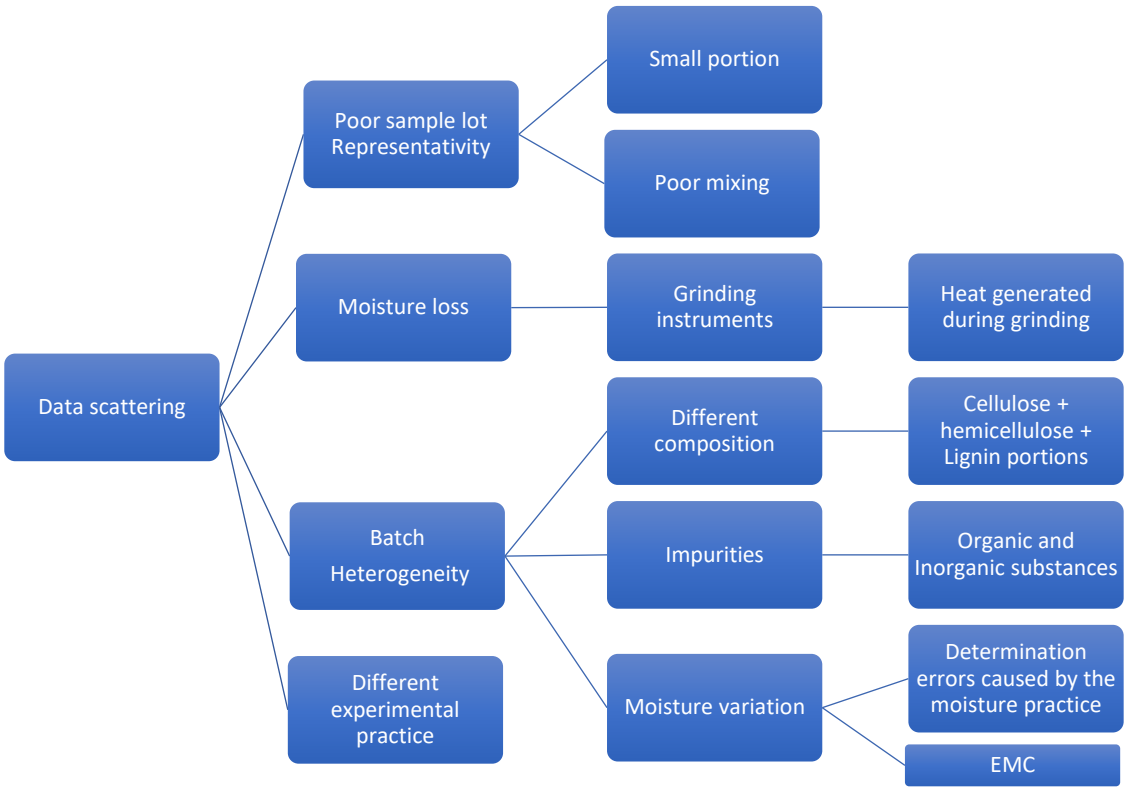

Figure 2.2. *Root cause analysis of possible reasons behind the data scattering*

Numerous factors contribute to the data scattering, starting with the poor representativity of the sample lot due to inadequate mixing or selecting a small portion from a larger batch. Additionally, moisture loss from using different grinding instruments, batch natural heterogeneity, and the executed experimental practices significantly contribute to data scattering. Enhancing the quality of results requires a thorough examination of the contribution of each factor to the calorific value and understanding how to mitigate them. Consequently, any improvement in the experimental setup ultimately reflects on repeatability and reproducibility. The BIOFMET survey indicates that sample heterogeneity and moisture variation have the most substantial impact on result accuracy [8]. To enhance results, factors identified in the root analysis must be neutralized, enabling the quantification of each source individually. This is achieved by standardizing the experimental practice and testing a unified sample under specific conditions.

For cycle 2, TUBITAK UME provided well-grounded, mixed, and homogenized samples (refer to section 2.3.2). These samples were dispatched to other institutes and subsequently tested, eliminating potential deviations caused by inconsistencies in sample lots. Moreover, using uniform samples mitigated deviations resulting from using different grinding instruments, where moisture loss can vary across different instruments [37]. This leaves two potential

sources of deviation in the new samples, either due to batch heterogeneity or different experimental practices. Quantifying both sources simultaneously is challenging due to possible interference. Therefore, the experimental practice was thoroughly discussed with partners. Various variations in the handling procedure were observed despite partners adhering to the same ISO standard. These variations arise from the standard's generality, lacking detailed criteria for each aspect of the experiment. Different biofuels require distinct approaches to ensure optimal repeatability and reproducibility. Consequently, a modified practice was proposed to minimize any deviation arising from different sample masses, applied pressure for pelletizing the samples, and the handling procedure.

2.4.3 Investigation for improved technical criteria – Cycle 1

The root cause analysis paved the way to further analyze the experimental practice and the technical parameters to drive optimized criteria, which were then tested and verified in cycle 2.

A- Pellet mass

The ISO standard suggests a sample mass range of 0.8–1.2 g, but it has been observed that ensuring complete combustion with such masses is challenging. In this investigation, PTB and TUBITAK encountered difficulties achieving complete combustion for the selected solid biofuels while adhering to the ISO standard recommendations. Consequently, a different set of masses was tested to identify the optimal mass range for wood chips and wood pellets.

The experiments revealed that a mass ranging from 0.3 to 0.7 g is suitable to achieve complete combustion at each institute. Moreover, standardizing the combustion mass at each institute ensures a relatively similar ash formation at the end of the combustion. This mass range is deemed suitable when working with hard-to-burn woody biomass and utilizing a well-mixed and homogenized sample. The newly recommended mass range takes into account diverse calorimetric bomb designs and variations in crucible material types and thicknesses. Commonly available crucibles in the market weigh between 10 to 14 g and are made of either fused silica or stainless steel. With heavier crucibles, heat transfer to the sample is slower, potentially resulting in incomplete burning. Conversely, when using a 5 g platinum crucible, certain sample parts may heat up rapidly, making it challenging to cope with sudden temperature rises, potentially leading to explosions or soot production as parts break down and fail to burn. However, incomplete combustion is not solely attributed to the crucible type; factors such as applied pellet pressure, for instance, play a crucial role in ensuring complete combustion. Additionally, it is recommended to use a balance with a resolution of 0.01 or 0.001 mg to ensure the accuracy and stability of the sample mass.

B- Applied pellet pressure

As BRML was the sole institute to achieve acceptable complete combustion using 1 g of the sample, it became imperative to comprehend the underlying reasons. In pursuit of this understanding, PTB conducted numerous tests involving different oxygen pressures, varied bomb sizes and heads, crucibles, and ignition aids. Despite these efforts, over 90% of the cases exhibited incomplete combustion when 1 g of the sample was employed, as explained in Appendix A. The pressure applied to form the sample pellet remained the only unexplored factor. Notably, the ISO standard lacks information regarding the applied pressure for pellet production or the characteristics of the pelletizer. While the standard specifies that the pelletizer should be capable of exerting pressure up to 10 tons, it remains unclear whether to apply the full 10 tons or engage in a trial-and-error process up to this limit to achieve a well-structured pellet.

In a systematic approach by PTB and TUBITAK, different sets of pellets weighing 1 g were produced by applying pressures of 0.5, 2, 5, and 10 tons to test for complete combustion, respectively. All other experimental conditions, such as the bomb vessel, the crucible, and the fuse setup, were maintained fixed. Each set was tested three times, and the bomb calorimeter was employed to visually assess the completeness of combustion, as presented in figure 2.3.

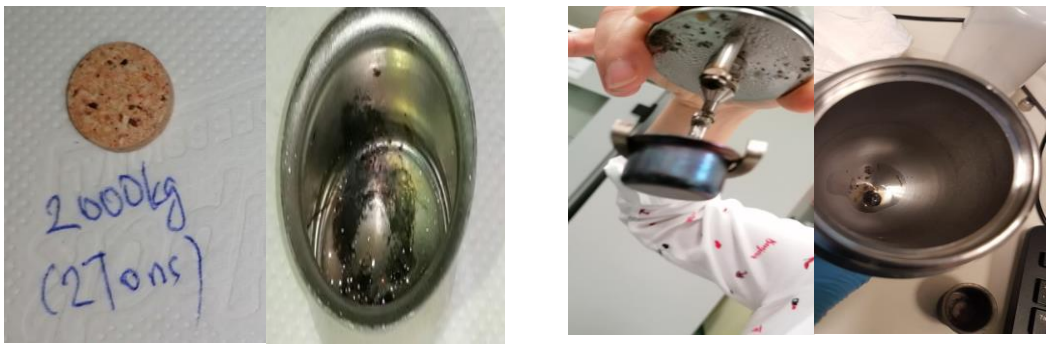

Figure 2.3. *The impact of the applied pellet pressure on complete combustion, (Left) shows the pellet under 2 tons, and (Right) shows the pellet under 10 tons as proposed by the standard.*

Figure 2.3 depicts a sample pellet after applying 2 tons of pressure (left photo) and the solid residuals formed following the combustion. Notably, it tends to form soot even with a smaller sample mass. Figure 2.3 also illustrates tests involving applying a pressure of 5-10 tons to form the pellet. In these cases, the sample exploded inside the bomb, scattering across the bomb head and vessel. These observations confirm the sensitivity of pellet pressure when dealing with finely powdered biofuel samples. Even when applying 10 tons of pressure, marks of breaking

points or segmentations in the pellet are observed, causing the possibility of forming loose powder during combustion. The coexistence of loose powder with turbulent gases generated during combustion may result in the whole sample blowing out of the sample crucible. Hence, if the bomb walls are cool, the sample will be extinguished before it can burn completely [38]. Therefore, a properly pelletized sample is more likely to undergo complete combustion. Applying 0.5 tons to 1 g of the sample resulted in almost all cases exhibiting complete combustion for both wood chips and wood pellets. This observation confirms that the most suitable pressure for pellet formation is 0.5 tons to ensure complete combustion. However, using 1 g of the sample is still recommended only when it is easy to burn or if uncertainties exist regarding the efficiency of sample division, the mixing process, or the batch representativity, as a larger sample would better represent the sample batch.

C- Thermochemical corrections

The thermochemical corrections (Q_N and Q_S) are frequently overlooked sources of error in calorific value measurements. Many industrial laboratories commonly rely on fixed corrections provided in the standards' appendix, based on average values of C, H, N, and S compositions of wood samples or values recommended by calorimeter providers. It is important to note that these fixed corrections do not account for the amount of air trapped inside the bomb vessel, especially when different bomb volumes are used or if the operator has not flushed the bomb vessel with oxygen before the experiment to replace the air inside. Such factors can alter the calorific value, as the trapped air is the primary nitrogen source, and Q_N is based on the quantity of NO_3 inside the bomb. Consequently, an inaccurate estimation of the amount of air inside the bomb can affect the value of the QN correction. The incorrect determination of Q_N and Q_S can result in offsets of 50–80 J in the final calorific value. Hence, the recommended correction approach is using ion chromatography (IC) or titration. Upon analyzing the liquid residual of several samples post-combustion through IC and titration, it was determined that flushing the bomb vessel results in an average nitrogen correction of 2–8 J, whereas not flushing the bomb vessel leads to a correction of around 20–40 J.

2.4.4 Results of cycle 2

Based on the above findings, the experimental strategy was optimized, and a united protocol was used for the measurements. The newly produced samples by TUBITAK were used in this cycle. Similar to cycle 1, the samples of wood chips high quality, industrial quality, and wood pellets were measured on a wet and dry basis, as shown in figure 2.4.

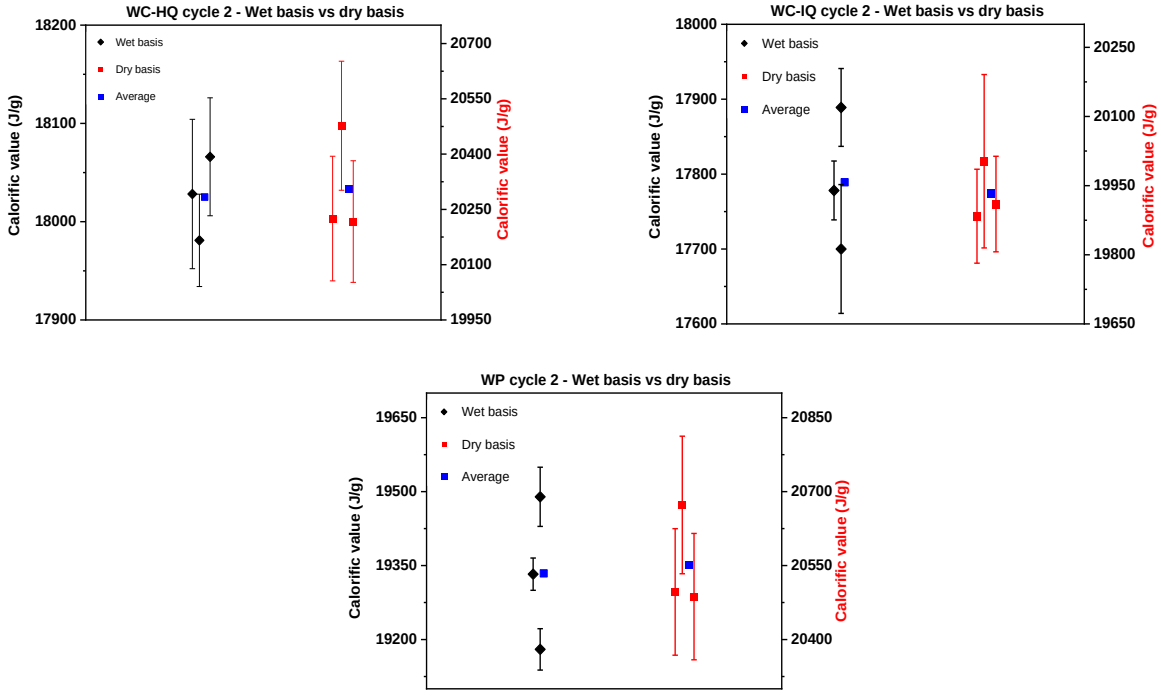

Figure 2.4. *Comparison between the calorific value on a wet and dry basis in cycle 2 for different types of biomass.*

Figure 2.4 shows a notable reduction in the scattering of results on the wet basis for cycle 2 compared to cycle 1 concerning wood chips. In cycle 1, the reproducibility difference for WC-IQ and WC-HQ was 800 J, whereas in cycle 2, it decreased to 189 J and 85 J, respectively. These values signify the improvement achieved by utilizing well-homogenized samples for wood chips. However, the scatter for wood pellets remained nearly constant, with 300 J in cycle 1 compared to 309 J in cycle 2. On a dry basis, the reproducibility difference for WC-IQ, WC-HQ, and WP decreased from 300 J, 600 J, and 312 J in cycle 1 to 120 J, 260 J, and 186 J in cycle 2, respectively.

Comparing the dry and wet basis of cycle 2, the reproducibility difference on the dry basis has decreased in both WC-IQ and WP samples, from 189 J to 120 J and 309 J to 186 J, respectively. However, for WC-HQ, there is an increase in the reproducibility difference from 85 J on a wet

basis to 260 J on a dry basis. This contradicts the conventional understanding that the difference should decrease after recalculating on a dry basis. This deviation suggests the presence of another error source in the experimental procedure that needs to be identified.

2.4.5 General root cause analysis – Cycle 2

As demonstrated in the previous section, the reproducibility for the WC-HQ measurements increases when calculating the calorific value on a dry basis instead of on a wet basis. The first prediction is an error caused during the moisture determination, which strongly influences the accuracy of the calorific value. Figure 2.5 shows the variance in moisture content for the analyzed WC-HQ samples across the three institutes. The moisture content for the remaining samples is provided in Appendix A in table A1.

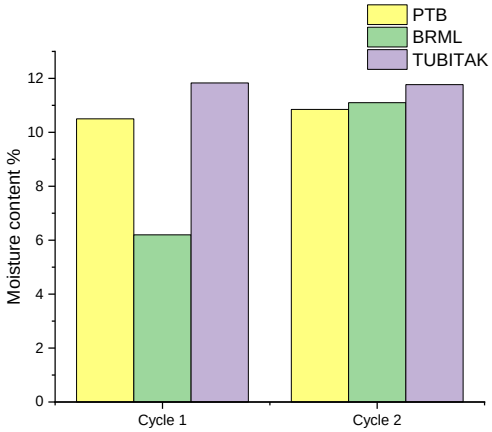

Figure 2.5. *The moisture content of the WC-HQ in the institutes for cycle 1 and cycle 2.*

Figure 2.5 reveals a substantial difference in moisture values during cycle 1 among the institutes, notably between BRML and TUBITAK, with a discrepancy of approximately 6%. In the case of cycle 2, the values exhibit relative consistency but not exact alignment, with a difference of about 0.6% between values. This variance in the moisture content of WC-HQ among the institutes in cycle 2 is attributed to various factors despite the samples being from the same batch and prepared identically, as previously mentioned.

Firstly, errors during moisture determination contribute to such discrepancies, depending on the type of oven used, heat distribution, sample placement inside the oven, and the adequacy of the sample tray for proper drying. The METefnet project's final report emphasizes the importance of a detailed investigation to assess the technical procedure of moisture determination, aiming

to identify error sources and uncertainties [39]. However, conducting such an in-depth investigation is beyond the scope of this work.

Secondly, differences in environmental conditions among the institutes, including relative humidity and temperature, represent another source of error. These conditions influence biofuel samples by changing the equilibrium moisture content (EMC), where the sample reacts with its surroundings, either gaining or losing moisture. Therefore, the sample mass serves as an indicator for evaluating the sample stability under varying environmental conditions [40].

2.4.6 Investigation for improved technical criteria – Cycle 2

A- Equilibrium moisture content (EMC)

If the sample mass remains consistent during the weighing process, it indicates that the sample has achieved equilibrium with its surroundings. In situations of high relative humidity, wood samples tend to absorb moisture; conversely, in low humidity conditions, they tend to lose moisture. This process is primarily influenced by the initial moisture content of the wood. Therefore, the time required to reach Equilibrium Moisture Content (EMC) is pivotal. ISO 14780, a standard addressing biofuel sample preparation, specifies that the sample can be left after grinding to reach equilibrium with temperature and moisture for 4 hours [16]. However, the standard does not explicitly emphasize the significance of EMC or impose an obligation to consider it. This criterion has proven inadequate due to frequent temperature and relative humidity fluctuations, necessitating sample readjustment when room conditions vary. Consequently, PTB conducted a test in a laboratory with 32% relative humidity to assess sample stability. The test involved allowing a freshly ground sample to sit on the balance until it reached a constant mass. The sample consistently lost moisture to the atmosphere, as indicated in table 2.2 by a mass loss. After 24 hours, the sample mass was observed to be stable up to 5 digits. The duration for stability is contingent on surrounding conditions and the nature of the sample.

Table 2.2. *Stability of sample mass as a function of time and EMC.*

EMC reached	Time (hrs)	Original mass: 1.1914 (g)	Moisture loss (%)
90.5%	2:30	1.1170	6.24
92.1%	4	1.1154	6.38
93.2%	5:30	1.1142	6.48
≈ 99%	24	1.1078	7.01

Based on the outcomes presented in table 2.2, the sample is not guaranteed to attain Equilibrium Moisture Content (EMC) within the initial 4 hours. Therefore, allowing the samples to reach equilibrium for 4 hours after grinding and then for an additional 4 hours before determining the calorific value is recommended. Alternatively, if the calorific value determination promptly follows, the sample can be left undisturbed for at least 16 hours.

To investigate the influence of varied EMC levels on the calorific value, 12 samples were selected from a freshly grinded batch of WC-IQ. The samples underwent testing at two distinct time intervals, as depicted in figure 2.6.

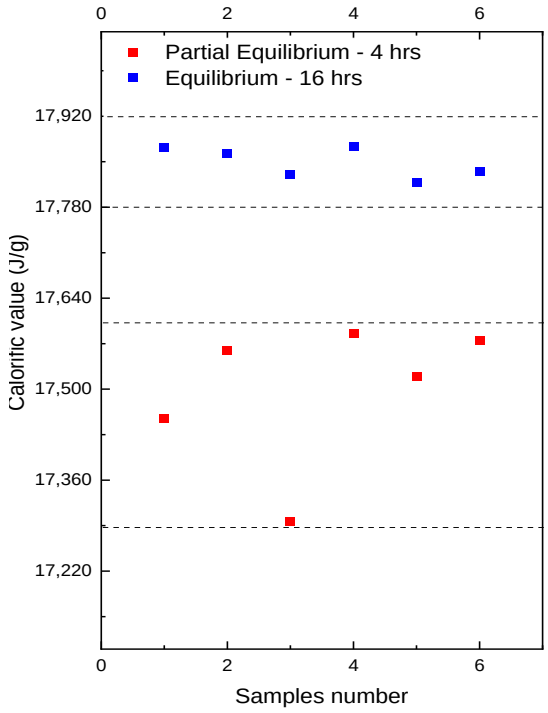

Figure 2.6. *EMC effect on the wet basis calorific value and the sample repeatability.*

Partial equilibrium refers to the tests conducted in the bomb calorimeter after grinding, lasting approximately 4-6 hours. These tests exhibit notable fluctuations in the determined calorific values (depicted by red symbols). After 16 hours, the samples underwent retesting, shown as equilibrium (represented by blue symbols in the figure). Achieving equilibrium would significantly enhance repeatability, reducing deviations between samples to less than 60 J compared to the 280 J observed in partial equilibrium. This improvement stems from the stability of the sample mass attributed to a more consistent moisture content. Laboratory conditions notably influence the impact of EMC on calorific value repeatability. A repeatability enhancement of up to 50–80% is realized, potentially causing the reproducibility difference to

decrease. Repeatability is pivotal in determining the final expanded uncertainty [41]. According to uncertainty calculations presented in section 2.5, where a fixed set of proposed uncertainty sources is outlined, a 50–80% improvement in repeatability is estimated to reduce the uncertainty by 15–30%. However, this value may vary widely based on the calorimetric setup and the uncertainty sources considered in the final uncertainty calculations. Notably, ISO 18125:2017 lacks information about uncertainty sources or their respective values. Therefore, section 2.5 will delve into a detailed discussion of uncertainty sources and their calculations.

B- Operator

The operator represents one of the contributing factors to data scattering in the measurement of calorific value and moisture content. Different operators may employ varying operating approaches and handling techniques, resulting in an expected deviation of approximately 20 J when different operators measure biomass samples. This estimation is based on tests conducted with stable and easily combustible materials, specifically liquid biofuels, as illustrated in Appendix A, figure A1. It is advisable to have the same operator conduct repeatability measurements to mitigate this factor. However, it is important to note that this factor remains inherent and cannot be entirely eliminated, particularly in the context of interlaboratory comparisons involving different institutes or between measurements performed by the biomass supplier or end-user.

2.5 Uncertainty sources

The following uncertainty considerations can help to unify the procedure of determining the uncertainty of a calorific value measured by bomb calorimetry. With that a better estimate about the accuracy of calorific values is accessible. Uncertainty is defined as a margin of error or dispersions attributed to any measured quantity [42]. To estimate the total uncertainty of the calorific value, all the variables that are part of eq. (2.1), eq. (2.2), and eq. (2.3) (see Section 2.3.4) must be highlighted and investigated for their individual uncertainty. Hence, each uncertainty source has been defined, and its contribution has been calculated in this study. Each of these sources can potentially impact the final calorific value. Figure 2.7 presents an Ishikawa diagram illustrating various uncertainty sources linked to the overall uncertainty of the final calorific value.

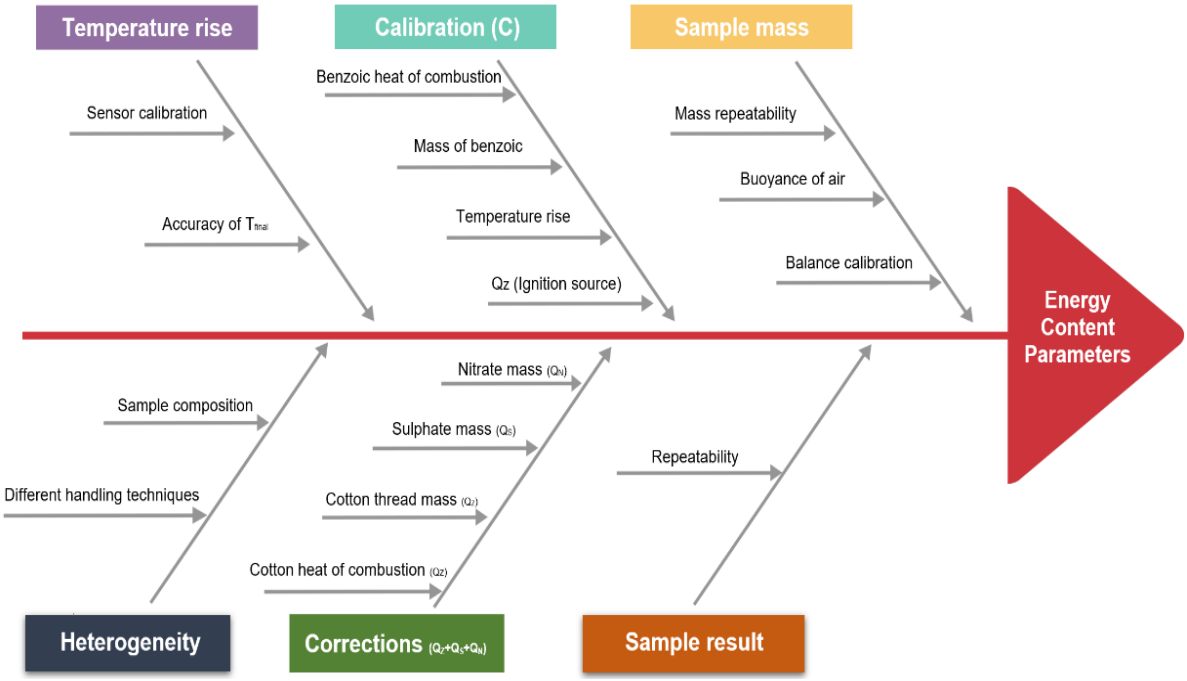

Figure 2.7. *Uncertainty sources associated with the determination of calorific value.*

2.5.1 Sample Mass

The uncertainty of the mass is a function of the mass repeatability, the uncertainty of the balance, and the buoyance of air as given in eq. (2.4), eq. (2.5) and eq. (2.6).

$$U_m(H) = U(m) * P \tag{2.4}$$

$$P = \frac{-C \times Delta\ T + (Qs + Qz + QN)}{m^2} \tag{2.5}$$

$$\mathrm{U}(m) = \sqrt{\left(\frac{\delta U(m)}{\sqrt{2}}\right)^2 + U^2(Balance) + U^2(buyoance)} \tag{2.6}$$

Where *U(H)* represents the mass uncertainty as a function of the calorific value, *U(m)* is the mass uncertainty, and *P* is the sensitivity coefficient. The uncertainty of the air buoyance can be calculated according to the formulas provided by Hashad [43]. The uncertainty of the balance can be found in the calibration certificate. If the certificate is unavailable, the balance must be calibrated manually using standard masses.

2.5.2 Temperature Rise

The precision of temperature measurements relies on the calibration of the sensor responsible for recording the rise in temperature resulting from sample combustion. Usually, such value would be provided by the manufacturer of the calorimeter, or it can be calibrated independently.

Most of the laboratories tend to use the values of the final calorific value and the temperature rise from the instrument. However, in the case of manual calculations based on the raw log data of the temperature from the instrument, the temperature values, T_a, $T_{final,,}$ and T_e must be accurately selected. These temperature values are recorded at specific times where these symbols refer to the beginning of the combustion, the end of the combustion, and the end of the experiment, respectively. Among these, the choice of T_{final} is pivotal, given that both T_a and T_e are known. The moment at which T_{final} is chosen should be consistent across all experiments. By maintaining fixed timing, any error in T_{final} selection during calibration will be mirrored in sample determination, effectively canceling out the error.

2.5.3 Sample result

This is the uncertainty caused by the repeatability of the performed measurements in the same laboratory at the hand of the same operator.

$$U(H_{rep}) = \frac{\delta(H)}{\sqrt{\mathrm{N}}} \tag{2.7}$$

Where $U(H_{rep})$ is the uncertainty of the repeatability, $\sqrt{N}$ is the number of measurements, and $\delta(H)$ is the standard deviation of the total measurements.

2.5.4 Calibration

The uncertainty of the calorimeter calibration (Heat capacity of the system *(C))* is calculated similarly to the fuel samples. Similar sources are considered in the uncertainty as the mass of the benzoic acid used, results repeatability, the thermochemical corrections, and the temperature rise. The only extra factor that needs to be added to the uncertainty is the heat of combustion of the reference material, benzoic acid, which is usually provided in the calibration certificate and ensures traceability to the SI unit.

2.5.5 Corrections (Q_N+Q_S+Q_Z)

The computation of acid corrections Q_N and Q_S adheres to the equations outlined in the ISO standard when ion chromatography is employed, as illustrated in table 2.3. Their uncertainties were derived based on these given equations. Ion chromatography is the recommended methodology for determining thermochemical corrections [44]. Q_N and Q_s are assumed to follow rectangular distributions, where the correction value might exist within any point of the uncertainty range. Q_Z is calculated based on the mass of the cotton multiplied by the cotton's calorific value. However, the fuse wire's contribution to the uncertainty is neglected as it does not burn during the combustion process. In the case of performing the thermochemical corrections based on titration, similar uncertainty is expected.

Table 2.3 *Uncertainty equations for the thermochemical and the ignition corrections.*

Quantity	**Equation**	**Uncertainty equation**	**Sensitivity coefficient (P)**	**Uncertainty**
Q_N	$0.97 \times m_{NO3}$	$U_{QN}(H) = U(Q_N) \times P$	-1/m	$U(Q_N) = \frac{\delta_{m_{NO3}}}{\sqrt{N}}$
Q_S	$3.14 \times m_{SO4}$	$U_{QS}(H) = U(Q_S) \times P$	-1/m	$U(Q_S) = \frac{\delta_{m_{SO4}}}{\sqrt{N}}$
Q_Z	$H_{cotton} \times m_{cotton}$	$U_{QZ}(H) = U(Q_Z) \times P$	-1/m	$U(Q_Z) = \sqrt{U_{Hc}^2(Qz) + U_{mc}^2(Qz)}$
H_{cotton}	Given in the calibration certificate	$U_{Hc}(Qz) = U(H_c) \times P$	M_c	$U_{Hc}(Qz) = \frac{U(H_c)}{2}$
m_{cotton}	Measured by balance	$U_{mc}(Qz) = U(m_c) \times P$	H_c	$U(m_c) = \sqrt{(\frac{\delta m_c}{\sqrt{N}})^2 + U^2(Balance)}$

Here, $\delta_{m_{NO3}}$ is the standard deviation of the determined nitrate mass, $\delta_{m_{SO4}}$ standard deviation of sulphate mass, m_{cotton} is the mass of cotton, and H_{cotton} is the heat of combustion from the cotton.

2.5.6 Sample Heterogeneity or reproducibility U (R)

This factor is introduced to consider the uncertainty caused by the reproducibility in case of comparison. Although this factor will slightly expand the uncertainty, yet it assures that the uncertainty covers the whole ranges of the calorific value measured by the other institutes. Moreover, it combines the uncertainties from the other institutes to develop a single overlapping uncertainty between the values. This factor assumes a rectangular distribution.

$$U(H_{Het}) = \frac{Maxmium\ average\ calorific\ value\ of\ X\ institute - Minmium\ average\ calorific\ value\ of\ Y\ institute}{\sqrt{N}} \quad (2.8)$$

2.5.7 Total final uncertainty

The total uncertainties of the calorific value on a wet and dry basis are derived respectively from eq. (2.2, and 2.3) which are given in section 2.3.4. The uncertainty of the wet basis is derived as follows:

$$U_{wet}^2(H) = U_C^2(H_w) + U_{dT}^2(H_w) + U_{Qz}^2(H_w) + U_{QN}^2(H_w) + U_{QS}^2(H_w) + U_m^2(H_w) \quad (2.9)$$

The total uncertainty on a dry basis:

$$U_{dry}^2(H) = U_{wet}^2(H_d) + U_{Rep}^2(H_d) + U_{Het}^2(H_d) + U_M^2(H_d) \quad (2.10)$$

Where $U_c(H_w)$ is the uncertainty of the heat capacity as a function of calorific value, $U_{dT}(H)$ is the uncertainty of temperature rise, $U_{Qz}(H_w)$ is the uncertainty of ignition, $U_{QN}(H_w)$ is the uncertainty of nitric correction, $U_{Qs}(H_w)$ is the uncertainty of sulphate correction, $U_m(H_w)$ the uncertainty of mass. In eq. (2.10), $U_{wet}(H_d)$ is the uncertainty of the calorific value on a wet basis, $U_{Rep}(H_d)$ is the uncertainty caused by the repeatability of the calorific value, $U_R(H_d)$ is the uncertainty of reproducibility in case of comparison and $U_M(H_d)$ is the uncertainty of the moisture content. Table 2.4 shows the uncertainties obtained during the laboratory comparison by the participating institutes.

Table 2.4. *Final expanded uncertainty (k=2) of each institute in cycle 2.*

Institute	Sample	H_{wet}	H_{dry}	W%	U_{wet}%	U kJ/kg	U_{dry}%	U incl. U(R) %
PTB	WC-HQ	18028	20225	10.86	0.23	78	0.38	0.83
	WC-IQ	17778	19884	10.59	0.22	75	0.38	0.51
	WP	19333	20497	5.68	0.17	70	0.34	0.63
BRML	WC-HQ	17981	20217	11.1	0.26	70	0.35	0.82
	WC-IQ	17889	19910	10.2	0.29	78	0.39	0.52
	WP	19180	20487	6.4	0.22	70	0.34	0.63
TUBITAK	WC-HQ	18066	20477	11.77	--	90	0.43	0.85
	WC-IQ	17700	20003	11.51	--	257	1.28	1.33
	WP	19490	20673	5.72	--	89	0.43	0.67

The final uncertainties of the calorific value on a dry basis U_{dry} are relatively identical in each institute, except for WC-IQ measured by TUBITAK. The latter is because the repeatability of WCIQ at TUBITAK was much higher, with around 0.46%, compared to around 0.16% for PTB and BRML. Therefore, it has caused a noticeable increase in the final uncertainty. Typically, this would have been an issue because the institutes' results would not overlap in a single point. However, by looking at the values of *U incl. U(R),* it can be observed that the final relative uncertainty became significantly extended with an average of maximum ± 1% for all samples.

This is also demonstrated in the previous results shown in figure 2.1 and figure 2.4 on a dry basis, where the uncertainty/error bar is widely extended in cycle 2 compared to cycle 1, where this factor was not implemented. The results are now clearly overlapping together in a specific range, for more information, see Appendix A, figure A2. This overlapping could only be obtained after calculating the heterogeneity/reproducibility uncertainty according to eq. (2.8) as shown in section 2.5.6. Nevertheless, the final relative expanded uncertainty of ±1% remains significantly better than the commonly cited industry or literature range of 2-5%. It is therefore recommended to consider the detailed uncertainty calculations to guarantee a precise determination of the calorific value. In a few cases, some uncertainty sources cannot be easily determined or do not significantly contribute to the final uncertainty. However, based on the findings in this work, it can be concluded that the uncertainty of the calorific value repeatability, the moisture, the sample mass, and the heat capacity of the system are the most crucial uncertainty sources that that should consistently be taken into account.

2.6 Analysis of biomass characteristics – CHNSO determination

Elemental analysis (CHNSO) is typically used as an alternative method to determine the energy content of biofuels and as an essential input in process modeling when simulating biofuels/biorefinery processes. Therefore, there was a need to evaluate this approach. However, unlike the energy content measurement, no comparison was performed as the other institutes collaborating on this project did not have an elemental analysis. Therefore, several tests were performed to determine the elemental analysis of the different types of biomass to evaluate the repeatability and compute the uncertainty to understand its range better.

2.6.1 Materials

The exact samples of wood chips of high quality (WC-HQ), wood chips of industrial quality (WC-IQ), and wood pellets (WP)—were utilized, which were supplied through the Danish Technological Institute (DTI) in Denmark.

2.6.2 Sample preparation

Similar to the calorific value, large samples are not suitable for use in the elemental analysis. Therefore, drying and grinding were necessary to lower the size into a fine powder and measure the value on a dry basis. Therefore, the samples were dried, and the fine powder was properly mixed to guarantee a reflective homogenized portion. Drying the biomass helps remove moisture, ensuring that the measured weight corresponds to the dry weight of the sample. This

is important because elemental analysis is typically reported dry-weight to provide consistent and comparable results.

2.6.3 Experimental setup and methodology

The elemental analyzer used in this chapter is the thermo scientific FLASH 2000 CHNS/O Analyzer. Five different measurements were performed for each sample following the operating procedure given in the instruments manual. The first step before using the instrument is calibration using a standard solution like Acetanilide or Sulphanilamide. Suphanilamide is used when sulfur needs to be determined. However, most elemental analyzers fail to determine very low sulfur composition in the ppm range, like in some solid biofuels. Therefore, other technologies, like mass spectroscopy, are used to accurately determine sulfur. Within this project, the BAM institute in Germany performed the measurements of sulfur and provided the values. Therefore, Acetanilide was used rather than Sulphanilamide. The solution is used to make a calibration curve, which will be used as a reference for determining CHN. After calibration, a sample made of the fine powder of wood pellets or chips is weighted on the balance. The sample mass is typically in the range of milligrams and introduced inside a tiny Tin capsule with 8 x 5 mm dimensions. This Tin capsule is introduced to the device through an Autosampler at the top of the device. The sample is then directed to an oven inside the device to combust the sample in the presence of a gas carrier like Helium or Argon, as can be seen in figure 2.8.

Figure 2.8. *CHNS analysis and sample preparation.*

The oven is typically on standby mode at 500 °C, while before starting the analysis, the temperature needs to be heated up to around 900 °C. After the sample is combusted, the flue gas is directed to a column made of copper oxide, where reduction reactions occur, resulting in

individual elements being produced. The gas enters a conductivity detector, where the signal is converted into concentration in a similar approach to Ion chromatography.

2.7 Results and discussion – CHNS determination

The elemental analysis generates results in the form of peaks displayed in chromatograms. Then, those peaks are converted through internal software to provide the final values in the form of the mass concentration of each element in the sample. However, it is important to highlight that the composition's sum must equal 100%. Therefore, the compositions of CHNS are summed up and deducted from 100% to calculate the oxygen content in the sample. However, it is worth mentioning that these outputs represent only the raw composition of the CHNSO and do not provide the uncertainty of each element. Therefore, an analysis was needed to specify the uncertainty sources. The uncertainty associated with these measurements can be caused by four potential sources as follows:

1. The uncertainty associated with weighting the sample and its repeatability can be determined using the same formulas as in equations 2.6 and 2.7, respectively.
2. The second source comes from the accuracy of the calibration solutions that were made using Acetanilide solution to generate the calibration curve. Any mistake in the calibration curve will be clearly reflected in the final measured values.
3. The third source comes from any fault or draft that might occur in the detector itself. However, if such an incident occurred, it would only be detected through the calibration curve, where deviations would be noticed compared to the reference calibration values. Therefore, sources number two and three are relatively connected.
4. The fourth source of uncertainty is the operator, as he/she must adhere to a specific unified procedure, for example, regarding which sample mass range to use across the measurements. Moreover, by assuring an impurity-free working atmosphere to avoid contaminating the samples. Therefore, this factor depends on the operator's level of proficiency in performing the measurements.

In reality, it is difficult to quantify some of these sources in case of deviations or errors mainly when caused by the instrument itself. However, if the operator maintained the same procedure and the calibration curve was correctly produced, the deviation between the calibration and determination is canceled out. Therefore, the common source of uncertainty for most measurements is associated with weighting the samples. The results of the CHNS analyzer, along with their uncertainties, are shown in table 2.5.

Table 2.5. *Results of elemental analysis and their uncertainty.*

Property	Wood chips - IQ	Wood chips – HQ	Wood pellet
C %	47.13 ± 0.34	47.08 ± 0.37	50.22 ± 0.30
H %	5.69 ± 0.14	5.61 ± 0.21	5.84 ± 0.047
N %	0.198	0.074	0.093
S % *	0.0125	0.0058	0.0069
O %	44.99	46.99	43.56
Ash % *	1.97	0.24	0.28
Moisture %	10.76 ± 0.538	11.24 ± 0.562	5.93 ± 0.2965

* Sulfur (S) was determined at BAM institute.

* Ash was determined at BRML institute.

The total elemental analysis (CHNSO) equal 100%. However, the ash and moisture content values are included in this table as they complete the biomass characterization. Notably, the maximum uncertainty in the elemental analysis is for the carbon content, with around 0.37% for WCHQ. Therefore, it is clear that elemental analysis has low uncertainty, and when used to calculate the energy content, it will not maximize its uncertainty. However, since other technologies like Mass Spectrometry might be needed in addition to the elemental analyzer to fully specify the composition of biomass, this makes it complicated for other laboratories as these technologies might not be accessible or available to everyone. Moreover, these instruments are more costly than the bomb calorimeter. Therefore, using CHNS analysis to estimate the calorific value might unnecessarily complicate the determination process.

2.8 Conclusions

This chapter comprehensively explained the potential error sources impacting the accuracy of solid biofuels' calorific value determination. These sources were quantified to provide laboratories, producers, and end-users with sufficient information on how to mitigate causes of deviation. Recommended criteria were introduced to improve the repeatability and reproducibility of results.

For hard-to-burn woody biomass, it is recommended to use a sample mass of approximately 0.3–0.7 g to ensure complete combustion. A balance with a resolution of 0.01mg or 0.001 mg is preferable for accurate sample weighing. The applied pressure to form the pellet is crucial for ensuring complete combustion, with a recommended pressure range of 0.5 to 3 tons.

Maintaining a bucket temperature between 22–24 °C in all experiments is essential to prevent deviations caused by variations in heat transfer rates. Utilizing titration methods or ion chromatography for thermochemical corrections is essential to ensure realistic and more accurate values. Allowing sufficient time for the sample to reach equilibrium moisture content is vital, with a recommended duration of 16 hours for direct determination or 4 hours after grinding and another 4 hours before determining the calorific value.

Detailed uncertainty sources were provided and highly recommended for users measuring calorific value with a bomb calorimeter. The maximum relative expanded uncertainty expected from the calorimetry is approximately ±1%, and any increase beyond this value should be investigated. The analysis improved the repeatability by around 50–80%, and the final relative expanded uncertainty was enhanced by 10–30%.

On the other hand, elemental analysis was used to determine biomass's CHNS composition and their uncertainties. The elemental analysis revealed unnecessary complications when used to estimate the calorific value as it requires other technologies for sulfur determination, which wastes time and effort. However, CHNSO determination is crucial when simulating biofuel/biorefinery processes since these data are the main building block in the model. Therefore, the results of the biomass characteristics that were obtained in this chapter will serve as the input data to the models performed in chapters 5 and 6 to study how these experimental measurements impact the process design and performance.

Nomenclature

PTB	Physikalisch-Technische Bundesanstalt
TUBITAK	National Metrology Institute from Turkey
BRML	Biroul Roman de Metrologie
CHP	Combined heat and power
WP	Wood pellet
WCIQ	Wood chips industrial quality
WCHQ	Wood chips high quality
CHNSO	Elemental analysis (Ultimate)
Ta	The beginning temperature of the experiment
Te	The end of the combustion phase
Tf	Final temperature of the experiment
H	Hydrogen
C	Carbon
N	Nitrogen
S	Sulfur
O	Oxygen
EMC	Equilibrium moisture content
H_{wet}	Heat of combustion on wet basis
H_{dry}	Heat of combustion on dry basis
U	Uncertainty
W%	Moisture content
Q_N	Nitrate correction
Q_S	Sulfur correction

CHAPTER 3

Chapter 3. Evaluating the Viability of EU's Sustainable Aviation Fuel Targets Through Biomass: Technical & Policy Aspects

3.1 Overview

In Chapter 2, different types of biomass were characterized and their uncertainties were determined. The importance of accurate measurement procedures not only contributes in avoiding financial loss for the biomass provider or the end user but also influences the process design, yield, and performance whenever those biomass/bio-based feedstocks are used to produce higher fuels. Consequently, as one of the main aims of this thesis is to evaluate the influence of biomass characteristics and their uncertainties on the production of sustainable aviation fuel, a prior analysis is presented in this chapter to evaluate the availability and feasibility of using biomass on a large scale as a primary feedstock for SAF production. Furthermore, the analysis compares the different feedstocks and pathways to determine the most promising SAF routes for implementation in the short and medium term. Additionally, the analysis provides insights into the potential of meeting the long-term SAF uptakes proposed by the EU mandates.

Based on:

Shehab, M.; Moshammer, K.; Franke, M.; Zondervan, E. Analysis of the Potential of Meeting the EU's Sustainable Aviation Fuel Targets in 2030 and 2050. *Sustainability* 2023, *15*, 9266. https://doi.org/10.3390/su15129266

3.2 Introduction

The International Civil Aviation Organization has implemented the Carbon Offsetting and Reduction Scheme for International Aviation (CORSIA). This scheme is designed to counterbalance any growth in emissions beyond the 2020 baseline levels by acquiring carbon credits from other sectors. It also outlines the sustainability criteria for the feedstocks used [45]. To be deemed sustainable according to CORSIA, a fuel must meet specific criteria, including reducing the carbon footprint, improving water quality, considering soil and air health, and respecting human and land rights. CORSIA is considered a temporary measure until the aviation industry can progress and adopt more sustainable technologies to mitigate its carbon footprint.

The European Union (EU) has actively taken measures to reduce aviation emissions by advocating for the adaption of SAF as a key solution for its decarbonization [46,47]. In 2021, the EU Commission proposed a gradual increase in the utilization of SAF at EU airports, leading to the development of the ReFuelEU aviation initiative and the introduce of a SAF mandate. On April 26, 2023, an agreement was reached between the EU Parliament and the EU Council, amending the initial proposal by the European Commission [48]. The agreed-upon SAF uptake at EU airports is set as follows: 2% by 2025, 6% by 2030, and 20% by 2035, with a maximum target of 70% by 2050. Notably, a sub-mandate is included to produce SAF from power to liquid process (PTL) as follows: 1.2% in 2030 and 5% in 2035, increasing to 35% by 2050, while the rest of SAF production should be produced through other means mainly via bio-based feedstocks. PTL involves converting renewable electricity from sources like solar or wind power into liquid fuels or by capturing CO_2 from a rich effluent stream, offering alternatives to conventional jet fuel.

Projections indicate a steady increase in SAF uptake in the EU from 2025 to 2035, driven by the commissioning of more SAF plants and their progression toward full capacity after initial operational years. As the SAF market matures, plants are expected to reach full capacity more swiftly, and production costs will decrease, resulting in an exponential uptake trajectory from 2035 to 2050. The SAF mandate presents several advantages, including boosting domestic economic growth, creating opportunities, and expanding the necessary infrastructure to meet the specified targets. Additionally, the mandate gives confidence to investors and stakeholders, encouraging support for the R&D and the commercialization of new technologies. Therefore, this chapter aims to evaluate the potential of meeting the SAF targets and assess the feasibility of achieving these projections based on existing technologies using bio-based feedstocks.

3.3 Methodology

The ReFuelEU initiative does not yet clearly state how realistic such SAF projections are achievable. To assess the feasibility of achieving the EU's SAF targets through bio-based feedstocks, a four-step validation process was undertaken:

1. **Quantification of Bio-Based Feedstocks:** The initial step addressed the significant challenge of limited feedstock availability, a key constraint on SAF production expansion. Various types of bio-based feedstocks suitable for SAF were quantified to evaluate their potential and identify supply limitations. This quantification aimed to determine if the EU possesses sufficient, sustainable feedstocks to meet the demands of SAF production.
2. **Comprehensive Analysis of SAF Conversion Pathways:** Multiple pathways exist for converting bio-feedstocks into SAF, each characterized by differences arising from utilizing diverse feedstock types and each technology's varying readiness levels. A thorough analysis of pathways defined by ASTM D7566 was conducted to identify the most promising and economically viable options. This assessment considered short and medium-term implementation possibilities.
3. **Calculation of SAF Production Capacity:** The SAF production capacity in the EU was calculated using the optimal pathways and feedstock quantities identified in the previous two steps. The capacity, measured in million tonnes (Mt) of SAF, was determined using the formula: *SAF Capacity (Mt) = Feedstock quantity (Mt) × Yield percentage of liquid hydrocarbon × SAF fraction in the liquid hydrocarbon*. Therefore, estimating the capacity of SAF production from each pathway shows which combination of feedstocks and pathways can supply enough SAF to meet the mandate targets.

3.4 SAF feedstocks availability and quantification

3.4.1 Bio-based feedstocks

Various feedstocks can be employed in producing SAF based on the chosen pathway. The analysis primarily focuses on bio-based feedstocks recommended by the European Renewable Energy Directive, aligning with the sustainability criteria outlined by CORSIA for SAF production [49,50].

Waste Oil, fats, and grease

Waste oils, fats, and greases (FOGs) encompass diverse waste types, including used cooking oil (UCO), greases, fatty acids, and animal fats. These by-products arise from cooking or food

preparation processes and can be sourced from commercial establishments or households. Typically used in the biodiesel sector, these oils serve as valuable feedstock.

Vegetable oils

Vegetable oils are derived from palm oil, soybeans, rapeseed, and sunflower crops, cultivated primarily for their oil-rich seeds. Collectively, these four crops contribute to over 87.3% of total vegetable oil production in 2022/2023 [51]. Widely employed in various applications, including food, industrial uses, and biofuel production, these oils are integral to SAF production.

Agricultural residues

Agricultural residues pertain to plant parts left after harvesting, processing, or consumption, including stems, leaves, husks, and shells. These residues offer organic matter and could be used for synthetic fuel production.

Lignocellulosic cover crops

Lignocellulosic cover crops are grown to cover soil, providing benefits like erosion control and enhanced soil health. Selected for fast growth and substantial biomass production.

Municipal solid waste

The organic fraction of municipal solid waste (MSW) includes biodegradable components from plant or animal sources within household and municipal waste. This fraction, comprising food waste, yard waste, paper products, and other organics, can be diverted from landfills and processed as fuel feedstock.

Primary and Secondary Forest Residual

Primary and secondary forest residuals are both forms of organic material remaining from the harvest of forests, but there are some key differences between those two [52,53]. Originating from undisturbed forests, primary forest residuals boast higher quality and energy content. In contrast, secondary forest residuals arise from regrown forests after disturbances like logging clearing for agriculture. While primary forest residuals are often more valuable, secondary forest residuals are more readily available for commercial use, given the protection status of primary forests. Access to primary forests may be restricted due to conservation efforts.

3.4.2 Feedstock quantification

Two distinct methodologies were examined for quantifying these feedstocks, relying on either their theoretical or actual availability. Theoretical availability refers to the quantity of the feedstock accessible for the entire bioenergy sector, irrespective of its current utilization. The theoretical quantification assumes a scenario where the entire mass of the available feedstock

is allocated to the production of sustainable aviation fuel. On the other hand, actual feedstock availability refers to the quantity of feedstock that fulfills the following criteria:

1. Sustainability
2. Ease of collection
3. consideration of competing demand from other sectors
4. Affordability and logistical viability

Various studies in the literature offer diverse results for quantifying these feedstocks in the European Union, as outlined in table 3.1 [54,55]. Theoretical projections are available for 2030 and 2050. However, concerning actual availability, only data predictions for 2030 are currently existing.

Table 3.1. *The EU's theoretical and actual available feedstock in 2030 and 2050 [54–57].*

Feedstock Type	Theoretical Available 2030 (Mt)	Theoretical Available 2050 (Mt)	Actual Available 2030 (Mt)
Waste oil and fats	5.3	9.9	2.4
Organic fraction in MSW	44–80	33–61	21.2
Agriculture residual	45–65	65–71	87.7
Cover crops	36–108	42–127	
Primary forest residual	41–68	45–75	5.1
Secondary forest residual	89–126	93–139	

According to table 3.1, the theoretical availability of waste FOGs, agricultural residues, cover crops, and forestry residuals that could be used in the bio-sector is expected to increase in 2050 compared to 2030. However, it is anticipated that the organic fraction of municipal solid waste will decrease by 2050 due to the EU's regulations aimed at reducing its production by following the waste hierarchy scheme [58]. The main focus is on the actual feedstocks, as those are the ones that are available and could be easily utilized to produce SAF. It can be seen that agriculture residuals, cover crops, and MSW would be largely available compared to forestry residuals.

3.5 Analysis of SAF pathways

The fuel industry comprises various pathways, each possessing unique characteristics and environmental impacts. A comprehensive understanding of these pathways is imperative for the aviation sector to effectively curtail its carbon footprint and facilitate the transition into a more sustainable future. The commonly approved ASTM pathways for SAF production are summarized and compared to ascertain their maturity levels in meeting SAF mandates.

1. **Fischer–Tropsch—Synthetic paraffinic kerosene (FT-SPK):** FT-SPK, is a pathway that produces SAF from non-petroleum-based feedstocks. This produced SAF is a drop-in fuel, compatible with existing aircraft engines without requiring modifications. The process involves converting syngas, derived from biomass gasification or other means, into hydrocarbons to produce a fuel with properties similar to conventional jet fuel.
2. **Fischer–Tropsch—Synthetic paraffinic kerosene with added aromatics (FT-SPK/A):** FT-SPK/A is a blend of FT-SPK and a small quantity of aromatic hydrocarbons (around 20%). These aromatics make the fuel match the characteristics of conventional jet fuels [59]. Moreover, this blending improves the fuel's cold-weather performance, addressing potential viscosity issues. FT-SPK/A is also a drop-in fuel, theoretically suitable for 100% use without blending with conventional jet fuel.
3. **Hydroprocessed esters fatty acids—Synthetic paraffinic kerosene (HEFA-SPK):** HEFA-SPK is typically produced by hydroprocessing renewable feedstocks like vegetable oils and animal fats. The process involves breaking down fatty acids into smaller hydrocarbon molecules, which are then combined with hydrogen to create HEFA-SPK.
4. **Hydroprocessing of fermented sugars—Synthetic Iso-Paraffinic fuels (HFS-SIP):** HFS-SIP is produced by fermenting sugars from renewable feedstocks like corn and sugarcane to create bio-alcohols, followed by hydroprocessing to generate various hydrocarbons. This multi-step process encompasses feedstock preparation, fermentation, hydroprocessing, refining, and blending.
5. **Alcohol-to-Jet synthetic paraffinic kerosene (ATJ-SPK):** ATJ-SPK is produced by converting bio-based alcohols, such as ethanol, into hydrocarbons suitable as a drop-in replacement for conventional jet fuel.
6. **Co-Processing of bio-oils with petroleum:** Co-processing involves blending and co-processing bio-oils with petroleum in traditional oil refineries to increase the proportion of renewable fuels, reduce the refinery's carbon footprint, and produce more sustainable aviation fuel.

7. **Catalytic hydrothermolysis synthetic kerosene (CHJ-SK):** CHJ-SK is typically produced through catalytic hydrothermolysis, a process involving heating a mixture of water and biomass in the presence of a catalyst. The resulting liquid is refined and blended to create a drop-in fuel.
8. **High hydrogen content synthetic paraffinic kerosene (HC-HEFA-SPK or HHC-SPK):** Produced from waste oils, fats, and algae, HC-HEFA-SPK involves treating the feedstock with hydrogen to remove oxygen and undesirable molecules. The hydrocarbons are then cracked and isomerized to create a synthetic jet fuel suitable for blending.

3.5.1 Comprehensive analysis of SAF pathways

In order to evaluate the SAF pathways, a set of criteria was chosen to compare and analyze their potential and readiness level to meet future demand, as shown in figure 3.1.

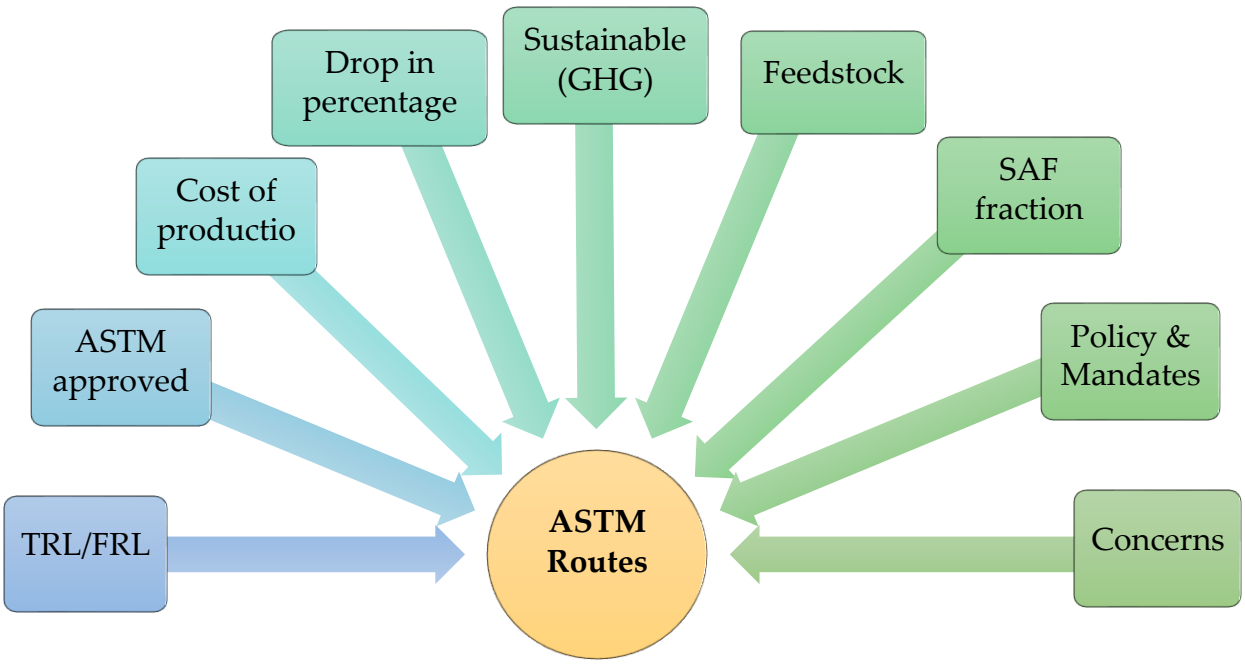

***Figure 3.1**. Criteria for SAF comparison.*

Policy and mandate denote the extent of endorsement provided to a specific pathway by the European mandate. *TRL (Technology Readiness Level) and FRL (Fuel Readiness Level)* represent technology and fuel readiness levels, respectively, ranging from 1 to 9. A score of 9 signifies full commercialization, while 1 corresponds to fundamental research principles. *ASTM approval* indicates the year when a pathway received approval for SAF production.

Production cost encompasses total capital expenditure (*CAPEX*), operational cost (*OPEX*), and *SAF cost* per tonne of fuel. SAF fraction signifies the percentage of SAF in the liquid hydrocarbon mix post-feedstock processing. *Feedstock evaluation* considers material types viable for SAF production, their availability, and the cost per tonne of supplying a specific feedstock.

Sustainability assesses pathways based on their greenhouse gas (GHG) emissions compared to conventional jet fuel, measured in gCO_{2e}/MJ. Comprehensive life cycle assessments (LCA) typically provide these values, covering the entire production cycle from planting and cultivating feedstock to the final fuel production. LCA is internationally standardized and widely used for assessing environmental impacts.

The drop-in percentage indicates the maximum blending ratio that can be supplied to current aviation engines without compromising safety. *Concerns* involve non-technical factors influencing decision-making, such as geopolitical implications or geographical limitations. *Geopolitical implications* refer to potential disruptions in the supply chain for a specific raw material/feedstock. *Geographical limitations* denote challenges in growing a feedstock in a particular area due to environmental reasons or resource scarcity. Table 3.2 provides a matrix for comparison between the different pathways.

Table 3.2. *Matrix for comparison for the SAF pathways.*

Routes	ASTM Approved	Supported by Mandates	Max Drop In %	TRL	FRL	Cost of Production (§)			Sustainability	Feedstock			SAF fraction %	Geopolitical/Geographical Concerns	References
						SAF Cost Dollar/Tonne	**CAPEX %**	**OPEX %**	gCO_2e/MJ	**Type**	**Availability (§§)**	**Cost Range (§§§)**			
FT-SPK	2009	Yes	50%	6–8	7–8	1866–2250	68–83	14–17%	7.7–12.2	Waste and biomass residues	High	Low	40–70%	NO	[59–62]
FT-SPK/A	2015		50–100%												
HEFA-SPK	2011	Only until 2030	50%	7–9	9	1100–1550	7–10	10–14%	13.9–60	Bio-oils, animal fat, Vegetable oils, UCO	Low	Med-High	20–55%	YES	[59–62]
HFS-SIP	2014	Yes	10%	5–7	5–7	2100–2900	N/A	N/A	32.4–32.8	Sugarcane, sugar beet	Med	Med-High	90–100%	Yes	[59–62]
ATJ- SPK	2016	Yes	50%	4–7	7	2100–2900	41–56	31–45%	23.8–65.7	Sugarcane sugar beet sawdust lignocellulosic residues (straw)	Med	Low	60–77%	Yes	[59–62]
Co-Processing Bio-Oils in Petroleum	2018	Yes	5%	N/A	N/A	N/A	N/A	N/A	N/A	Fats, oils, and greases (FOG)	Low	Med-High	N/A	YES	[59,63]
CHJ-SKA	2020	Yes	50–100%	6–7	6	N/A	N/A	N/A	N/A	Triglycerides such oils as soybean, jatropha, and camelina Oil	Low	Med-High	33%	YES	[64]
HC- HEFA-SPK	2020	Yes	10%	4	6	N/A	N/A	N/A	N/A	Algae	N/A	Med-High	N/A	NO	[64]

N/A refers to the lack of reliable data. § *The CAPEX and OPEX* are represented as a percentage of the total SAF cost per tonne. §§ The *availability* is described in three categories. *High* refers to enough available feedstocks; *medium* indicates average availability; and *low* refers to limited feedstock. The data is based on Tables 1 and 2. §§§ The feedstock cost is described in three categories. *High* refers to an expensive feedstock in the range of USD 300–2000; *medium* indicates an average cost in the range of USD 200–1500; and *low* refers to a cheap feedstock in the range of USD 50–300. The range of costs provided is a rough value and unreliable data, as the prices change significantly depending on market stability and demand.

By analyzing the pathways based on the *maximum drop-in percentage*, it becomes evident that FT-SPK/A and CHJ-SKA can offer fuel that is entirely suitable for use in the existing aviation fleet without requiring blending. This is because these pathways produce SAF with properties closely resembling conventional jet fuel, including approximately 20% aromatics [59]. This aromatic content satisfies safety regulations concerning engine sealing. In contrast, the capacity of current co-processing of oil in refinery remains low at approximately 5%, influenced by a combination of technical and economic factors. A primary technical challenge of co-processing comes from the distinct physical and chemical properties of bio-oils compared to petroleum [63]. This dissimilarity can impact the refining process's stability and the end product's quality. Additionally, using bio-oils may lead to complications such as fouling and corrosion of refinery equipment. Although co-processing of bio-oils with petroleum holds significant potential for reducing the carbon footprint of the refining industry, further research and development are required to address technical challenges and enhance economic viability.

Considering *Technology Readiness Level (TRL), Fuel Readiness Level (FRL), Capital Expenditure (CAPEX), Operational Cost (OPEX), and SAF cost per ton*ne, the conclusion takes a different turn, with HEFA emerging as the most promising option. Several factors contribute to this:

1. The feedstocks used in HEFA, such as vegetable oils and animal fats, need less extensive processing, leading to reduced capital investment for the production facility. Consequently, only around 7–10% of the jet fuel's cost is attributed to capital expenses. In contrast, capital costs represent a substantial portion of the jet fuel cost in other pathways, such as FT and ATJ.
2. The HEFA process is a proven technology with a history of use in biodiesel production over many years. This well-understood technology can be readily adapted for producing SAF.
3. HEFA demonstrates a relatively high yield conversion compared to other pathways, indicating that a relatively small amount of feedstock, when processed, results in approximately 90% liquid hydrocarbon. This efficiency reduces both capital and operating costs.
4. Side streams produce valuable co-products like glycerol, which can be sold to offset the plant's operating costs.

Examining feedstock availability and cost unveils a different outcome, emphasizing the abundance and cost-effectiveness of waste and biomass residuals, which can be obtained in

relatively large quantities at reasonably low costs. MSW emerges as the most economical feedstock due to established policies facilitating its collection and sorting. Consequently, pathways capable of harnessing such feedstocks possess the highest potential for widespread implementation. However, this depends on the country and the region. In this context, the FT process takes the lead, followed by ATJ and HFS-SIP, benefiting from their respective feedstocks' mid-range availability and cost. HEFA lags at the bottom of the ranking due to its reliance on less widely available and comparatively more expensive feedstocks. When utilizing waste oil like Used Cooking Oil (UCO), feedstock costs vary based on location and existing infrastructure for oil collection. It is crucial to note that the *cost per tonne* for these feedstocks may exhibit considerable fluctuations depending on market conditions. On the contrary, algae is theoretically more abundant due to its ability to grow in different environments, including freshwater, seawater, and wastewater, with year-round harvesting potential. However, despite these advantages compared to other crops, it's still an immature process, expensive, and has a difficult feedstock to quantify. Therefore, it is excluded from this comparison because of its current state.

Sustainability is evaluated based on the emissions caused by each pathway when utilizing different types of feedstocks. Therefore, it can be noticed that a range for each pathway is provided. The FT process remains the most sustainable among all processes, producing 7.7–12.2 gCO_{2e}/MJ compared to the conventional jet fuel baseline of 89 gCO_{2e}/MJ. This results in significant emissions savings. Other processes also meet sustainability criteria and reduce overall emissions depending on the feedstock, with HEFA ranking second, followed by ATJ and HFS-SIP.

Based on the *SAF fraction*, which represents the percentage of SAF in the liquid hydrocarbon mix, it reveals that HFS-SIP yields the highest SAF fraction, up to 100%. Following this, ATJ, FT-SKA, and HEFA. The SAF yield fraction holds paramount importance in considering production processes' economic viability and sustainability.

Considering *geopolitics and geographical constraints* is crucial when evaluating the feasibility of implementing a specific SAF pathway on a large scale. This consideration gains significance in light of recent energy crises resulting from geopolitical events such as the Russian war in Ukraine. Evaluating the feedstocks employed in each pathway reveals notable geopolitical concerns associated with HEFA, co-processing of oils, and CHJ-SKA. These concerns arise from the reliance on feedstocks that are not widely available within the EU and are dependent

on imports. Therefore, highlighting the supply chain's vulnerability is crucial for the EU's energy policy. For example, approximately 50% of the EU's Used Cooking Oil (UCO), the main feedstock for HEFA, is imported from China. With escalating tensions and trade disputes between China and the US, coupled with considerations of NATO's 2022 strategic concept document addressing China, there's a reasonable assumption that these critical feedstocks could be compromised in the event of sanctions [65]. Consequently, widespread adoption of these processes could jeopardize the aviation sector, as any disruption in the feedstock supply chain in the Indo-Pacific region would paralyze the industry. Paradoxically, these geopolitical concerns may drive demand for locally sourced and sustainable feedstocks, potentially moving the EU closer to energy independence. While domestically-sourced used cooking oil (UCO) could be utilized for SAF production, yet it requires substantial investment to develop the necessary infrastructure.

It is highly noticeable that there is a lack of alignment between the EU committees tasked with shaping energy and foreign policies. This can be demonstrated by the fact that there is a tendency to use imported feedstocks from countries classified, according to several ministries of foreign affairs in the EU, as non-friendly states. Moreover, the devastating Israeli war on Gaza has triggered a disruption in the supply chain in the Red Sea, threatening around 40 % of the EU's trade with Asia and the Middle East. This development revealed the importance of geopolitics in shaping the energy policy. Although the EU seeks to strengthen economic ties with the Middle East to import renewable feedstocks and electricity, its foreign policy during the recent events has fallen short, triggering a backlash and campaigns across the Middle East seeking to halt and boycott trade with the EU. Therefore, there is a need to align the EU's foreign and energy policies by putting cooperation and sustainability at heart and having a balanced foreign policy to avoid possible escalations, only then can a secure and sustainable future be achieved.

On the other hand, the majority of raw oil feedstocks are cultivated in East Asia, South America, parts of Europe, and the United States. Palm oil, the most consumed vegetable oil globally, poses a significant risk of carbon leakage for the EU despite its complete ban as a feedstock for biofuel production [66,67]. This risk arises because the cooking oil used in the EU is predominantly imported, potentially containing substantial amounts of palm oil, thereby indirectly challenging the EU's ban on palm oil for biofuel production. The rationale behind the ban comes from the major environmental concerns associated with palm oil production,

including deforestation, biodiversity reduction, threats to wildlife, and various labor rights violations.

The *geographical limitations* and the environmental conditions required for the growth of oil crops prevent the EU from cultivating palm, soybean, or sunflower oil on a large scale for SAF production. Regions with humid conditions, high rainfall, and sufficient sunlight, such as East Asian and South American nations, are notably suited for cultivating palm and soybean oils [68]. Simultaneously, Russia and Ukraine emerge as major producers of sunflower oil, benefitting from the widespread fertile lands and favorable weather conditions [69]. Consequently, it can be inferred that various vegetable oils not only pose potential geopolitical concerns but also face geographical limitations due to unsuitable climate conditions within the EU. In contrast, sugar cane and beet thrive in the EU and are primarily utilized for sugar production. However, they are not deemed highly sustainable as feedstocks for SAF production for several reasons. For example, sugarcane and beet require a substantial amount of water, triggering a debate over prioritizing resources between food and energy. Consequently, planting a dedicated sugar crop to produce sustainable aviation fuel is deemed neither reasonable, sustainable nor economically viable.

It is essential to acknowledge that this section serves as an overview of potential geopolitical and geographical implications for SAF production. A more in-depth analysis, employing a systematic thinking approach, is recommended. Scholars like Zahra et al. have explored the imbalance in food and biofuel markets amid the Ukraine–Russia crisis. A similar methodology would be needed for bio-based SAF to provide comprehensive insights into potential challenges and viable solutions [70].

3.5.2 Most promising and economically viable pathways

The comprehensive evaluation presented in table 3.2 leads to the cumulative conclusion that the three most viable options for widespread implementation within the context of SAF mandates are HEFA, FT-SPK, and ATJ pathways. This conclusion is derived from the observation that these pathways currently have the highest TRL and FRL, coupled with reasonable CAPEX and OPEX in comparison to the other pathways. Consequently, they exhibit the potential for swift implementation shortly after mandate issuance, facilitating the achievement of short-term SAF goals. Projections indicate that post-2030, other processes will likely start commercial operations. HEFA, although already commercially operational, cannot

be considered in the long-term as the backbone of the SAF industry due to its multiple drawbacks.

On the other hand, FT-SPK shares similar advantages with HEFA, boasting high TRL and FRL, yet it stands out as it can utilize multiple waste feedstocks that are easily accessible at a low cost. Furthermore, FT-SPK demonstrates low emission production, ranging from 7.7 to 12.2 gCO_2e/MJ, compared to the jet fuel baseline of 89 gCO_{2e}/MJ [71]. If adopted widely within the European Union, the FT-SPK process avoids potential concerns that could disrupt SAF production, such as geopolitical implications or feedstock limitations. Additionally, FT-SPK has the unique potential to produce SAF with blended aromatic content, paving the way for its use as a 100% drop-in fuel in the near future, which provides it with a distinctive advantage over most other pathways.

It is crucial to emphasize that this analysis primarily considers pathways approved by ASTM D7566. While other pathways like methanol to jet and waste pyrolysis are in the research phase, their full potential remains unclear and requires a detailed study.

3.5.3 Aviation fuel demand

The anticipated growth in global passenger and freight traffic, averaging 4.1% annually [4], suggests a corresponding rise in aviation fuel utilization. Historical data on jet fuel demand indicates a linear pattern of increase. However, there is inconsistency in EU projections for future jet fuel demand within the literature. O'Malley et al. project a linear growth in demand, aligning with historical data, estimating 62.8 and 71.1 million tonnes (Mt) for 2030 and 2035, respectively [57]. Conversely, a recent European Union Aviation Safety Agency report suggests a relatively stable jet fuel demand in 2030 and beyond, indicating minimal change. The report projects estimated demand figures of 46 Mt in 2030, 46 Mt in 2040, and 45 Mt in 2050 [72]. These projections are derived from modeling work conducted under the ReFuelEU aviation initiative framework.

Predicting precise future jet fuel demand proves challenging due to the absence of public announcements from fuel producers and airports [72]. Factors such as introducing more fuel-efficient engines, which allow for equivalent travel distances with reduced fuel consumption, further contribute to this uncertainty. Additionally, the commercialization of new aircraft types relying on hydrogen, ammonia, or batteries, adds complexity to forecasting. Collectively, these factors contribute to a stabilizing effect on the demand for conventional jet fuel in the future.

3.6 Capacity of SAF production in the EU in 2030

HEFA, FT-SPK, and ATJ emerge as the most promising processes to stimulate the SAF market. An estimation of the maximum possible SAF production in 2030 was conducted based on the actual available feedstocks. This estimation was used to validate the potential of meeting the SAF targets set by the mandates. The 2030 bio-based feedstocks target is 4.8% of the total EU jet fuel demand [48]. The quantity of SAF produced varies according to the feedstock type and the chosen conversion pathway, which transforms feedstocks into a mix of liquid hydrocarbons, including SAF. Yield factors from literature data shown in table 3.3 were applied to convert feedstock quantities into SAF quantities, offering insights into the potential of meeting SAF targets with the current existing technologies.

Table 3.3 *Yield values for different SAF pathways [59,61].*

Process	Feedstock Type	Liquid Hydrocarbon Yield %	SAF Fraction %
HEFA	Waste FOGs	90	59
FT-SPK	Bio-based feedstocks	20	60
ATJ	Bio-based feedstocks	13	77

The average values were utilized for calculations. It's crucial to note that actual yield values may fluctuate in practice, influenced by the specific feedstock and process configuration. Figure 3.2 illustrates the estimated SAF production using different feedstocks and pathways within the EU.

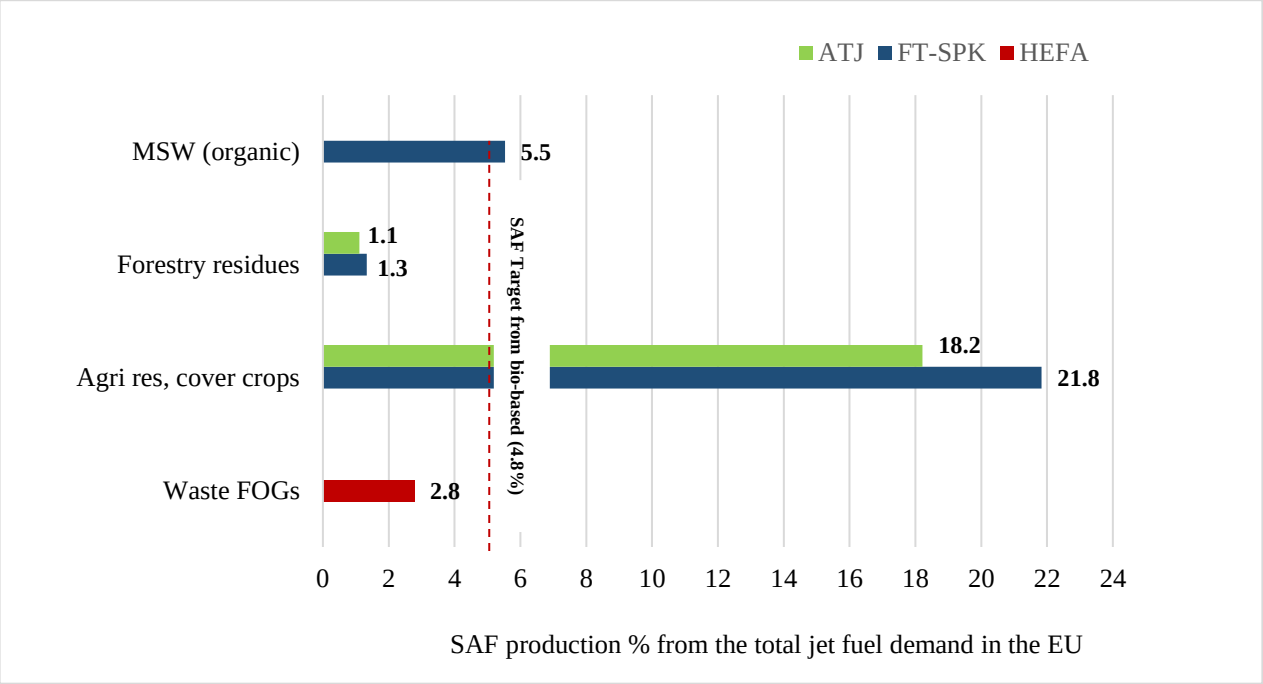

Figure 3.2*. Estimated SAF production based on the available feedstocks in the EU by 2030.*

Waste FOGs and forestry residues alone appear insufficient to meet the EU's SAF uptake in 2030. Conversely, agriculture residuals, cover crops, and MSW demonstrate the capability to fulfill all EU targets for bio-based feedstocks. The most reasonable scenario involves employing a combination of pathways and feedstocks, depending on the economic viability of each feedstock in each region. ATJ and FT-SPK, in many cases, can utilize the same feedstock for SAF production, excluding MSW, which is exclusive to FT-SPK. Overall, FT-SPK surpasses ATJ due to its flexibility in using a broad range of feedstocks and providing higher yield values, resulting in increased SAF production capacity. Consequently, FT-SPK holds the potential to meet SAF targets in 2030 and beyond.

It is crucial to note that, by focusing solely on yield values from table 3.3, HEFA appears to have the highest potential for SAF production due to its high conversion rate. However, due to feedstock limitations concerning waste FOGs, HEFA could only contribute approximately 58% toward meeting the SAF target. The maximum overall SAF production from combined bio-based feedstocks reaches 31.4% of the total EU jet fuel demand, approximately 14.44 Mt. This value is obtained by summing SAF production from different feedstocks. For SAF production from the same feedstock, the value of FT-SPK was considered over the ATJ since it has a higher production capacity.

3.7 Capacity of SAF production in the EU in 2050

The preceding analysis indicates that leveraging currently available biomass with existing commercial technologies could successfully meet SAF targets in the EU by 2030. Beyond 2030, biomass production is anticipated to remain relatively stable, with no significant upsurge. Consequently, it is reasonable to conclude that the actual available feedstocks for SAF production in 2050 will not experience a substantial increase compared to 2030. This assumption is strengthened by the likelihood that any increase in biomass feedstocks would encounter competition from other bio-sectors, partially diverting them from SAF production. Moreover, other factors contribute to the anticipated stability in biomass production, including the impacts of climate change, water scarcity, and more strict land usage policies aimed at preserving biodiversity. A hypothetical scenario was constructed to explore the long-term potential of utilizing biomass, assuming that the available feedstocks for SAF production in the EU in 2030, as detailed in table 3.1, will remain identical in 2050, as shown in figure 3.3.

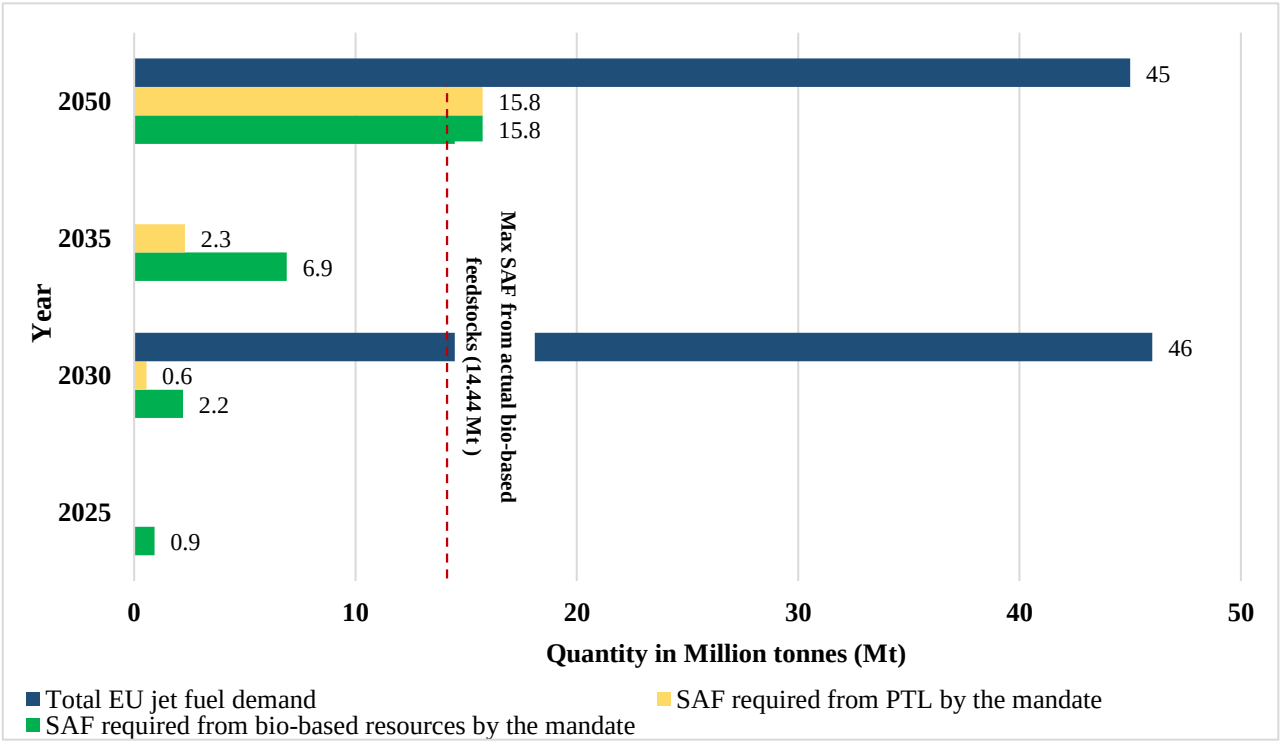

***Figure 3.3**. The potential of Biobased SAF to meet the EU targets in 2050.*

The foreseeable challenge lies in the deficit between the maximum achievable SAF production from existing bio-based feedstocks, totaling 14.44 Mt, and the mandated target of 15.8 Mt of SAF production from bio-based sources by 2050, as outlined in the European SAF mandate [48]. This implies a shortfall of 1.35 Mt, necessitating additional production to fulfill the set

target. By applying average yield conversion values from table 3.3, this 1.35 Mt SAF shortage translates to an extra requirement of 2.4 Mt of waste Fats, Oils, and Greases (FOGs) or approximately 10.8 Mt of agricultural residuals and cover crops in 2050.

In the hypothetical scenario where all biomass in the EU's bio-energy sector is exclusively channeled for SAF production, a theoretical surplus of SAF production exceeding 230% of the total EU jet fuel demand could be achieved. While this is impossible to occur yet, it shows that there is theoretically enough available biomass to meet the EU's demands. Therefore, with the right policy framework in place to divert more biomass from other sectors to SAF production, this would secure enough feedstocks to meet the SAF demand in 2050. Nonetheless, implementing such a policy requires extensive deliberations and considerable time.

An alternative approach involves exploring the option of importing these feedstocks from the Balkan region, given its proximity to EU states and the advantage of avoiding overseas imports, which causes an increase in emissions. Unlike the EU, where most waste materials are recycled, the Balkans often dispose of waste in landfills [73]. However, the feasibility of providing such substantial quantities and validating their technical and economic viability needs a thorough evaluation. Moreover, the apparent scarcity of actual biomass availability in the EU pushes the need for innovative technologies like Power-to-Liquid (PTL) and Methanol to Jet (MTJ). These new technologies are anticipated to play a major role in the SAF industry's future. Especially considering the suitability of these technologies for utilizing diverse carbon dioxide sources, including CO_2 rich streams from cement and steel industries or direct carbon capture from the air. This conclusion aligns with the EU's vision of having a dedicated sub-mandate for PTL and simultaneously pushing towards obtaining the accreditation of the MTJ pathway by the ASTM committee.

3.8 Policy barriers in the proposed mandates

The analysis has shown that there is real potential to use biomass for SAF production and to fulfill the SAF production from bio-based feedstocks in 2030, as specified by the mandate. However, the current proposals/Mandates of SAF are under continuous reformation and development. Therefore, there is a need to highlight the various challenges associated with SAF production, supply, and utilization to become a reference for future improvement. Moreover, identifying and understanding these challenges is important for formulating an effective policy framework. Such challenges can be summarized as follows:

1. **Global cooperation for international flights:** The absence of agreements on managing international flights with or without SAF certification poses a challenge. Existing mandates primarily govern domestic flights or those originating or concluding within the mandate's jurisdiction. Therefore, a global framework is essential to prevent carbon leakage and ensure policy alignment.
2. **Tankering practices:** The handling of tankering practices remains unclear. Tankering involves flights being overfilled with traditional jet fuel to avoid refueling in the EU, due to higher SAF costs. Clear procedures are needed to deter such practices, safeguarding the competitiveness of the EU aviation industry.
3. **Overlapping production of SAF and other synthetic fuels:** Mandates lack clarity on addressing potential overlaps between SAF and other green synthetic fuels, especially when both utilize the same feedstocks. A well-defined policy is required to navigate these overlaps and ensure sustainable production.
4. **Importing feedstocks from non-EU countries:** The policy framework for importing feedstocks from non-EU countries, particularly from East and South Asia, needs attention. Unregulated cultivation and harvesting of these feedstocks may lead to deforestation, competition with food production, and other environmental concerns. Ensuring sustainable practices is crucial to avoid land abuse and negative impacts on local communities. Moreover, to avoid the imported feedstocks being a source of carbon leakage.

3.9 Technical barriers for sustainable aviation fuel deployment

In the foreseeable future, SAF is anticipated to significantly contribute at covering aviation fuel needs, particularly dominating long international flights. On the contrary, hydrogen and electric airplanes are expected to find their niche in smaller jets and shorter distances. However, the large production of SAF requires addressing various technical challenges which represent problems and require potential improvements [74–76].

1. **Feedstock availability:** SAF, primarily derived from renewable and waste resources like waste oils, plant oils, and lignocellulosic biomass, faces limitations in feedstock availability. Scaling up production could lead to competition with food crops or result in environmental impacts. Identifying promising and sustainable feedstocks through life cycle assessments is crucial to enhance their utilization to accelerate SAF production.
2. **Feedstock competition:** The same feedstocks suitable for SAF production also have applications in other modes of transport, including maritime ships and railways, posing a challenge of competing demands.
3. **Economic viability:** SAF production is currently more costly than conventional aviation fuel, posing a challenge for airlines to justify the additional expense, particularly when operating on tight profit margins.
4. **Commissioning time:** Existing SAF production capacity falls short of demand, necessitating the design and commissioning of additional factories to booster SAF production. This challenge may lead to increased costs and disruptions in the supply chain due to the long waiting time for such plants.
5. **Infrastructure:** The infrastructure for SAF production, transportation, and storage at airports is still underdeveloped, requiring the construction of new facilities to accommodate the increased use of SAF.
6. **Energy intensity and process yield:** SAF production requires a significant amount of energy, potentially resulting in increased greenhouse gas emissions if produced from non-renewable sources. Utilizing renewable electricity and enhancing the process yield are crucial for emissions reduction and boosting production capacity.
7. **SAF compatibility:** The term SAF can be misleading, as different technologies yield compositional variations among SAF blending components. Even with the same technology, distinct producers may yield different products. SAF compatibility challenges arise from different airports storing and distributing various SAF types, necessitating a focus

on ensuring a compatible mix for safety purposes. Additionally, the ability to mix different types of SAFs remains unclear. According to the ASTM standards, blending two or more SAF types for commercial flights is prohibited. However, it is noteworthy that distinct SAF blends can be combined if individually approved and reidentified as Jet A/A-1 fuel.

Addressing these multiple challenges is essential to foster the widespread adoption of SAF in the aviation sector seamlessly.

3.10 Conclusions

This chapter comprehensively assessed various bio-based feedstocks, SAF pathways and their potential to meet the SAF targets mandated by the European Union. The analysis covered the availability of sustainable bio-based feedstocks in the EU that meet the sustainability criteria in order to fulfill the short- and medium-term SAF goals. The available feedstocks in the EU can fulfill the targets in 2030. However, by 2050, a deficit of 1.35 Mt of SAF is expected due to the EU's lack of available bio-based feedstocks. This deficit necessitates additional policy frameworks to redirect more biomass towards SAF production to meet the long-term SAF demand.

There is no silver bullet when choosing a pathway; a diversified portfolio of pathways is essential for optimizing SAF production. HEFA, ATJ, and FT-SPK emerge as the most promising and economically viable choices in the short and medium term. HEFA would flourish firstly as it serves as a catalyst to stimulate the SAF market and increase the demand due to its high TRL level, despite its concerns regarding sustainability, feedstock availability, and potential geopolitical implications. On the other hand, FT-SPK stands out as the most flexible pathway with high sustainability credentials, exhibiting substantial emissions decrease of approximately 7.7 to 12.2 gCO_{2e}/MJ compared to the conventional jet fuel baseline of 89 gCO_{2e}/MJ. However, this investigation reveals that existing technologies, irrespective of feedstock or process configuration, fall short of efficiency to meet the long-term large commercial demand. This highlights persistent limitations and practical challenges associated with biomass utilization as a primary feedstock for SAF production. This necessitates further investigation and development of new process concepts to increase the overall conversion efficiency. Therefore, facilitating the adoption of technologies like power to liquid is crucial for the successful expansion of the SAF industry toward achieving net-zero aviation. Moreover, pushing forward with the non-approved ASTM pathways like the methanol to jet would help to

broaden the understanding of alternative SAF production technologies and eventually obtain ASTM accreditation.

Lastly, SAF compatibility poses a challenge in achieving a 100% drop in fuel, as the ability to mix different SAF types remains unclear. Overcoming these challenges relies on significant research and development investments to enhance existing technologies and eventually perform repeatable tests for 100% SAF in long commercial flights to obtain more data. On the other hand, geopolitical implications are an essential element that must be considered while shaping energy policy and deciding which technology or feedstock to use. Furthermore, the energy and foreign policies of the EU need to align to secure a long-lasting, sustainable trade with the rest of the world.

Nomenclature

SAF	Sustainable aviation fuel
HEFA	Hydroprocessed Esters Fatty Acids
Alcohol to Jet	ATJ
FT-SPK	Fischer-Tropsch Synthetic Paraffinic Kerosene
TRL	Technology readiness level
FRL	Fuel readiness level
GHG	Greenhouse gas emissions
IPCC	Intergovernmental Panel on Climate Change
CORSIA	Carbon Offsetting and Reduction Scheme for International Aviation
PTL	Power to liquid
Mt	Million tonnes
UCO	used cooking oil
MSW	Municipal Solid Waste
FOGs	Fats, oils, and greases
ASTM	American Society for Testing and Materials
FT-SPK/A	Fischer-Tropsch—Synthetic Paraffinic Kerosene with added aromatics
HFS-SIP	Hydroprocessing of Fermented Sugars—Synthetic Iso-Paraffinic fuels
CHJ-SK	Catalytic Hydrothermolysis Synthetic Kerosene
(HC-HEFA / HHC-SPK)	High Hydrogen Content Synthetic Paraffinic Kerosene
CAPEX	Total capital expenditure
OPEX	Operational expenditure
LCA	Life cycle assessment
WGS	Water gas shift reactor

CHAPTER 4

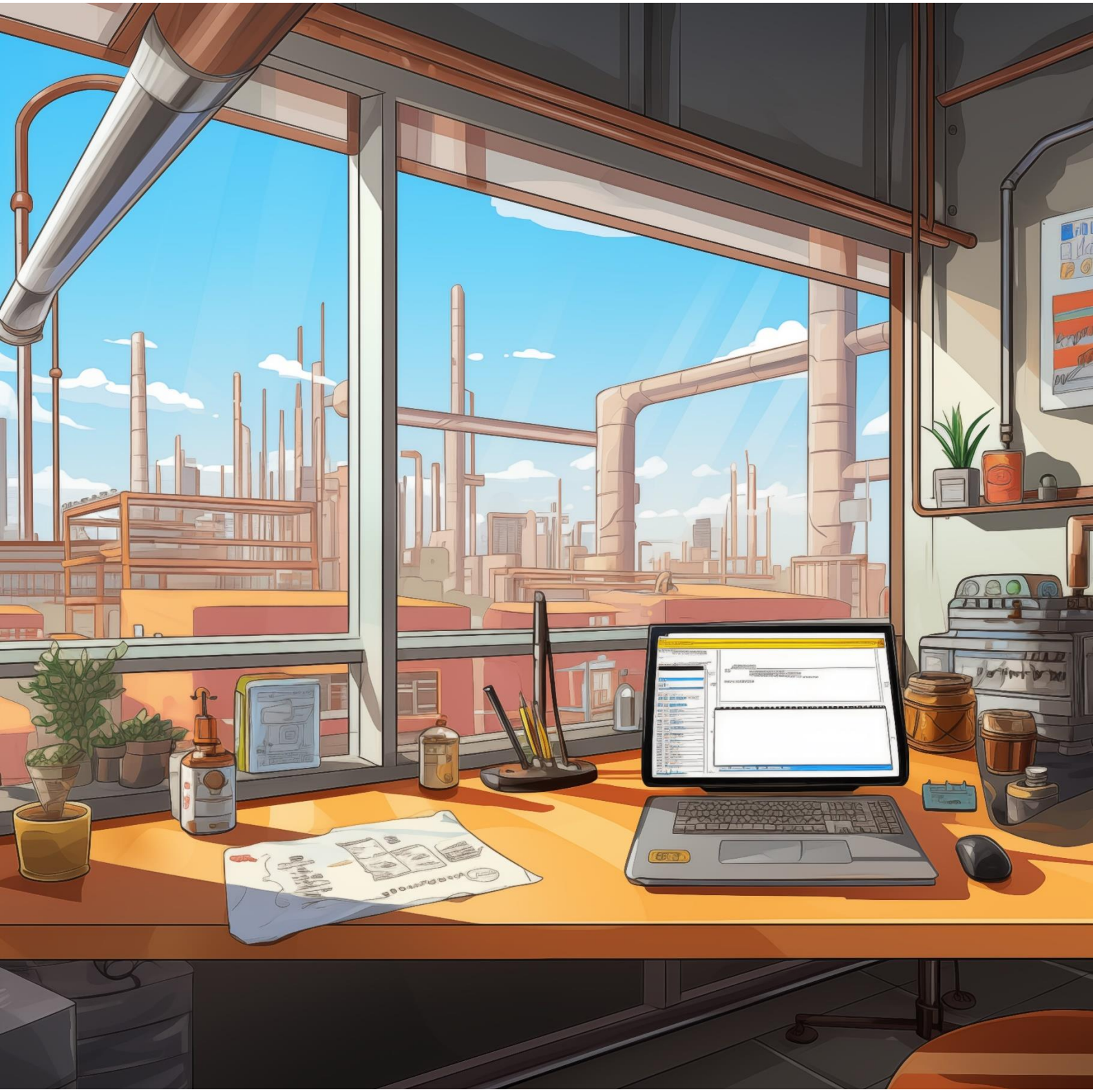

Chapter 4 – Methodology of Process Simulation and Techno-Economic Analysis

4.1 Overview

The most promising processes for SAF production were determined in Chapter 3. Biomass gasification coupled with Fischer Tropsch (FT) was selected as an approved ASTM pathway for SAF production. On the other hand, Methanol-to-Jet (MTJ) was chosen as non-approved ASTM pathway. An overview of the tools and methodologies needed for process simulation, Monte Carlo simulation, as well as techno-economic analysis are highlighted in this chapter. This methodology was subsequently used to analyze the FT pathway (chapter 5) and MTJ pathway (chapter 6).

4.2 Process simulation

The models were constructed using the available literature data with a focus on using experimental data that is highly cited and published in reputable journals, as will be shown in Chapters 5 and 6. Aspen Plus V12.1 was used to simulate the processes and calculate the material and energy balances of the process streams. For the Fischer Tropsch, the Peng-Robinson equation of state combined with the Boston-Mathias equation was used for property prediction since it is suitable in the presence of heavy hydrocarbons, which is expected from the FT process [77]. However, for the upgrading part of the MTJ process, Peng-Robinson (PR) was adapted as it was prominently used in the literature. The biomass feed rate was fixed in the models at 300 tonnes/hour. Three different types of biomass were used to evaluate their suitability in SAF production: 1) wood chips of high quality (WC-HQ), 2) wood chips of industrial quality (WC-IQ), and 3) wood pellets (WP).

The input data for the model, along with the uncertainties of the biomass characteristics, were taken from the experimental measurements presented in Chapter 2. For each of these models, FT and MTJ, two different configurations were simulated and evaluated. The first configuration is based on biomass-to-liquid (BTL), and the second one is based on biomass power-to-liquid (PBTL). The difference between the two configurations is in the H_2/CO ratio, where extra hydrogen is needed to reach the ratio of 2:1. In the BTL process, the hydrogen is obtained through a water gas shift (WGS) reactor. In the second case of PBTL, external hydrogen is added as a process stream rather than a WGS reactor to reach the required H_2/CO ratio. It should be mentioned that the external hydrogen source, whether green or blue hydrogen generated

through electrolysis or steam methane reformer, will not be simulated. Moreover, a Monte Carlo simulation was performed to study the influence of the change in the biomass characteristics on the yield of SAF. The outputs of the models and the Monte Carlo simulation were used to assess the economic performance of the produced fuels.

4.3 Heat integration

Heat integration (HI) is a systematic approach to improving the energy efficiency of industrial processes. Improving the energy efficiency of these processes relies on minimizing the external heating and cooling demand by reusing the waste energy already available in the system to heat or cool the process streams [78].

In heat- or mass-exchange systems, there exists a critical point, known as the pinch or pinch point, where the driving force for energy or mass exchange is at its minimum. The successful design of these systems hinges on identifying the location of the pinch point and utilizing the information it provides to optimize the entire network. The first step typically determines the minimum temperature, representing the smallest temperature difference between streams entering or leaving the system. Typically, the minimum temperature value is between 5°C – 20°C. This step is followed by constructing a temperature interval to determine the hot and cold streams. These steps help to define the minimum number of heat exchangers needed to utilize the energy available in the system. However, the detailed calculations of the pinch point approach are only required if the heat integration will be performed through manual calculations. However, in this thesis, the implementation of heat integration within the production processes was carried out through the utilization of Aspen Energy Analyzer v12, a software developed by Aspen Technology [79]. The software is part of the Aspen Plus package, which enables the creation of flowcharts for modeling process flows and allocating utilities. The software performs the analysis automatically, and the output consists of composite curves to show the heating and cooling demands, as well as the mass flows of the external utilities (if needed). This information is essential, especially during the techno-economic evaluation, as utilities are one of the main contributors to the operating cost of most industrial processes. Performing heat integration is a common procedure in process design since it can provide several benefits, including:

- Reduction of energy consumption and costs by recovering heat
- Reducing greenhouse gas emissions as it decreases the resources needed for heating or cooling

- Improving product quality by providing more precise and consistent temperature control

4.4 Flowsheet optimization

In a complex process where multiple units of operation and recycle streams are needed, optimization becomes important to specify the optimum operating conditions that minimize or maximize a specific objective. In this thesis, sensitivity analysis in Aspen Plus was done to optimize the operating conditions. The sensitivity analysis is done by systematically varying key operational variables such as temperature, pressure, etc., and assessing their impact on performance metrics such as product composition or yield. Exploring the system's sensitivity to these variables helps pinpoint which operating conditions lead to the best results. This data-driven approach enhances process efficiency and minimizes resource consumption and production costs, making it an indispensable tool for more sustainable and economically viable industrial operations.

4.5 Monte Carlo simulation for biomass characteristics

Uncertainty analysis aims to quantify the variability of outputs due to the uncertainty of inputs. Therefore, the uncertainty in SAF product quality caused by the variation of biomass characteristics has to be analyzed. The experimental data of biomass characteristics and their uncertainties presented in Chapter 2 provided the input variables for the models. A Monte Carlo simulation was used to quantify the uncertainty of SAF production where the different input variables of biomass characteristics were changed randomly (within specified ranges) and simultaneously. After performing sensitivity analysis in the Aspen model, three parameters, namely carbon, hydrogen, and moisture content, were considered for the uncertainty assessment since those parameters are the most influential in producing hydrocarbons. Four steps were followed to perform the Monte Carlo simulation, as shown below:

1- Biomass characteristics were measured experimentally, and their uncertainties were determined, as discussed in Chapter 2.
2- Using the determined uncertainties and based on their distributions (Normal or rectangular), 1.000 random values covering the whole uncertainty range were generated using a Python code, see Appendix B.
3- The Aspen model was coupled with Python to run the model 1.000 times using the randomly generated values, see Appendix B.

4- The output data was recorded, and the uncertainty was calculated according to a normal distribution K=2, which represents 2 times the standard deviation value, corresponding to 95% coverage.

4.6 Techno-economic analysis

Techno-economic analysis (TEA) of a chemical process is the assessment of the financial viability of the process. The analysis involves estimating the revenue, operating costs (OPEX), and capital costs (CAPEX) associated with the process and then determining whether the process is profitable or not [80]. Moreover, the TEA helps to provide suggestions for process optimization where a significant cost reduction might be needed [81].

4.6.1 Net production cost

The net production cost (NPC) can be defined as the ratio between the total annualized production costs and the annual product output. To calculate the NPC, the total capital investment (TCI /CAPEX) and operational cost (OPEX) are required. The mass and energy flows through the system obtained from the Aspen simulation will help determine the yield and utility requirements. This information is then used to compute the CAPEX and OPEX. Part of the CAPEX is the equipment cost. The equipment costs (EC) for the major unit of operation like the FT, methanol reactor., etc., were calculated using the following formula:

$$EC = \mathrm{EC}_{ref}.\left(\frac{\mathrm{S}}{S_{ref}}\right)^{D}.\left(\frac{CEPCI_{Project\ year}}{CEPCI_{ref}}\right) \qquad 4.1$$

Where EC_{ref} represents the same purchased cost expressed of the reference year, S indicates the actual size of the equipment, S_{ref} is the reference capacity of the equipment, and D is a scaling factor. $CEPCI$ is the chemical engineering plant cost index. CEPCI value for this study was considered for June 2023. In other words, this value reflects the increase in cost due to inflation compared to the reference cost, which is given to a specific year, depending on the equipment. CEPCI is published monthly by Chemical Engineering magazine and is widely used in the chemical industries. Some of the secondary equipment, such as heat exchangers and flash drums, were directly taken from the process simulation using Aspen Process Economic Analyzer v12 [82]. These calculated equipment costs are only part of the TCI. Albrecht *et al*. have provided a description of how to calculate the overall total capital investment (TCI) and the total operating cost (TOC) as follows [83]:

Total Capital Investment (TCI) = Fixed Capital Investment (FCI) + Working Capital (WC) 4.2

The fixed capital investment (FCI) can be divided into two categories: direct fixed cost and indirect fixed cost. The direct cost typically contains the equipment cost, installation, piping, and other capital requirements needed during the construction phase. The indirect capital cost is associated with other administrative costs like legal expenses, contract fees, etc [83]. The working capital represents the funds necessary to support the ongoing operational needs for the implementation of the project. The working capital (WC) was assumed to be 10% of the total capital investment (TCI). Since TCI represents the total capital cost across the plant's lifetime, this value needs to be annualized to calculate the yearly contribution of CAPEX to the product cost.

$$ACC = \text{FCI}.\left(\frac{i * (1+i)^t}{(1+i)^t - 1} + \frac{1}{9}\right) \quad 4.3$$

Where ACC represents the annualized capital cost, i is the interest rate, and t is the plant's economic life. The second term of the equation represents the WC.

In addition, the total operating cost (TOC) represents the ongoing yearly operational cost that sustains the operation of the plant. The TOC will be estimated based on 2023 prices. After determining the TOC and ACC, the annualized capital cost can be calculated according to equation 4.4.

The plant's total annualized cost (TAC) is calculated by summing up the TOC and the ACC.

$$TAC = TOC + ACC \quad 4.4$$

The NPC was calculated by dividing the TAC by the annual production of fuels (AP), as shown in Equation 4.5.

$$NPC = \frac{TAC}{AP} \quad 4.5$$

The NPC is commonly expressed in Dollars ($) per mass fuel (tonne).

4.6.2 Cost uncertainty analysis

Sensitivity analyses were carried out for OPEX and CAPEX, in which the value of each contributing element was changed separately to determine the variables that have the highest impact on the cost of SAF. Several parameters were chosen based on the sensitivity analysis. As proposed by Sinnott et al., a normal distribution with a standard deviation of 20% for the initial values of each variable was assumed [81]. Ten thousand random values were generated using Python code for these selected variables. The random values cover the whole range of uncertainty for each parameter. The Monte Carlo simulation was used to estimate the overall probability distribution in the cost of SAF. This method was selected for its ability to factor in a range of values for various inputs and the ease of interpretation of the results obtained [84].

Moreover, the biomass influence on SAF yield was explained in section 4.5. This uncertainty in yield was translated into cost by varying the cost model between the minimum and maximum SAF production to estimate the NPC value. The overall uncertainty cost represents the sum of the uncertainty caused by the feedstock characteristics plus the uncertainty caused by OPEX.

4.7 Efficiency and Performance Evaluation

The performance of the processes was evaluated based on several criteria, such as plant efficiency, SAF yield, SAF fraction, carbon conversion, and energetic jet fuel efficiency. The plant efficiency represents the conversion efficiency from biomass and utilities to SAF. It is calculated by dividing the energy content of SAF by all energy inputs into the system. When other by-products are considered, such as electricity or heat, it is called the overall plant efficiency. However, these formulas can be adapted to fit the process. The assessment focused on SAF due to comparable methodologies used in existing literature, facilitating comparisons between this data and previous studies. The carbon conversion rate determines the proportion of carbon atoms entering the system from biomass that ultimately ends up in the liquid fuel product. It serves as a critical indicator for assessing the maximum fuel yield attainable from a given biomass source. Energetic jet fuel efficiency (EJFE) measures the thermal efficiency of the produced jet fuel divided by the total heat input into the system. A summary of the equations used is shown in table 4.1 [85].

Table 4.1. *Definition of process performance parameters based on jet fuel [85].*

SAF yield	$\boldsymbol{Y_{SAF}} = \frac{\dot{m}_{\boldsymbol{SAF}}}{\dot{m}_{\boldsymbol{Biomass}}}$
SAF fraction	$f_{SAF} = \frac{\dot{m}_{SAF}}{\dot{m}_{Products}}$
Carbon conversion	$\eta_C = \frac{\dot{n}_{Carbon\ in\ product}}{\dot{n}_{Carbon\ in\ biomass}}$
Plant efficiency	$\eta_{tot} = \frac{\Sigma\, \dot{m}_{SAF} * LHV_{SAF}}{\dot{m}_{Biomass} * LHV_{Biomass} + P_{ext} + Q_{ext}}$
EJFE	$EJFE = \frac{\dot{m}_{SAF} * LHV_{SAF}}{\dot{m}_{Biomass} * LHV_{Biomass} + Q_{ext}}$
Conversion efficiency of products	$\eta_{tot-fuel} = \frac{\Sigma\, \dot{m}_i * LHV_i}{\dot{m}_{Biomass} * LHV_{Biomass}}$

Where $\dot{m}$ and $\dot{n}$ are the mass and molar flow rate, respectively, *LHV* is the low heating value. Meanwhile, P_{ext} and Q_{ext} are the external electricity and heat used in the system. These equations are fixed and utilized in chapters 5 and 6 to evaluate the performance of the processes.

4.8 Conclusions

The chapter has summarized the tools and software that will be combined to fulfill the objectives of this thesis. Aspen Plus was the basis to perform the process simulation and modify the configurations to maximize the production of SAF. Moreover, the methodology of coupling Aspen with Python was explained to perform the Monte Carlo simulation. The Monte Carlo simulation will be the basis for studying the influence of biomass characteristics on SAF production and its net production cost, as will be discussed in chapters 5 and 6.

Nomenclature

TEA	Techno-economic analysis
FT	Fischer Tropsch
MTJ	Methanol to Jet
NPC	Net production cost
EC	Equipment cost
CEPCI	Chemical engineering plant cost index
FCI	Fixed capital investment
TCI	Total capital investment
WC	Working capital
ACC	Annualized capital cost
TAC	Total annual cost
HI	Heat integration
Y_{SAF}	SAF yield
$\int_{SAF}$	SAF fraction
EJFE	Energetic jet fuel efficiency
η_{c}	Carbon conversion
η_{tot}	Plant efficiency
$\eta_{tot\text{-}fuel}$	Conversion efficiency of products
LHV	Lower heating value
BTL	Biomass to liquid
PBTL	Biomass power to liquid

CHAPTER 5

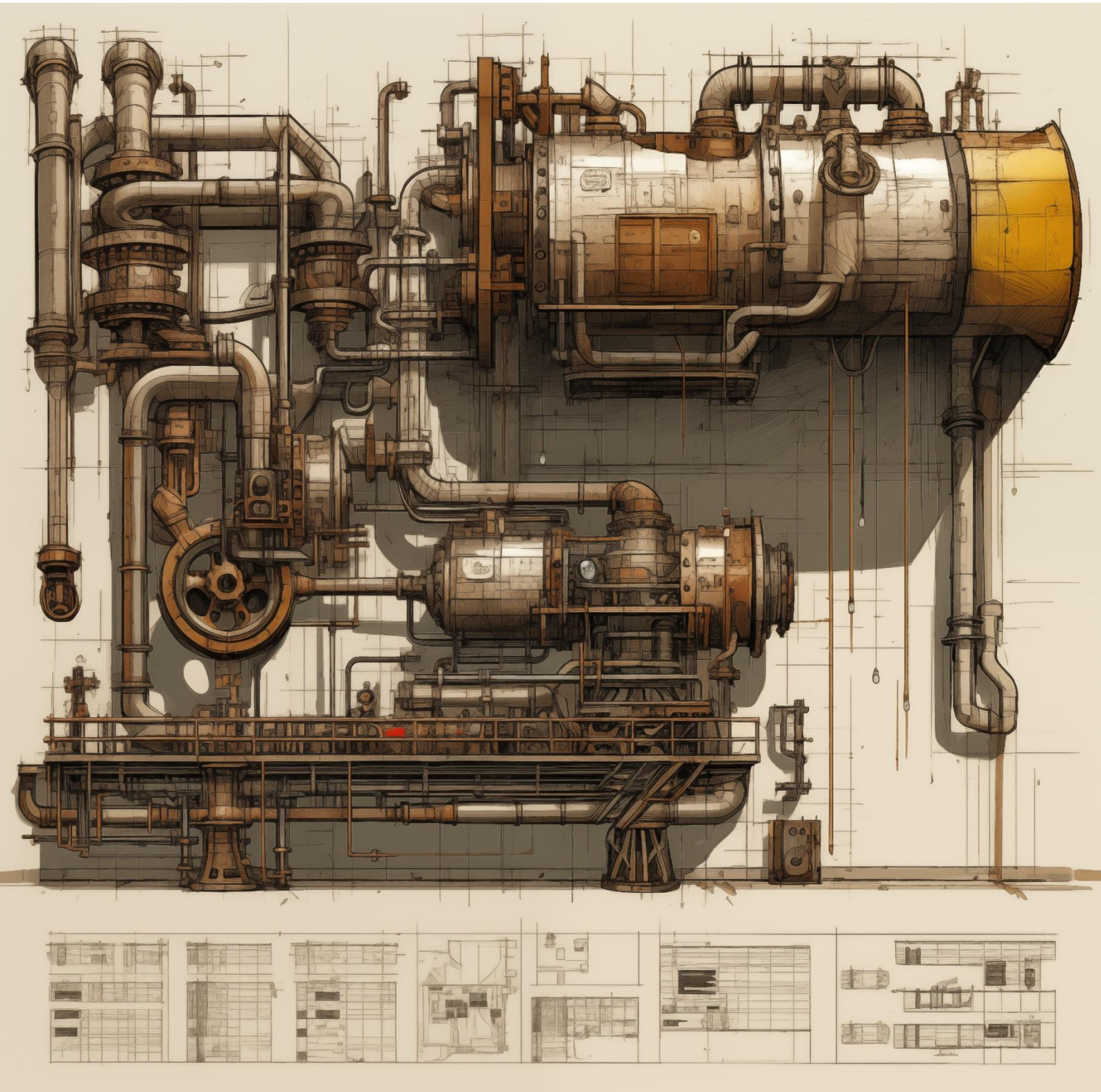

Chapter 5. Biomass to SAF – Fischer Tropsch Pathway

5.1 Overview

Two configurations of biomass gasification coupled with the Fischer Tropsch process were simulated in Aspen Plus. The influence of the biomass characteristics and their uncertainties on the yield of SAF was analyzed using Monte Carlo simulation, following the methodology explained in section 4.5. Moreover, the results obtained from the process simulation and the Monte Carlo were utilized to perform the techno-economic analysis (TEA) to determine which process configuration is more economically viable.

Based on:

Shehab, M., Ordóñez, D. F., Bui, M., Moshammer, K., & Zondervan, E. (2023). The influence of biomass characteristics and their uncertainties on the production of sustainable aviation fuel. In 33rd European Symposium on Computer Aided Process Engineering (Vol. 52, pp. 2089-2094). (Computer Aided Chemical Engineering; Vol. 52). Elsevier. https://doi.org/10.1016/B978-0-443-15274-0.50332-2

Shehab, M.; Moshammer, K; Zondervan, E. Techno-economic analysis of the production of sustainable aviation fuel from biomass via Fischer Tropsch and Methanol pathways (*Ongoing manuscript*)

5.2 Introduction

As previously proven in Chapter 4, biomass has the potential to fulfill the SAF mandates in the short and medium range. However, there is an evident lack of information when it comes to evaluating the overall technical and economic viability of adopting biomass to SAF on a large commercial scale through the Fischer Tropsch process coupled with gasification. Therefore, such evaluation is needed to validate the realistic potential of biomass utilization for SAF production. Unit selection is a crucial element in the process design of biomass to SAF process. Two significant aspects are decisive in shaping the output of the process: syngas production and purification and the upgrading section.

5.2.1 Syngas production and purification

Gasification technology is the central unit of operation responsible for producing the syngas. Properly selecting this equipment plays a pivotal role in ensuring the highest yield of SAF is achieved. Gasification refers to the thermal decomposition of biomass particles within a closed reactor, known as a gasifier. The process typically occurs at elevated temperatures of 600-1000 °C. This process results in the formation of syngas, which is a mixture of CO and H_2, along with other compounds such as CO_2, CH_4, and H_2O. The syngas produced during gasification can be purified and used to synthesize special chemical products or generate heat and electricity. Gasification occurs in the presence of an external oxidizing agent, such as air, O_2, or steam.

The equivalent ratio (ER) is a crucial parameter, with ER < 1 indicating that the stoichiometric amount of the oxidizing agent is insufficient, as gasification is an intermediate step between pyrolysis and combustion. A stoichiometric amount refers to the theoretical quantity of air or any other oxidizing agent needed for the complete combustion of the fuel. Gasification possesses a distinctive quality as a technology capable of transforming various types of waste, ranging from municipal solid waste (MSW) to agricultural or crop residues, into a valuable and high-quality energy source. The gasifier can be classified into different categories, whether on how the heat is supplied or the type of the gasifier reactor and flow direction. The heat is provided to the gasifier, either as autothermal (direct) or allothermal (indirect) [86]. In autothermal gasification, the essential heat is directly generated through partial oxidation within the gasifier using air or oxygen.

Conversely, in the case of allothermal, heat is derived from the combustion of a fraction of the feedstock, char, or clean syngas in a separate reactor [87]. This heat is then transferred through exchangers utilizing preheated bed material. It is worth mentioning that when using air as an

oxidant agent, the syngas produced would have a low heating value due to the nitrogen dilution. In comparison, oxygen produces medium to high-quality syngas with a higher heating value and a low tar content. On the other hand, comparing the gasifiers based on the reactor type is another common approach. Figure 5.1 shows the different types of reactors and their application.

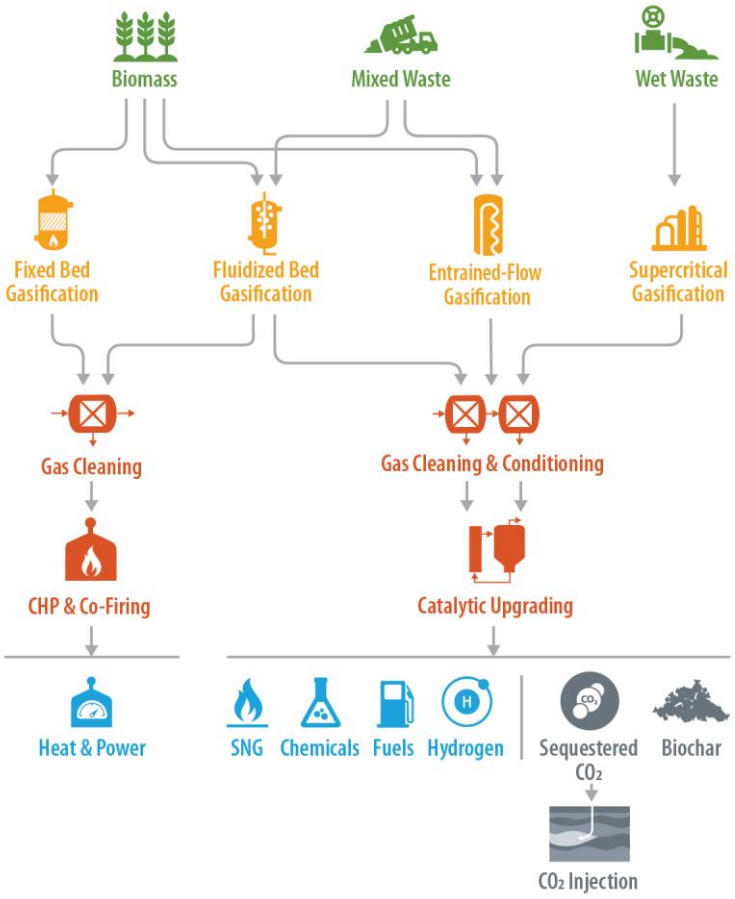

Figure 5.1. *Flow diagram of different gasification technologies [88].*

The fluidized bed is one of the most common gasifier types used on a large commercial scale [89]. The gasifier contains a sand-like bed material that is fluidized (the gas stream lifts the bed material and gets a liquid appearance). Fluidized-bed gasifiers generally operate at temperatures of 800–950°C [90]. On the other hand, Entrained flow gasification is getting a lot of attention as it can produce very high-quality syngas with negligible tar formation compared to the fluidized bed. Firstly, the short residence time required for effective gasification necessitates finely grinding the feedstock, which can be challenging for fibrous biomass materials. Secondly, the high alkali content of molten biomass ash can cause corrosion of the gasifier's refractory lining, significantly reducing its service life [91].

After gasification, syngas cleaning is followed to remove any impurities, as this is an essential step before converting it into higher hydrocarbons by Fischer-Tropsch or methanol synthesis processes. Syngas is primarily composed of CO and H_2 and often contains impurities like sulfur compounds, particulate matter, and various contaminants that can poison catalysts and reduce the efficiency in the upgrading section. A comprehensive cleaning process is employed to obtain syngas suitable for the Fischer Tropsch process or any other upgrading pathway. This process typically involves removing sulfur compounds through desulfurization techniques. Acid gas removal technologies such as Selexol and Rectisol are widely used due to their suitability to capture H_2S with high efficiency along with capturing CO_2 as a side stream. Particulate matter like ash can be removed through filtration or cyclones.

On the other hand, tar is formed during biomass gasification, which typically contains a complex mixture of organic compounds. Tar removal is necessary for syngas quality because tar can have several detrimental effects, such as clogging the pipelines and damaging the downstream equipment, making syngas production less efficient. Several technologies can be used for tar removal. However, selecting the suitable technology depends on the type of gasifier, feedstock, and tar concentration in the syngas. Thermal cracking is a common approach where the syngas is passed over a high-temperature catalyst to break down the tar into small gaseous molecules. However, other technologies, such as wet scrubbing or filtration, are also used.
In wet scrubbing, the syngas is passed over a liquid solvent such as water or oil. Rapeseed methyl ester (RME) is typically used for wet scrubbing, where the oil is regenerated and reused. Unlike thermal cracking, the wet process does not require extensive cost and still achieves a high tar removal efficiency.

The last step in preparing the syngas for upgrading in the FT reactor is to ensure that the ratio of H_2:CO of 2:1 is achieved. This is achieved using a water gas shift reactor or an external hydrogen source. WGS reactors can be classified into several categories based on the operating conditions and the type of catalyst utilized. Based on their operating conditions, it can be either a high-temperature shift (HTS) or a low-temperature shift (LTS).

The HTS is typically operated at temperatures of 350-450°C, while the LTS is operated at temperatures of 180-250°C [92,93]. Selecting which type of WGS depends on the application. In the case of producing higher hydrocarbons through the FT reactor, the WGS aims to increase the amount of H_2 production to a reasonable level without significantly losing all the CO. Therefore, a LTS can be utilized. Another way to classify the WGS process is based on the

catalyst type, which can be either a clean shift or sour shift catalyst [93]. Sulfur compounds in the syngas are poisonous to some WGS catalysts and can cause catalyst deactivation [94]. Iron and Copper are considered clean shift catalysts, while cobalt-based catalysts are classified as sour shift catalysts. The composition of sulfur and the process configuration and operating parameters play an important role in selecting the catalyst suitable for the process.

5.2.2 Upgrading section

Fischer-Tropsch synthesis is a chemical process that aims to convert syngas (CO and H_2) into a petroleum-like product in the presence of a catalyst, depending on the length of the hydrocarbon chain targeted. The produced liquid is typically named FT crude. The FT crude can be upgraded into a wide range of transportation-grade liquid hydrocarbons. FT process is flexible and not dependent on which feedstock was used to produce the syngas. The FT process is a form of polymerization where the hydrocarbon formation is governed by the Anderson-Schulz-Flory (ASF) distribution. ASF distribution is a probability distribution that describes the chain length distribution of products in the FT process. The ASF distribution is characterized by a single parameter, α, which is the chain growth probability. The chain growth probability is the probability that a monomer will add to a growing chain during each step of the FT reaction. A higher chain growth probability leads to a higher proportion of longer-chain products. The ASF distribution is shown in equation 5.1 [80].

$$w_n = (1-\alpha)^n \alpha^{n-1} \tag{5.1}$$

Where *n* refers to the carbon number/atom, w_n is the weight fraction of carbon number. The ASF is typically used to predict the product distribution of the FT process and to optimize the production of specific products. The value of α depends on the catalyst and the application. Iron (Fe) and cobalt (Co) are the preferable catalysts for the Fischer-Tropsch process when the focus is on the production of longer-chain hydrocarbons [95]. However, other catalysts could be coupled with FT, such as nickel (NI) and ruthenium (RU), which have high CO hydrogenation. However, Nickel has high selectivity towards methane, making it unsuitable, while RU is highly expensive compared to Fe and Co catalysts [96]. Like the WGS reactor, the FT reactor can be classified based on the operating conditions, as shown in table 5.1.

Table 5.1. *Comparison between the FT setups [97,98].*

Setup	Temperature	Pressure	Reactor type	Product
Low temperature Fischer Tropsch (LTFT)	180 - 250	20-40	Fluidized bed/ Circulating - catalyst	Diesel, gasoline, and wax production.
High temperature Fischer Tropsch (HTFT)	300 – 375	30-60	Fixed bed (generally)	Short-chain linear alkenes

Table 5.1 shows that the LTFT is more suitable for SAF production since long-chain alkanes are produced in this process. Moreover, the LTFT process requires less temperature and pressure, making it less energy-intensive than the HTFT. As wax (> C20+) is produced in this process, a hydrocracker is needed to convert it back into the SAF range of C8 to C18.

Hydrocracking (HC) is a catalytic process that breaks down long hydrocarbon chains into shorter, more valuable compounds by adding hydrogen at high pressure [99]. This rearrangement process is commonly used in petroleum refining to convert heavy hydrocarbons into gasoline and middle distillates. Currently, most available middle distillate in the market is derived from crude oil hydrocracking [100]. However, HC also plays a significant role in FT wax processing [101]. Table 5.2 provides an overview of the operating conditions, the technology employed, and conversion rates for various HC processes.

Table 5.2 *Different types of HC and their conditions [102,103].*

	Conventional HC	**Mild HC**	**FT waxes HC**
Pressure (MPa)	10- 20	5-8	3-7
Temperature (°C)	350-430	380-440	324-372
H2/feedstock (m3/m3)	800-2000	400-800	500-1800
Reactor technology	Trickle bed	Trickle bed	Trickle bed
Conversion (%)	70-100	20-40	20-100

After the LTFT process, the wax hydrocracking aims to maximize the middle distillate yield. On the other hand, bifunctional metal/acid catalysts, such as NiMo and NiW catalysts, are widely associated with hydrocracking. As FT wax is sulfur-free, Lee et al. proposed using Pd and Pt-loaded catalysts for their excellent overall efficiency. This efficiency is attributed to their high hydrogenation/dehydrogenation activity in the cracking of heavy hydrocarbons [104].

5.3 Methodology

The methodology combines different tools, as previously described in Chapter 4. Process simulation is followed by Monte Carlo simulation and a techno-economic assessment. The FT pathway was evaluated based on two different configurations. Firstly, as a conventional Biomass-to-Liquid (BTL) process as commonly available in the literature, and secondly, as a combination of Power & Biomass-to-Liquid (PBTL). Process simulation was used to determine fuel production's mass and energy flows to assess their yield, efficiency, and economic performance.

5.4 Model description - Biomass to clean syngas

Two flowsheets were developed in Aspen Plus to reflect the configuration of BTL and PBTL. The main difference between those two configurations is how the necessary H_2/CO 2:1 ratio can be reached. This is a crucial criterion for the upgrading process in the FT reactor. However, this section of the process will highlight biomass conversion to clean syngas, which is an initial step before the upgrading process, as shown in figure 5.2.

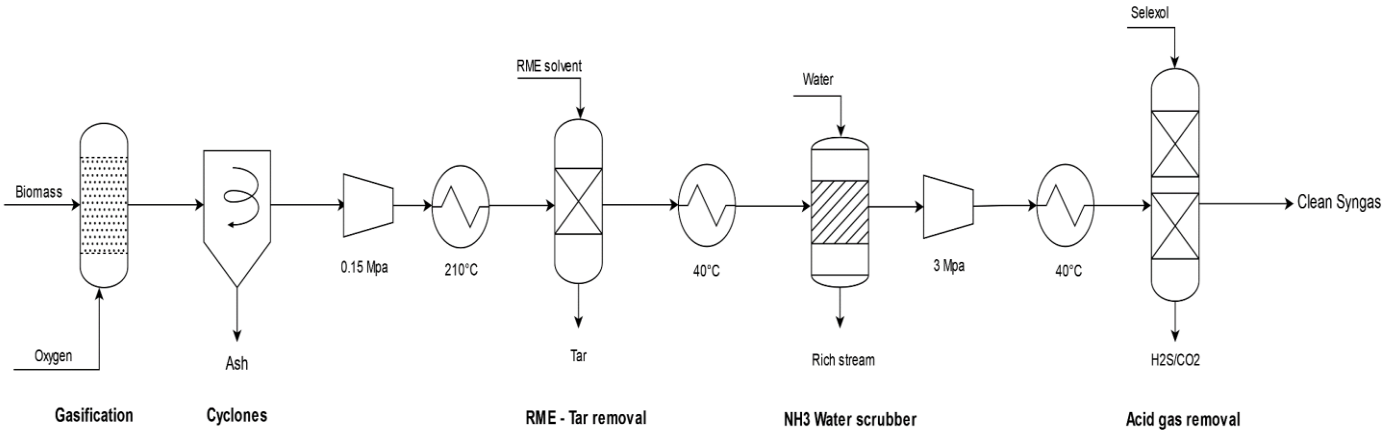

***Figure 5.2**. Flow diagram of biomass gasification and syngas cleaning*

In this model, the biomass is assumed to have gone through pre-treatment, which typically involves drying and cutting the biomass into suitable sizes (3-6 mm) to be fed into a fluidized bed gasifier [105]. However, the particle size can vary depending on the type of reactor chosen. The produced syngas contains mainly CO, CO_2, CH_4, H_2, ash, tar, and other impurities, depending on the type of biomass used and the operating conditions. The gasifier used in this process was adapted from an existing pilot plant at Aston University in the UK [106]. The gasifier temperature is set to operate at 845 °C, which is suitable for producing high-quality

syngas without excessively increasing the energy input, which could unnecessarily raise the cost of the gasifier [90].

Moreover, as the model was based on an equilibrium approach where Yield and Gibbs free energy reactors were utilized to simulate the gasification process, a temperature above 800 °C was required [106,107]. that is because below 800 °C, only a kinetic model would be capable of reflecting the gasification reactions [108]. Therefore, the higher the gasifier temperature, the more acceptable it is to use an equilibrium model [107]. Moreover, higher temperatures guarantee the reduction of tar formation. On the contrary, exceeding 900 would risk the potential of having a reverse water gas shift reaction, which influences the yield of syngas. Therefore, based on this information, a temperature of 845 °C was deemed suitable. It is worth mentioning that the optimum temperature changes depend on the type of gasifier, feedstock, and gasifying medium.

Oxygen was selected as the gasifying medium. The oxygen is assumed to have been obtained from an air separation unit (ASU). The oxygen equivalent ratio (ER) was set to be 0.21, corresponding to 81 tonnes per hour (t/h). The equivalent ratio represents the amount of oxygen fed to the gasifier relative to the stochiometric quantity required to obtain complete biomass combustion. Therefore, optimizing the gasifier ER is crucial to maximize the CO and H_2 while lowering the concentration of carbon dioxide and unwanted impurities. An effective gasification process will operate in an ER of 0.2 to 0.4 [109,110]. Any value less than 0.2 would lead to a noticeably dominant pyrolysis reaction and the formation of more CH_4 and tar. In contrast, for ER more than 0.4, more oxygen is supplied for the combustion reaction, increasing the CO_2 and H_2O produced [111,112]. It is assumed that there is no need for steam as a thermal moderator [106]. This part of the process is unified across all configurations, as producing clean syngas is essential before feeding the gas to the upgrading section.

The produced syngas goes through cyclones to remove the ashes. The ash-free syngas still contains tar, H_2S, and NH_3, which were formed during the process. It is essential to remove those compounds before feeding the syngas to the next upgrading steps, as these elements can be poisonous to the catalysts present in the water gas shift reactor and the FT reactor. Wet scrubbing was used to remove tar using rapeseed methyl ester (RME) as solvent. Water scrubbing is assumed to remove the NH_3, while for H_2S, an acid gas removal unit (Selexol) was considered [113]. However, to ease the simulation in the syngas cleaning part, these units were simplified and replaced with separators while assuming a slight loss in syngas due to the

separation processes [114,115]. This configuration can be rearranged in case of using different types of feedstocks containing different compositions or rearranging to adapt to the upgrading section. For example, sulfur should be removed before the WGS and FT reactors.

However, due to the WGS reaction, a significant quantity of CO_2 is produced. Therefore, a carbon capture unit will be typically needed. However, for economic reasons, it would be more advantageous to utilize a WGS catalyst that is sulfur tolerant, followed by integrating an acid gas removal after the WGS, where it will be capable of capturing both H_2S and CO_2 [116,117]. It is estimated that up to 90% of CO_2 can be captured with such a setup [113]. Therefore, it helps to avoid the extra need to add a dedicated carbon capture unit after the WGS reactor. The clean syngas produced after gasification typically have an H_2/CO ratio of 0.77 – 0.9, depending on the type of sample used, whether wood pellets or wood chips. This ratio of H_2/CO is not suitable for FT or methanol synthesis; therefore, a WGS is integrated to convert more carbon monoxide into carbon dioxide and hydrogen using super-heated steam supplied at a temperature and pressure of 440 °C and 4.4 MPa, respectively. When combined with Fischer Tropsch, this process is typically called conventional BTL, as shown in figure 5.3.

The WGS reactor is modeled as an equilibrium reactor in the Aspen Plus, which operates at 220 °C and 1.5 MPa [118]. Utilizing an equilibrium reactor (REquil) is recommended in the literature [106]. However, the reactor is controlled by the input of steam; therefore, in the design specs in Aspen Plus, the steam flow rate is varied to reach an H_2/CO ratio of 2:1. These design specs were fixed across all samples and simulation cases along with the operating conditions of the gasifier and the WGS reactor temperatures to assure a fair comparison between different cases.

A ZNO bed (Zinc oxide) is added to remove the traces of sulfur down to 0.01 ppmv before entering the FT or the methanol reactor [119]. In the case of PBTL, as shown in figure 5.4, an external hydrogen source is introduced with the syngas to raise the H_2/CO to 2:1 instead of utilizing WGS. This process is significantly advantageous as there is no loss in carbon, and it does not sacrifice it to produce hydrogen. Instead, the external hydrogen source fulfills the required ratio. Moreover, since there is no WGS reactor, there is a significant reduction in the production of CO_2. Therefore, in the PBTL case, the acid gas removal unit will come after NH_3 removal, as shown previously in figure 5.2.

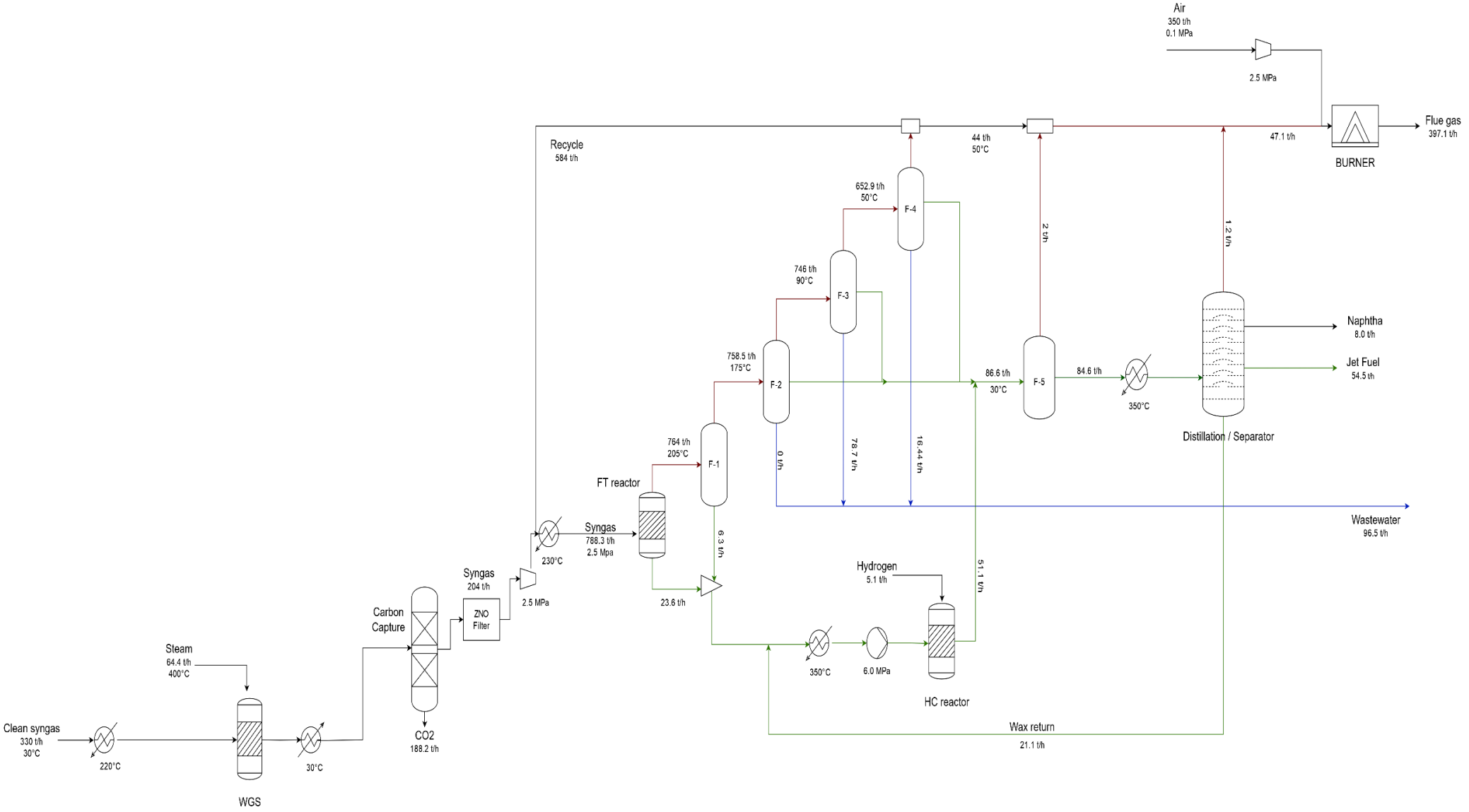

***Figure 5.3**. Flow diagram of biomass to liquid (BTL) – WP feedstock*

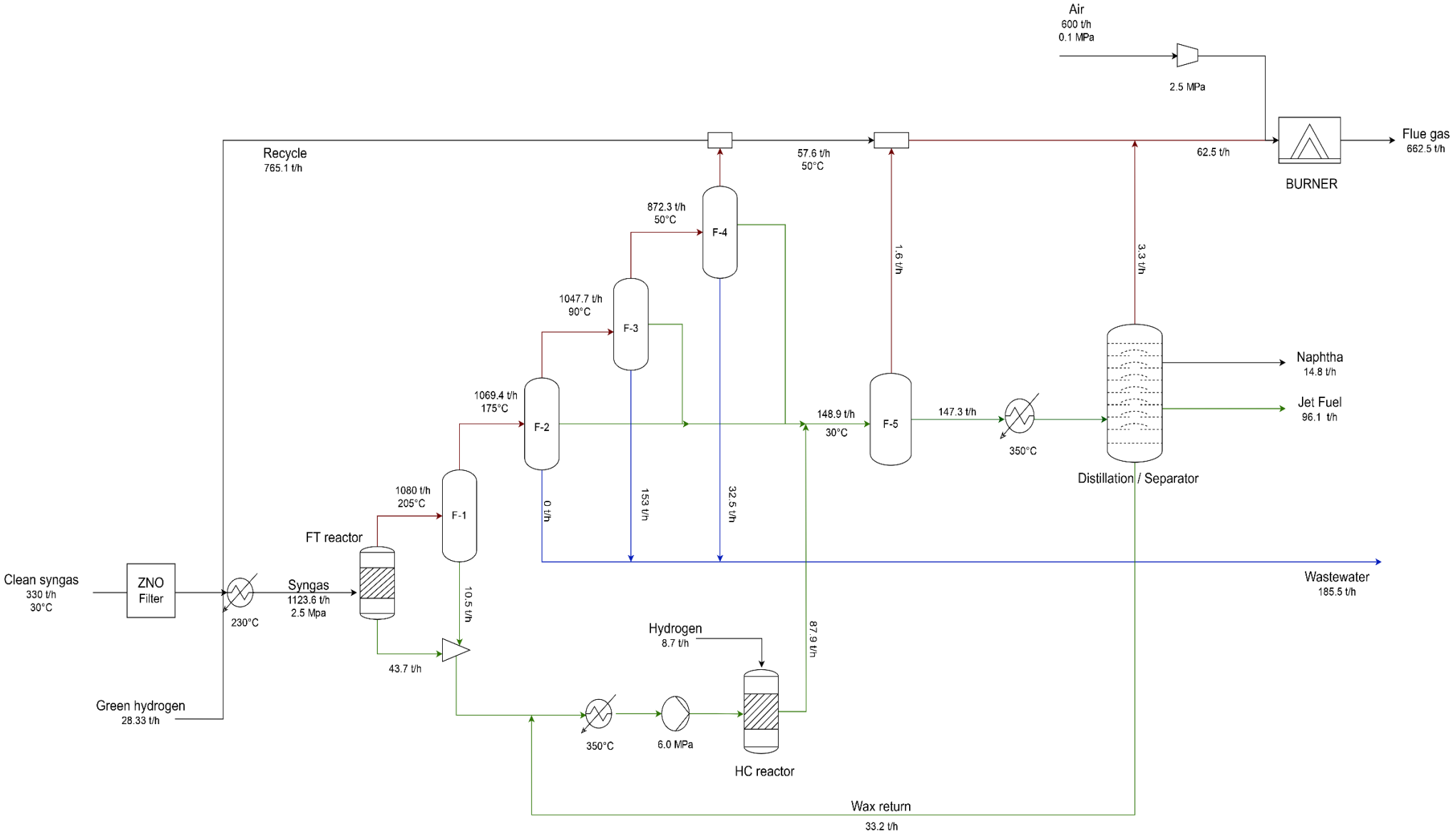

***Figure 5.4**. Flow diagram of Power Biomass to liquid (PBTL) – WP feedstock*

5.5 Model description - Upgrading

5.5.1 Fischer Tropsch

Syngas with an H_2/CO ratio of 2:1 is suitable to be fed to the FT reactor. The product distribution of the FT reactions follows the Anderson-Schulz-Flory (ASF) distribution, as previously given in Eq. (5.1). [120]. The cobalt-based catalyst is typically suitable for producing long-chain hydrocarbons with α of 0.95 [121]. The catalyst is assumed to have a 40% CO per pass molar conversion. It means only 40% of the CO in the syngas will react with H_2 to be converted to higher hydrocarbons. This percentage will not make the process economically feasible; therefore, a closed-loop design was implemented where a recycle stream is sent back to the FT reactor to increase the overall CO conversion in the process. This recycle stream leads to the increase of FT crude. However, to avoid build-up in the system, a purge stream of around 5% was introduced [122]. This stream was used for combustion to generate heat for the system.

It is worth mentioning that this particular part of the process was modeled by adapting parts of the process explained by Diego [80]. The FT reactor was set to operate at 230 °C and 2.5 MPa [118]. The higher the temperature, the more light gases are produced, which is not recommended in the case of targeting the production of long-chain hydrocarbons like SAF. On the other hand, very low temperature in the FT process leads to slow reactions. Therefore, selecting 230 °C as the temperature helps to balance the production of long-chain hydrocarbons while ensuring that the reactions are fast due to the higher temperatures.

5.5.2 Wax hydrocracking (HC)

A platinum-based catalyst was selected due to its suitability for dealing with FT wax [123,124]. For simplification, the hydrocracker model was based on the yield distribution, which mainly aims to break down parts of C_{19} to C_{30} into smaller chain hydrocarbons in the presence of hydrogen. The final yield obtained after hydrocracking contains C_1-C_4, C_5-C_{10}, and C_{11}-C_{20}, as 3%, 13%, and 69% mass weight, respectively [80].

5.5.3 Product separation

As previously shown in figures 5.3 and 5.4, flash separators were coupled with the FT reactor to separate the waxes and liquid hydrocarbons from the light gases. The liquid hydrocarbons are collected and distilled to obtain different hydrocarbons, including Naphtha, SAF, and Diesel. Since the main purpose of the upgrading section is to maximize the production of SAF, the diesel fraction was sent back to the HC to produce more SAF.

5.6 Model optimization and validation

Several factors in the process require optimization and validation, starting from the gasification output, where essential parameters such as the cold gas efficiency, syngas heating value, and H_2/CO ratio have to correspond to what would be typically expected from a gasification process. The cold gas efficiency is defined as the ratio between the energy present in the syngas and the energy content of the biomass. The cold gas efficiency was in the range of 60.6% to 65% across the different samples. This is consistent with the typical range in the literature [125]. The results of syngas heating value and H_2/CO obtained in this study compared with the literature are shown in table 5.3.

Table 5.3. *Results of the gasification process.*

Source	H_2/CO	Higher heating value (HHV) of syngas- MJ/M_3
This thesis	0.77 – 0.9	10.8-9.84
Venugopal et al., [126]	0.71	9.85
Couto et al., [127]	0.67	10.4
NNFCC project [128]	0.93	----

It can be seen from Table 5.3 that the results lie within the range of the literature. However, it is essential to highlight that the output from the gasifier changes depending on which gasifying medium, reactor, feedstock, or operating conditions are utilized. Therefore, any variation in these inputs would consequently change the syngas' composition and the gasifier's performance. Consequently, these changes would influence the downstream processes; for more information, see Appendix B.

On the other hand, catalyst selection in the FT reactor is another vital aspect that controls the production of liquid hydrocarbons. A cobalt catalyst with α of 0.95 and 40% per pass CO conversion was selected as proposed by Diego [95]. This is because for the low-temperature FT process (180–250 °C), cobalt-based catalysts are known to produce predominantly unbranched alkanes (C_nH_{2n+2}). However, the methane selectivity observed in experiments is consistently higher than predicted by the ASF distribution. To address this discrepancy, the approach proposed by König et al., which introduces a correction factor for methane was followed [80]. This yield factor for the methane yield was w_{CH4}= 0.04 for an α value of 0.95. This yield factor was obtained experimentally for FT product distributions. To ensure the catalyst is indeed

suitable for SAF production, the fractional conversions were manually calculated and evaluated, as shown in figure 5.5 [95].

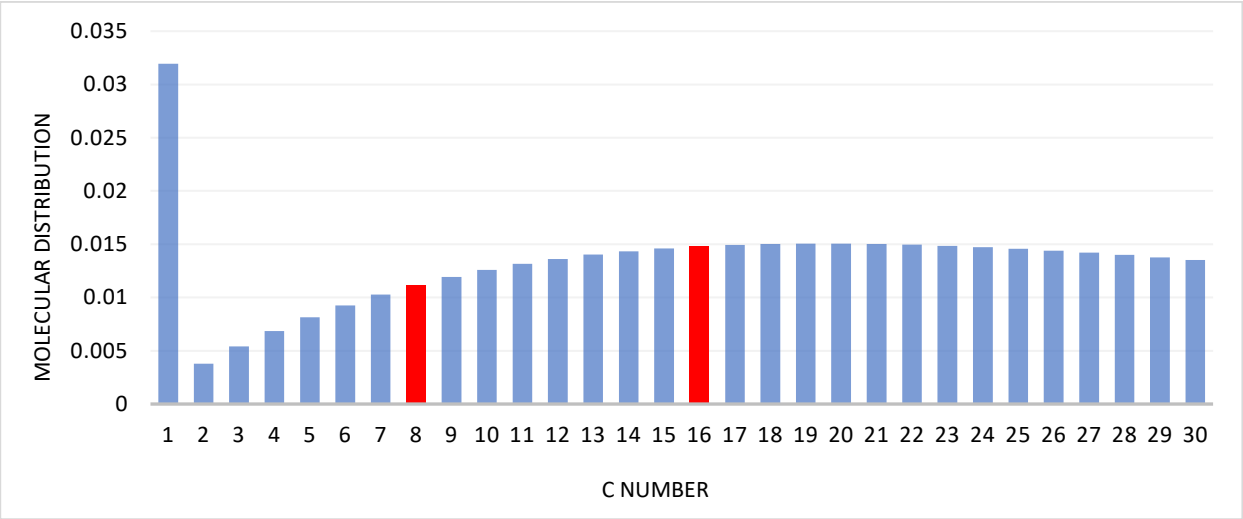

***Figure 5.5**. Cobalt catalyst with Alpha of 0.95 and 40% CO per pass molar conversion*

It can be seen that the SAF fraction in the range of C_8 to C_{18} is present when utilizing a cobalt catalyst. Those validations were necessary before analyzing the results and economically evaluating the processes. Heat integration is essential to optimize the production process by analyzing the potential energy savings due to HI. The HI was performed using Aspen Energy Analyzer v12. An approach temperature of 10 °C was selected. The approach temperature refers to the minimum temperature difference between the hot and cold streams coming out of the heat exchanger. This method allows us to assess if there is a need for external utilities like heating or cooling. The result of HI is shown in figure 5.6.

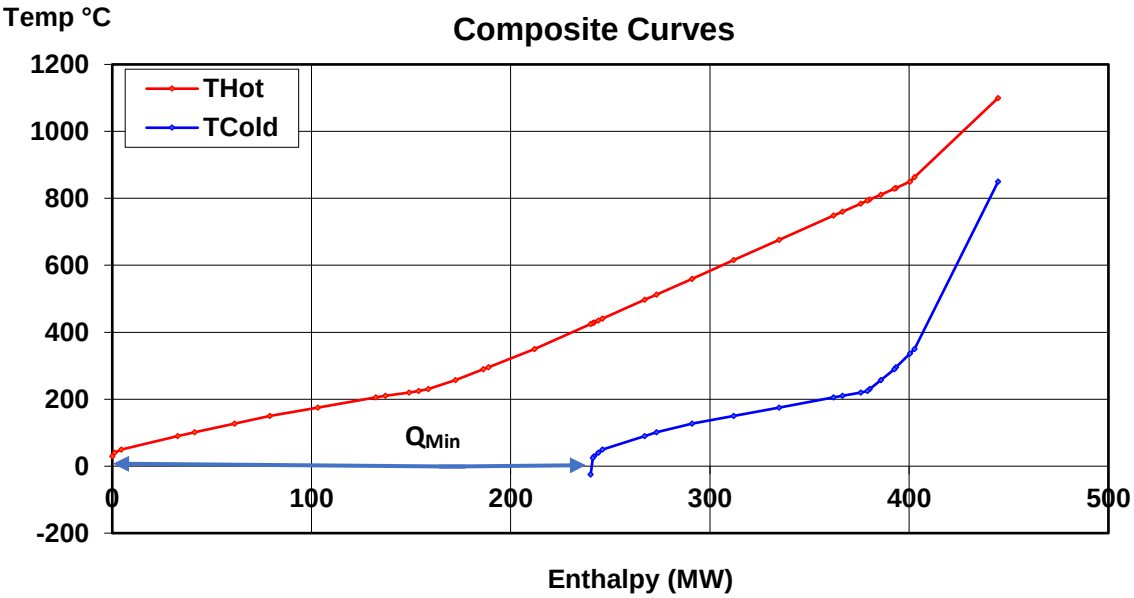

***Figure 5.6**. Heat integration results from Aspen Energy Analyzer for BTL WP.*

The graph shows that the heating demand exceeds that of the cooling demand. In other words, more energy is available in the hot streams to raise the temperature of the cool streams. Therefore, Q_{min} represents the extra available energy that requires external utilities; in this case, cooling water was utilized. This energy can be a source of income by generating steam and electricity. The cooling demand Q_{min} is 240 MW and 363 MW for BTL and PBTL, respectively. The reason behind the additional need for cooling water in the PBTL case is that the FT streams have higher flow rates than BTL, which requires extra cooling utilities. Moreover, the quantity of cooling water depends on the temperatures of the different streams as well as if a different sample of wood chips is utilized rather than a wood pellet. The change in the sample will influence the flow of the stream, which consequently influences the cooling and heating demand requirements.

5.7 Simulation Results

5.7.1. FT crude distribution

To evaluate the performance of the FT process, the range of produced hydrocarbons from the simulation must be checked to validate the presence of SAF, as shown in figure 5.7.

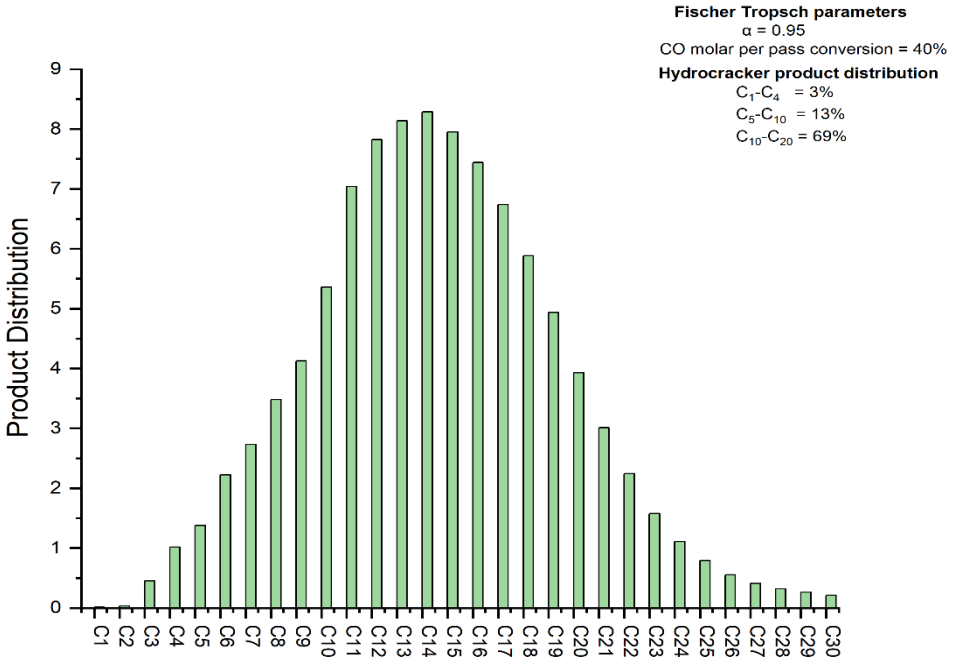

Figure 5.7*. Product distribution of FT crude.*

Figure 5.7 shows that the hydrocarbons in the range of C_8 to C_{18} are maximized, which assures that most of the product is SAF. The FT crude is then sent to a series of flash drums where the different fractions are separated.

5.7.2 SAF distribution

As the FT crude contains the SAF range, the final distilled product should be checked by comparing its physical characteristics with the conventional jet fuel A-1. The ranges of the characteristics are given in the ASTM standard D7566. Table 5.4 shows the results of the comparison between the standard and the SAF obtained from the simulation results in Aspen Plus.

Table 5.4. *Properties of conventional jet fuel vs SAF from WP feedstock.*

Properties	**Conventional jet fuel A-1**	**BTL - SAF**	**PBTL - SAF**
Density	775-840	757.4	757.2
Net heating value	> 42.8	44.1	44.1
Average boiling point	150 – 300	234.5	233.9
Flash point	> 38	60.1	64
Freezing point	Max. -47	-52.8	-53

The comparison shows that the net heating value, average boiling, and flash point lie within the range given in the standard. However, the density differs from the conventional jet fuel. This difference is expected as the model assumes jet fuel to contain only paraffins, while in reality, jet fuel contains paraffins, alkenes, and aromatics. The jet fuel typically has 7-20% aromatic[59]. Therefore, the standard does not authorize the utilization of SAF coming from the FT process as 100% fuel; instead, it has to be blended with conventional jet fuel. Therefore, this fuel will typically undergo a blending process where the final product will be experimentally tested to validate that every characteristic matches the jet fuel A-1 before being used in an airplane.

5.7.3 SAF yield

The same simulation procedure was repeated for the different samples of wood chips, high-quality and industrial-quality. Figure 5.8 shows the SAF yield obtained from the different samples and configurations.

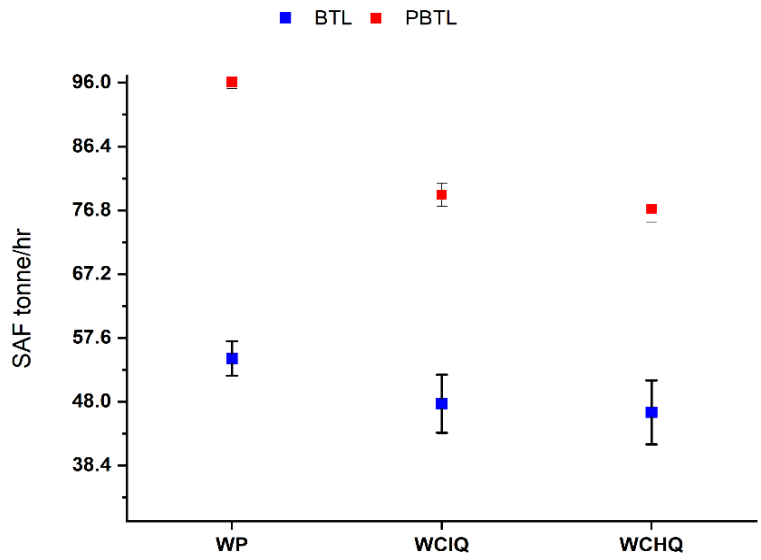

***Figure 5.8**. SAF yield of different feedstocks in the BTL and PBTL configurations.*

Figure 5.8 reveals that WP produces the most SAF in the BTL and PBTL cases compared to the other feedstocks of WCIQ and WCHQ, respectively. From WP, more SAF can be produced because it contains more carbon in its composition, which allows for the production of more carbon monoxide, which can be upgraded in the FT reactor to produce more hydrocarbons. Moreover, WP has low moisture and ash content, which yields high-quality syngas. WCIQ produces less SAF than WP but more than WCHQ. This is because WCIQ has a slightly higher carbon and hydrogen content in its composition than WCHQ, and therefore, it produces more syngas. However, it is crucial to highlight that this model does not consider the possible technical difficulties that might emerge due to the excess presence of ash, tar, or higher moisture content samples. In the case of PBTL, it follows the same pattern as BTL; however, it produces more SAF compared to BTL. This is because there is no WGS reactor; therefore, more carbon dioxide can be converted into higher hydrocarbons in the Fischer Tropsch reactor. Figure 5.9 gives a better insight into the carbon flow diagram in the process. The graph template was adopted from Dossow et al. [129].

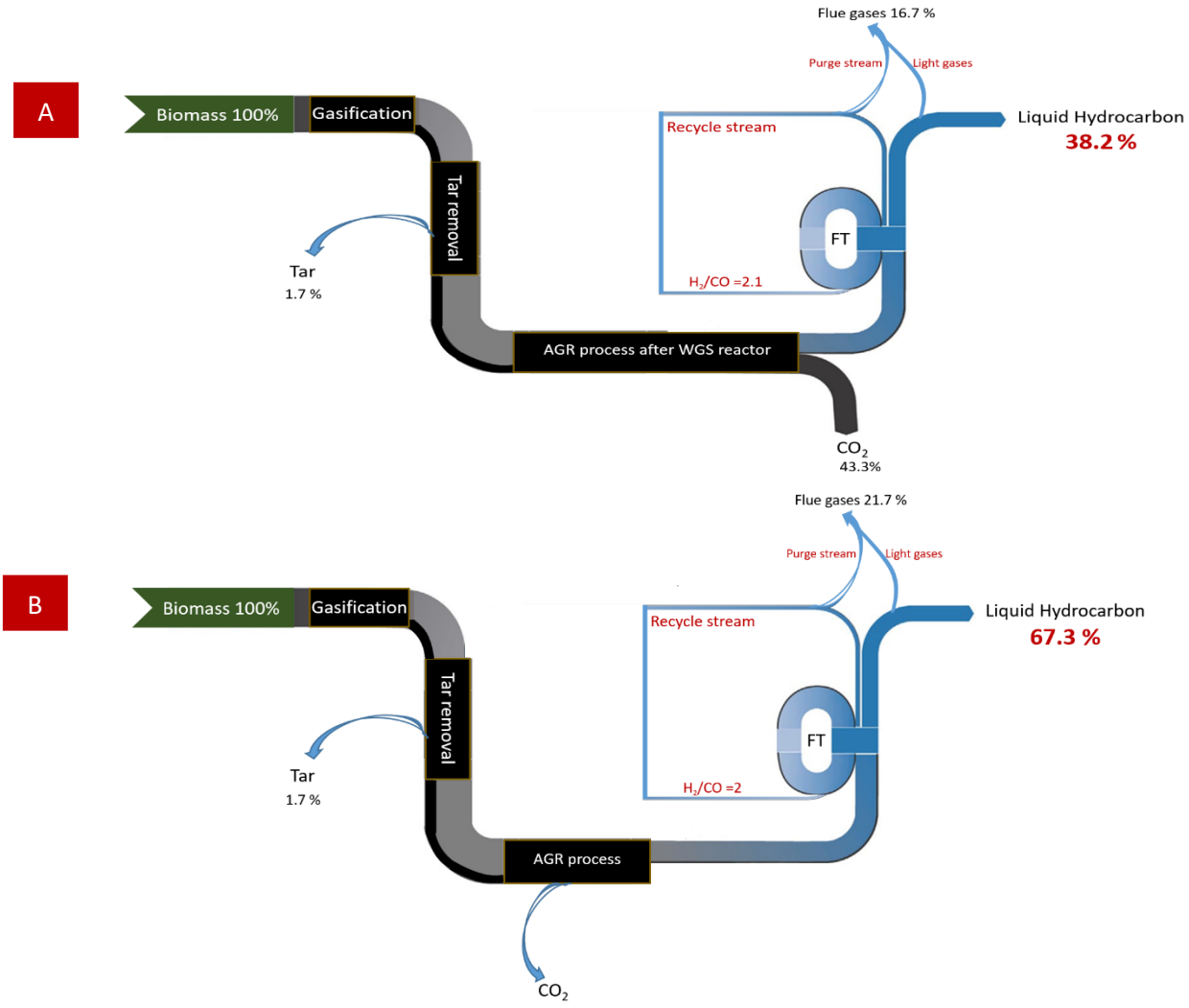

***Figure 5.9**. Carbon flow diagram for BTL (A) and PBTL (B) – WP feedstock. (The original schematic of the graph was taken and adopted from Dossow et al. [129])*

PBTL produces more hydrocarbons; therefore, the carbon flow diagram shows that over 67.3% of the carbon has been converted into liquid hydrocarbons. On the other hand, since there is no WGS reactor, only 9.3% of carbon is wasted in the form of carbon dioxide compared to the BTL, where around 45.8% is wasted. However, this setup of PBTL could be further improved to reach over 97% carbon conversion into liquid hydrocarbon when a reversed water gas shift reactor (RWGS) is included [130]. However, RWGS is not fully commercial and has a TRL level 6 [131]. Therefore, when assessing the pathways based on the current commercial state for the fast adaptation of SAF, a choice has been made to exclude adding the RWGS reactor.

5.7.4 Monte Carlo Simulation

After evaluating the performance of the processes, it was essential to analyze how the uncertainty of the different biomass characteristics influenced the final yield. Therefore, Monte Carlo simulation was chosen for this purpose, as explained in section 4.5. The experimental data of biomass characteristics obtained in Chapter 2 was utilized as the inputs for the model, where the range of each value was varied according to the uncertainty distribution of each parameter. The uncertainty distribution was normal for carbon and hydrogen content, while it was rectangular for the moisture content since the standard proposes only two measurement data points for moisture determination. Therefore, it is safe to assume that the moisture uncertainty follows a rectangular distribution. The utilized values in this simulation were taken from table 2.5 in Chapter 2.

Using a Python code capable of generating normal and rectangular distributions, 1000 random values of each parameter were generated and saved in an Excel sheet. This Excel sheet was connected to the Aspen model using a different Python code, as explained in Appendix B. Every parameter was changed alone while the rest was maintained fixed in order to study which parameter's uncertainty has the most influence on the process yield. Moreover, all biomass elements were changed simultaneously to study the overall impact on the yield. However, it is essential to highlight that the concentration is always constant at 100%. Therefore, oxygen was assumed to vary, whether by increasing or decreasing, to guarantee that the composition was fixed at 100%. It is worth mentioning that oxygen was not experimentally determined; rather, it was calculated after measuring all the other characteristics and deducting their sum from 100%. The results of the Monte Carlo simulation show that the uncertainty of SAF yield follows a normal distribution, as shown in figure 5.10.

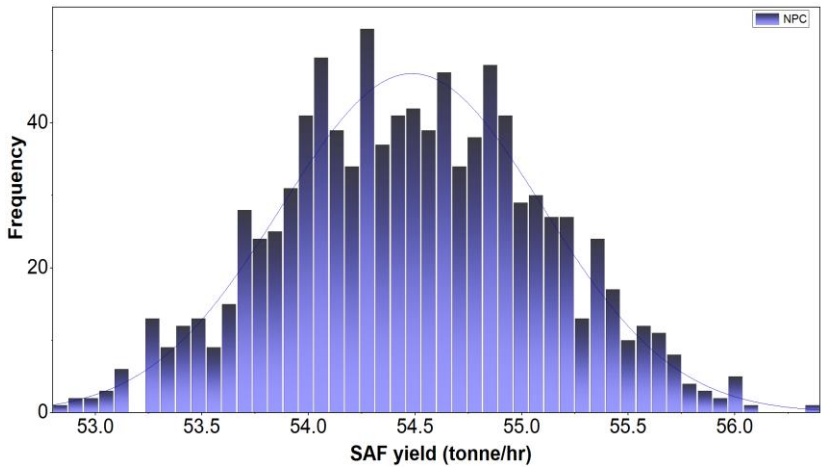

***Figure 5.10**. The results of Monte Carlo distribution for WP*

Since the yield followed a normal distribution, the expanded uncertainty was calculated as two times the standard deviation. The detailed results of the Monte Carlo simulation are summarized in table 5.5.

***Table 5.5.** Results of Monte Carlo simulation for WP.*

WP Feedstock – BTL Case (WGS)				
	Moisture content (MC) ± 5 %	Carbon (C) ± 0.30 %	Hydrogen (H) ± 0.047%	CH + Moisture (Overall uncertainty)
Average SAF yield (t/h)	54.48	54.48	54.48	54.48
SD (t/h)	0.49	0.36	0.0014	0.70
Expanded uncertainty of SAF % (K=2) 95%	1.79	1.32	0.005	2.58
Relative value = Biomass parameter uncertainty /expanded uncertainty	0.36	4.4	0.12	--
WP Feedstock – PBTL Case (hydrogen)				
Average SAF yield (t/h)	96.13	96.13	96.13	96.13
SD (t/h)	0.35	0.28	0.01	0.49
Expanded uncertainty of SAF % (K=2) 95%	0.72	0.58	0.02	1.03
Relative value = Biomass parameter uncertainty /expanded uncertainty	0.14	1.93	0.43	--

The simulation shows that the impact of biomass uncertainty on the SAF yield varies significantly depending on the process configuration. The BTL configuration seems to widen the impact of the uncertainty of the biomass characteristics on SAF yield. To understand the reasons, looking at the individual uncertainty parameters is vital. At first glance, it is noticeable that the moisture content seems to be the most influential parameter, as the SAF yield has an uncertainty of 1.79% compared to 1.32% and 0.005% for carbon and hydrogen, respectively. However, the uncertainty of each parameter is not the same. Therefore, the conclusion changes by calculating the relative value where the biomass parameter's uncertainty is divided by its expanded uncertainty. Here, where the carbon content becomes the most influential parameter. This leads to the conclusion that any inaccurate measurement in the laboratory for these parameters would result in a wrong assessment of their contribution to the yield. In the PBTL case, the overall expanded uncertainty of SAF yield and the relative value for carbon and moisture were decreased compared to the BTL case.

On the other hand, the relative value of hydrogen has increased. This can be explained by the fact that carbon has the highest percentage in the composition, so when it changes, it impacts the CO produced in gasification, consequently impacting the WGS and FT reactor, which also relies on the quantity of CO. Therefore, despite the low uncertainty of carbon, it can cause a more considerable impact. However, the reason behind the overall reduction in the PBTL case to 1.03% is that there is no WGS reactor; consequently, there is no carbon loss in the form of CO_2, and the impact of carbon is decreased on the overall CO production. Therefore, hydrogen becomes the key factor in the FT reactor, where any slight change becomes more observable in the results. The same method was applied to WCIQ and WCHQ, where a similar pattern was detected. The overall uncertainty for WCIQ and WCHQ was 4.38% and 4.81% for the BTL case and 1.76% and 1.95% for the PBTL case, respectively. The detailed values of WCIQ and WCHQ are presented in Appendix B in tables B1 and B2.

WP has the lowest overall uncertainty compared to all other feedstocks since it is a high-quality material, has fewer impurities, and is easy to measure experimentally. Therefore, the uncertainty of carbon and hydrogen content in WP was lower than that of WCIQ and WCHQ. Therefore, the lower the uncertainty in biomass characteristics, the lower its impact on the SAF yield. This shows the importance of accurately measuring the biomass characteristics or any other feedstock before the process design phase. Such information helps to provide insights about the possible implications in case of a sudden exchange in characteristics during operation. Moreover, knowing the contribution of biomass characteristics on the SAF yield helps to

estimate how these characteristics influence the production cost of SAF. This will be discussed in detail in the following section.

5.7.5 Techno-economic analysis

In the economic evaluation, four distinct scenarios were considered as follows:

1- Calculating the NPC for the BTL case without external hydrogen
2- Calculating the NPC for the PBTL case, assuming the source of external hydrogen is electrolysis (Green hydrogen)
3- Calculating the NPC for the BTL without WGS and coupled with external hydrogen assuming the source is blue hydrogen produced from methane steam reformer (HMBTL)
4- Calculating the NPC for the BTL without WGS and coupled with external hydrogen, assuming the source is blue hydrogen produced from coal (HCBTL)

It is essential to highlight that the graphs will be drawn mainly for the WP as a feedstock and for the configurations of BTL and PBTL. However, the other scenarios, along with the use of different wood feedstocks, are included in the study. Several assumptions had to be made to start evaluating the process, as shown in table 5.6. The production cost will be calculated for all configurations at a fixed biomass, electricity price, and annual operating hours.

Table 5.6. *Economic parameters and assumptions for the TEA [80,132–134].*

Parameter	**Value**
Location	Germany
Project year	2023
Plant lifetime	20 years
Interest rate	10%
Electricity	120 €/MWh
Wood Pellet	225 €/tonne
Wood chips	152 €/tonne
Green hydrogen	5.05 €/kg
Blue hydrogen - Methane	1.53 €/kg
Blue hydrogen - Coal	2.18 €/kg

The first step needed to calculate the NPC is to estimate the CAPEX by summing the purchased cost for every piece of equipment using equation 4.1, given in section 4.6. The reference cost, capacity, year, and unit of scale were taken from the literature data as summarized in table 5.7.

Table 5.7. *Parameters for calculating the equipment cost reported in Millions of US dollars (MUSD).*

Equipment	**EC_{ref}**	**Unit**	**S_{ref}**	**Design variable**	**Unit**	**D**	**Reference year**	**Reference**
Dry biomass handling	4.7	MUSD	8.87	Biomass input	kg dry/s	0.31	2010	[83,135,136]
Gasification	18.9	MUSD	17.8	Biomass input	kg dry/s	0.75	2010	
ASU	36.8	MUSD	76.6	Oxygen flow	t/hr	0.5	2010	
Cyclone	0.91	MUSD	68.7	Total gas flow	M_3/s	0.7	2004	[137]
AGR	59.5	MUSD	9909	H_2S /CO_2 mole flow	Kmol/s	0.7	2006	[130]
NH_3 scrubber	5.2	MUSD	1.446	NH3 mole flow	Kmol/s	0.67	2010	[136]
Tar removal	0.732	MUSD	47.1	MW	MW	0.7	2003	[138]
FT reactor	22.4	MUSD	310	FT feed	MW	0.7	2015	[135,139]
Hydrocracker	16.49	MUSD	378	Tonne/day	Tonne/day	0.67	2007	
Burner	2.62	MUSD	20	Heat duty	MW	0.83	2014	[83]
WGS	2.78	MUSD	150	Total gas feed	Kg/s	0.67	2014	

Distillation	10	MUSD	100	Feed	t/hr	0.7	2018	[81]
Pump	0.1	MUSD	10	Liquid flow	M_3/s	0.36	2010	[130]
Compressor	5	MUSD	10	Power consumption	MW	0.67	2010	

The value of the chemical engineering plant cost index (CEPCI) was utilized to consider the inflation and the change in cost across the years. The base value was 803.3, representing the CEPCI in June 2023, as previously explained in Chapter 4, equation 4.1. Note that the value changes every month until an accumulative value is taken at the end of each year. Along with the purchased cost, other factors like piping, instrumentation, and indirect capital costs were calculated through a set of assumptions as part of the purchased cost, as shown in Appendix B in Table B3. The fixed capital investment (FCI) equals the direct and indirect capital costs.

Meanwhile, the total capital investment (TCI/CAPEX) equals FCI plus the working capital (WC). The WC represents 10% of the TCI. The total TCI for BTL and PBTL for wood pellets were 2163.62 and 2182.82 million dollars, respectively. Although the PBTL scenario excludes the WGS and the ASU cost, yet its TCI is more than BTL. The PBTL process produces more liquid hydrocarbons; therefore, the unit operation needed for this configuration is larger in size, which makes it more expensive than the BTL configuration. Whatever hydrogen source is used in the PBTL process, it will not change the TCI since the cost of producing hydrogen, whether green or blue, is considered part of the operating cost (OPEX). Therefore, the TCI for PBTL is fixed for all cases of hydrogen variants. The equipment costs represent the biggest part of the annualized capital cost distribution, as shown in figure 5.11.

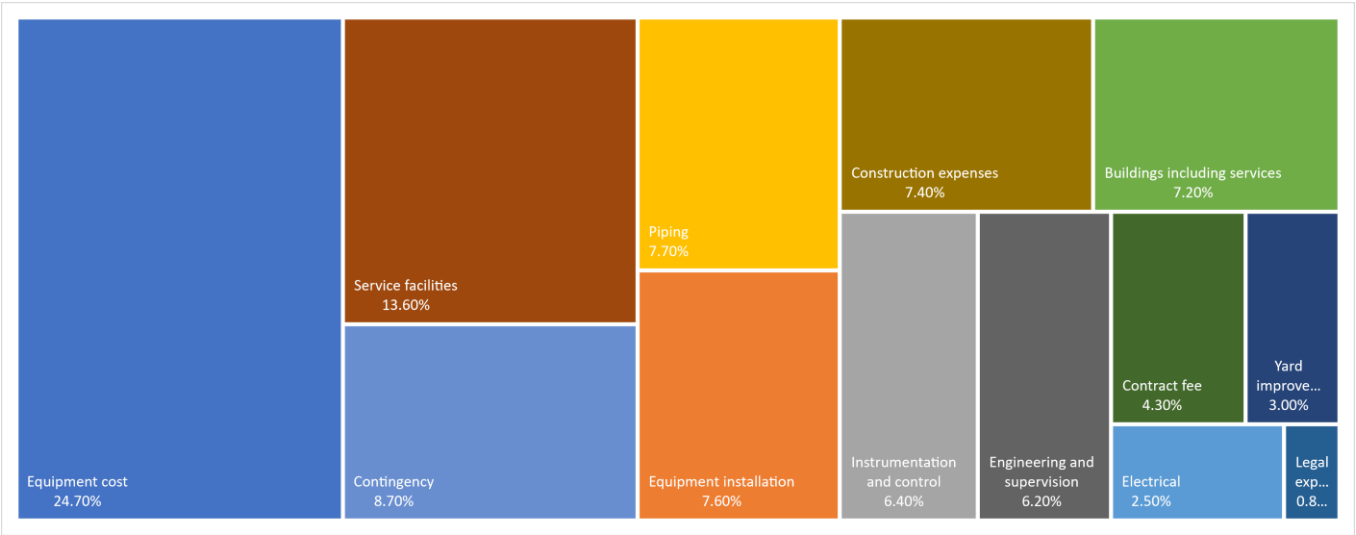

Figure 5.11. *Breakdown of annualized capital cost (ACC).*

This breakdown is fixed for both the BTL and PBTL cases as the sum of direct and indirect costs represents the annualized capital cost (ACC), calculated as a function of the purchased equipment cost. Therefore, any change in the purchased equipment cost will automatically influence the rest of the elements (e.g., piping), leading to a constant ratio. If direct or indirect cost assumptions change, then the ACC will differ between the BTL and PBTL cases. Figure 5.12 shows how much every piece of equipment contributes to the total installed equipment costs in BTL and PBTL cases.

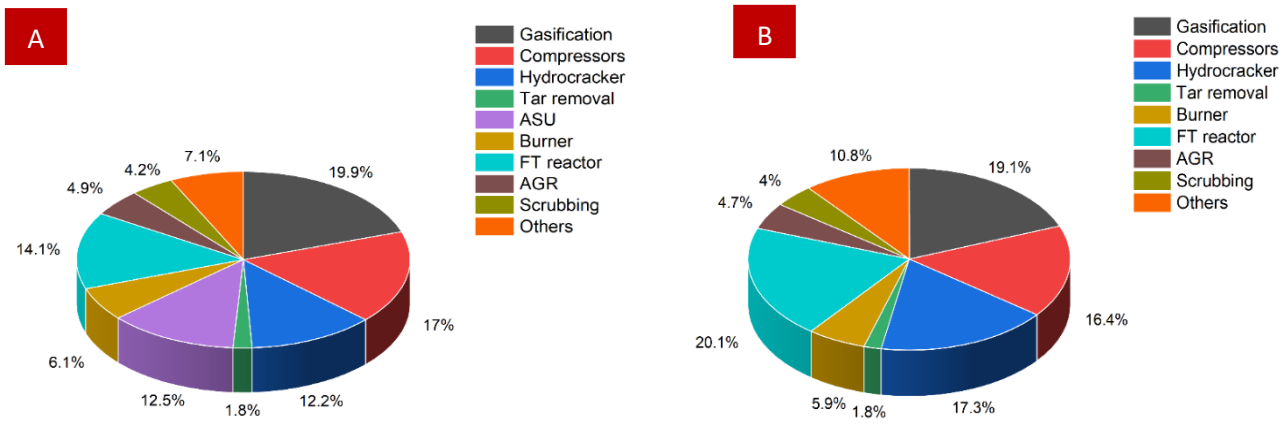

Figure 5.12. *Installed equipment cost distribution for the configurations BTL (A) and PBTL (B)- Wood pellet as feedstock.*

The gasifier and the FT reactor represent the major contributors to equipment costs, with around 19.3% and 13.6% of the total equipment costs, respectively. In the case of PBTL, they represent 19.1% and 20.1%, respectively. This is due to the larger FT crudes and recycle streams in the

PBTL case, which require larger reactors. It should be mentioned that WCIQ and WCHQ follow a similar trend; therefore, they have not been reported here. On the other hand, figure 5.13 shows the breakdown of the total operating cost (TOC).

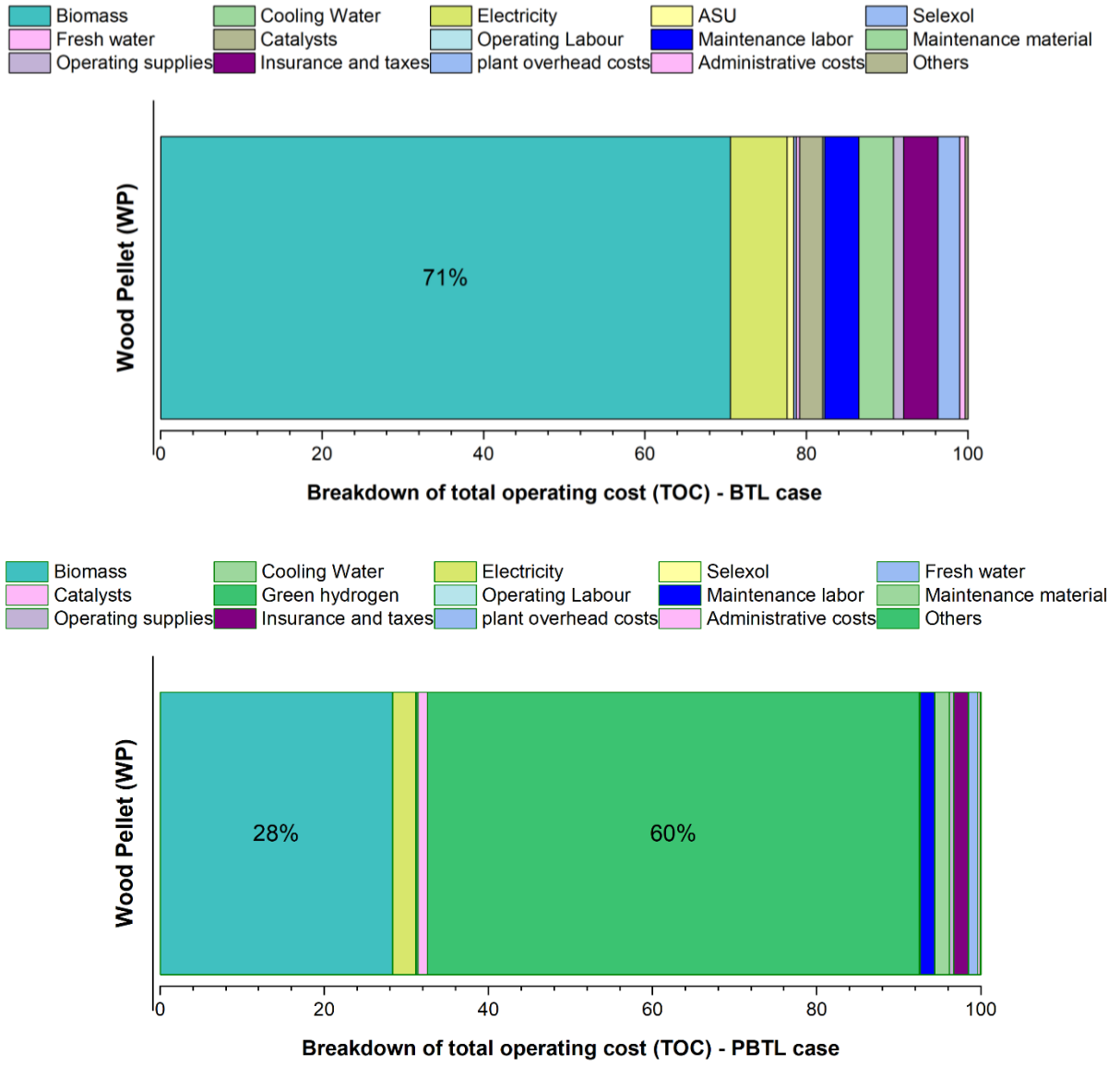

Figure 5.13 *Breakdown of total operating cost (TOC) for BTL and PBTL – FT- WP feedstock.*

The result shows that the biomass cost represents the main contributor in the BTL case with over 70% of the total operating cost. In comparison, it is the second contributor in the PBTL case with around 28% when green hydrogen is used. However, this change depends on the cost of biomass as well as the source of external hydrogen. In the case of utilizing blue hydrogen produced through methane or coal (HMBTL/HCBTL), biomass cost will still represent the main contributor, with around 48.6 %and 42.9%, respectively. This pattern would not differ significantly in the case of utilizing WCIQ or WCHQ. After calculating CAPEX and OPEX,

the net production cost was computed as a unit of dollars per tonne. Figure 5.14 provides a summary of the NPC results for all scenarios as well as for all feedstocks.

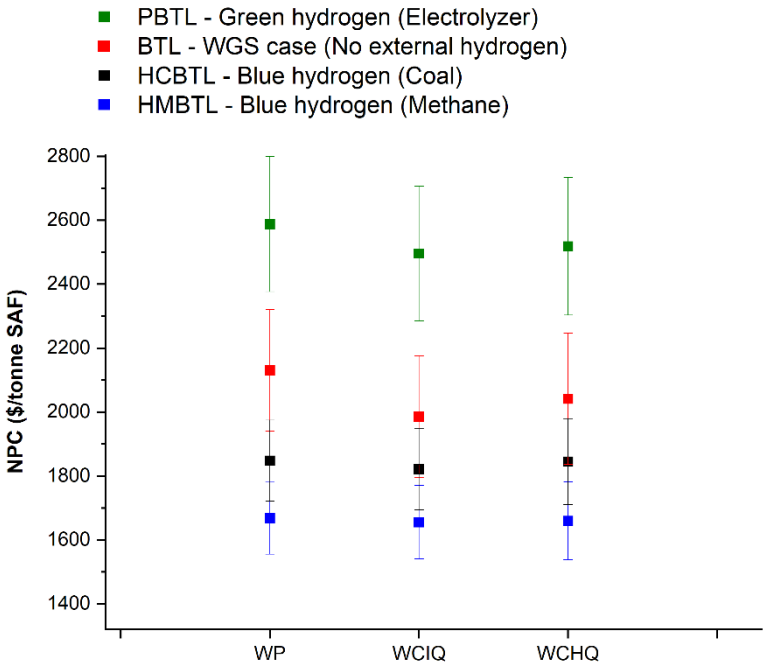

***Figure 5.14**. NPC results of BTL and PBTL using different wood types and hydrogen sources - FT*

The figure reveals that the most economically attractive scenario to produce cheap sustainable aviation fuel, regardless of the type of wood, is by utilizing blue hydrogen from a steam methane reformer (HMBTL-FT). The cheapest SAF was produced from WCIQ at 1655 dollars per tonne. In contrast, the most expensive SAF was produced from PBTL (green hydrogen) configuration using WP at 2588 dollars per tonne SAF. BTL is the second most expensive option between blue and green hydrogen. This is because BTL produces less fuel overall, which leads to higher NPC values.

On the other hand, when comparing the different samples, it is noticeable that WCIQ is the sample with the cheapest SAF production in all scenarios despite producing less SAF than WP. This is because wood pellets are typically more expensive to produce than wood chips. However, it is essential to highlight that this assessment does not consider the carbon footprint caused by producing blue hydrogen from methane or coal. However, it is fair to assume that HMBTL setup can be a key element in decarbonizing the aviation sector in the short term as it substantially lowers emissions compared to conventional jet fuel and produces SAF at a low cost. It deserves to be mentioned that the error bars on the graph represent the cost uncertainty for each case, which is explained in detail in the following section.

5.7.6 Uncertainty analysis

Typically, the best way to estimate the cost uncertainty as well as the yield is through historical data, which shows the fluctuation in the selling price or the production, respectively. The uncertainty represents a combination of factors, mainly due to the fluctuation in production capacity caused by the uncertainty of the feedstock, the utilities, and the supply chain, amongst other factors.

However, since these sustainable processes are not implemented commercially, such uncertainty analysis is crucial to provide more insights into the process. The uncertainty on SAF production caused by the feedstock was analyzed previously in section 5.7.4. This section aims to utilize the obtained data to study how it influences the cost of SAF. On the other hand, CAPEX and OPEX are another source of uncertainty. Therefore, sensitivity analysis is required to specify the critical variables that influence the economic assessment the most. The parameters in OPEX and CAPEX were varied by 20% to determine which parameter is decisive in influencing the cost of SAF, as shown in figure 5.15.

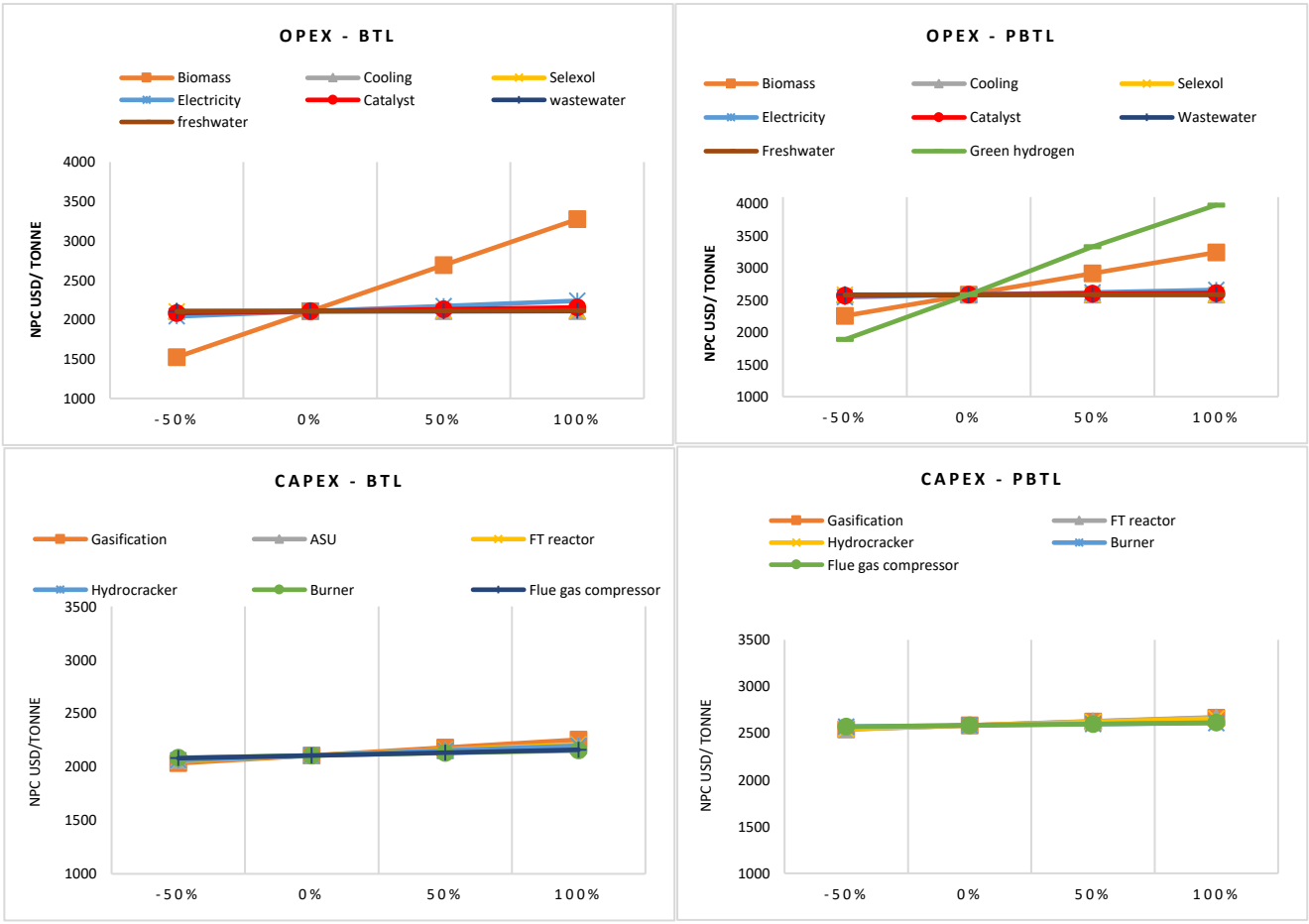

***Figure 5.15**. Sensitivity analysis for OPEX and CAPEX for BTL (left) and PBTL (right).*

The sensitivity analysis results show that biomass cost is the most influential parameter for the BTL case. This means one of the main objectives for cost improvement for this process is the utilization of a cheaper feedstock that can be used for SAF production. Electricity comes next as the second most influential parameter. On the other hand, for the PBTL case, the cost of green hydrogen is the most influential parameter, followed by biomass and electricity. It is worth mentioning that the same conclusion would apply to the HMBTL and HCBTL configurations; however, only BTL and PBTL are displayed here to avoid confusion. The sensitivity analysis for CAPEX in both cases of BTL and PBTL shows that it is barely influential on the NPC of SAF. Therefore, to perform the Monte Carlo simulation for the uncertainty assessment of SAF cost, biomass, electricity, and hydrogen were simultaneously changed. Similar to the procedure explained in section 4.5 for Monte Carlo simulation, 10,000 random values as normal distribution were generated for each parameter. Figure 5.16 shows the Monte Carlo distribution for BTL and PBTL.

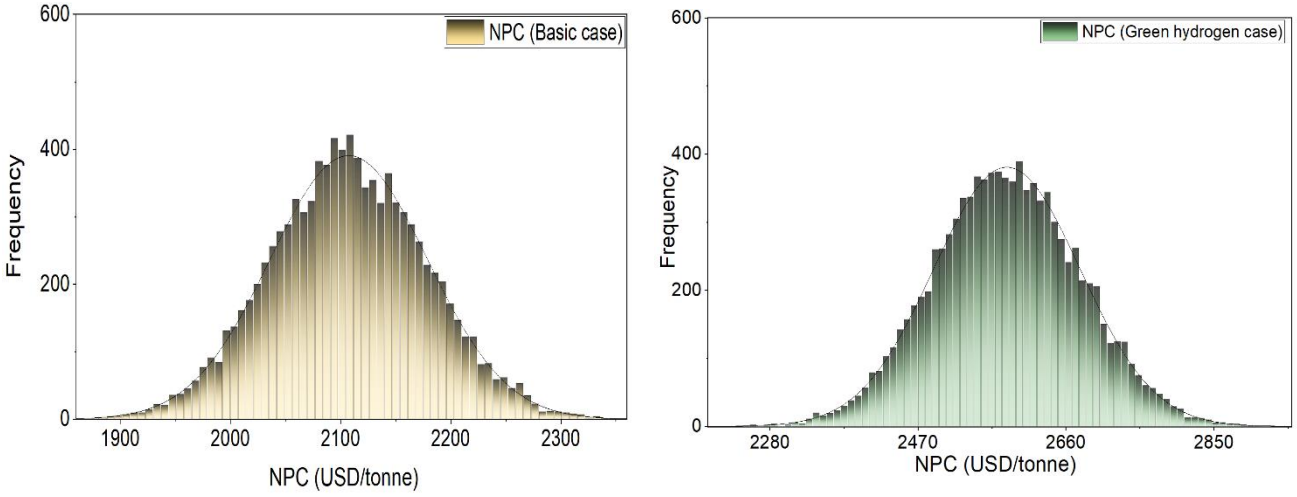

Figure 5.16*. Monte Carlo distribution for the NPC of BTL (A) and PBTL (B) – WP feedstock.*

The results of the Monte Carlo simulation follow a normal distribution in the BTL and the PBTL configurations. The same conclusion is extended for HMBTL and HCBTL setups as well as for the other feedstocks of WCIQ and WCHQ. The uncertainty caused by the variation in OPEX parameters was calculated as two times the standard deviation k=2, 95% coverage. It should be mentioned that in section 5.7.4, biomass characteristics were varied to estimate the uncertainty of SAF's yield. Using the estimated yield uncertainty, the impact on cost was estimated by generating 10,000 random values for the yield covering the upper and lower limits to obtain the uncertainty of the NPC. The results are summarized in table 5.8 for all different scenarios and feedstocks.

Table 5.8. *The primary outcomes of the uncertainty analysis of SAF cost.*

Factor (NPC)	BTL -FT	PBTL -FT	HMBTL -FT	HCBTL-FT
Results of wood pellets (WP)				
Cost uncertainty (U) due to Biomass characteristics uncertainty - WP	2.24	0.90	0.89	0.89
Cost uncertainty (U) due to OPEX uncertainty K=2, 95% - WP	6.67	7.26	5.92	5.96
Overall Cost Uncertainty (WP)	8.91	8.156	6.81	6.85
Results of wood chips industrial quality (WCIQ)				
Cost uncertainty (U) due to Biomass characteristics uncertainty - WCIQ	3.81	1.54	1.54	1.54
Cost uncertainty (U) due to OPEX uncertainty K=2, 95% - WCIQ	5.79	6.89	5.40	5.48
Overall Cost Uncertainty (WCIQ)	9.6	8.43	6.94	6.99
Results of wood chips high quality (WCHQ)				
Cost uncertainty (U) due to Biomass characteristics uncertainty - WCHQ	4.2	1.71	1.72	1.72
Cost uncertainty (U) due to OPEX uncertainty K=2, 95% - WCHQ	5.86	6.84	5.53	5.52
Overall Cost Uncertainty (WCHQ)	10.06	8.55	7.25	7.24

Each wood type was evaluated for the four different scenarios, and a Monte Carlo simulation was implemented for all these cases. The results show that the uncertainty caused by the utilities has a higher impact than the uncertainty caused by the fluctuation in yield caused by the uncertainty of the biomass characteristics. For wood pellets, biomass characteristics and OPEX influence the cost in the range of 0.89% – 2.24% and 5.92% – 7.26%, respectively. The BTL scenario has the highest uncertainty caused by the biomass characteristics, while its impact on PBTL is relatively marginal.

On the other hand, OPEX plays a significant role in both cases; however, it is more influential in the PBTL, with a maximum uncertainty of 7.26% when utilizing green hydrogen. However, the accumulative impact of both branches of uncertainty leads to the conclusion that the BTL scenario has a higher level of uncertainty on the final overall price of SAF compared to the PBTL configuration. It deserves to be mentioned that the accumulative uncertainty was assumed to be independent. Therefore, the values of uncertainty were summed together. These results clearly show that the configuration and the nature of the reactions in the process would maximize or minimize the uncertainty.

On the other hand, WCHQ has the highest overall uncertainty on the cost, which leads to the conclusion that the higher the uncertainty of biomass, the higher its influence on the process. While it is important to highlight that this analysis only provides numerical values, it is fair to assume that OPEX and biomass characteristics are not the only parameters influencing the SAF cost. There are other influential aspects, like supply chain fluctuation, sudden factory emergencies, or market instability. Moreover, OPEX was assumed to change by 20%. However, after the recent energy crisis caused by the Russian war in Ukraine, energy costs spiked in some countries in the EU to exceed 200%. Therefore, these values should not be considered as absolute values.

5.7.7 Efficiency evaluation and validation (BTL VS PBTL)

A comparison between the developed models and the literature was performed following the equations given in section 4.7. The products flow rates were taken from the model, while the LHV was calculated from the experimental results. Table 5.9 shows this comparison adapted from the Astonios, et al [85].

Table 5.9. *Comparison between the FT process performance and the literature [85,118,140].*

Study	**Technology**	**Y_{SAF}**	**f_{SAF}**	**EJFE**	**η_{tot}**	**$\eta_{tot\text{-}fuels}$**
König et al [51]	rWGS – FT	9.3%	43.9%	29.3%	28.5%	67.0%
Zang et al [64]	rWGS – FT	6.3%	46.7%	27.0%	26.7%	57.8%
Astonios et al [45]	CO2FT	20.8%	75.5%	51.2%	51.6%	69.2%
	LTFT	25.4%	90.7%	70.9%	66.4%	78.1%
This study	BTL-FT	18.2%	87.1%	32.1%	31.8%	38.3%
This study	PBTL-FT	32.1%	86.7%	56.6%	55.9%	68.1%

The pathways investigated in this study present a middle ground between the other technologies. Moreover, despite the availability of information on BTL in the literature, yet the assessments made for SAF are only available for power-to-liquid technologies using electrolyzers and renewable CO_2. Therefore, the models developed in this chapter cover this gap in the literature. It can be noticed that there is a significant improvement in the yield of SAF in PBTL over conventional BTL or PTL technologies. This is noticeable in the values of the Y_{SAF} and f_{SAF} for PBTL, which have higher values than their respective performance values found in the literature. Therefore, it is safe to say that the PBTL configuration is the most suitable for producing SAF.

5.7.8 Efficiency uncertainty

Calculating the efficiencies relies heavily on biomass's LHV, as shown in the previous section. The LHV data is derived from the experimental measurement performed in Chapter 2 and calculated from the HHV as proposed by J.S Lee [141]. The LHV was 19.3 MJ/kg. Studying

how impactful the accuracy of these experimental measurements is on the efficiency evaluation is essential since there is no plant data for such an investigation. The energy content of biomass has an uncertainty of ± 1% up to ± 5%, depending on how accurate the experimental procedure was. Therefore, EJFE, η_{tot}, and $\eta_{tot\text{-}fuels}$ were evaluated after changing the LHV of biomass within that range's upper and lower limits.

BTL-FT was considered as a case study. The EJFE, η_{tot}, and $\eta_{tot\text{-}fuels}$ had an uncertainty of around ± 1.61%, 1.57%, and 1.92%, respectively, at uncertainty of biomass LHV at ± 5%. When the uncertainty of LHV is ±1%, EJFE, η_{tot}, and $\eta_{tot\text{-}fuels}$ had an uncertainty of 0.32%, 0.31%, and 0.38%, respectively. Therefore, the efficiency uncertainty has decreased by a factor of 5, corresponding to the reduction in the LHV's uncertainty. This accuracy was achieved thanks to the enhanced experimental practice that ensured accurate characterization of the energy content. This shows that the measurement uncertainty directly influences the process performance and efficiency. The lower the biomass energy content uncertainty, the higher the efficiency accuracy. It deserves to be mentioned that the uncertainty values were calculated using the average difference between the upper and lower uncertainty values obtained when varying the LHV.

This information is valuable for process designers as it helps them estimate a realistic range of uncertainties for unit operations and process efficiency in situations where historical data is unavailable, such as with new sustainable processes. Therefore, at this stage of process development, these inputs are crucial to provide a better insight into the process performance. It is worth mentioning that the efficiency fluctuation will be reflected in the process in the form of potential operational difficulties. For example, the sudden increase or decrease in biomass characteristics like moisture, energy content, etc., could influence the equipment and the steady operation of the plant. For instance, the sudden increase in the biomass's energy input might lower the gasifier's temperature and produce low-quality syngas, eventually reducing the overall SAF production. Consequently, higher biomass feed might be needed to maintain the production capacity in a steady state, causing an increase in cost. Meanwhile, if the gasifier temperature suddenly increases due to higher energy content, overheating might occur, leading to a safety hazard. Therefore, the accurate characterization of biomass and its uncertainty is essential to achieve a proper, sustainable, and safe design.

5.8 Conclusions

Wood pellets produce more sustainable aviation fuel than wood chips because they have higher carbon and hydrogen content, regardless of configuration. Therefore, this leads to the production of more syngas of high quality, which is suitable for upgrading in the FT process. Configuration-wise, the PBTL produces more SAF than BTL and conventional PTL technologies as it is more efficient than both. On the other hand, the process configuration affects the SAF yield and its uncertainty. The BTL setup expands the yield uncertainty due to the carbon loss in the WGS reactor, where part of the CO is consumed to produce hydrogen and CO_2, which triggers an accumulative effect of CO loss in the system. It is worth mentioning that the assessment did not consider the possible technical issues associated with the uncertainty of the biomass characteristics, which could influence the process performance even more, which increases the impact on the SAF yield.

From a techno-economic perspective, wood chips-industrial quality produced the cheapest form of SAF compared to all other feedstocks. Configuration-wise, SAF produced from HMBTL -FT (methane blue hydrogen) is more economical than SAF from PBTL (green hydrogen), HCBTL -FT (coal blue hydrogen), and BTL setups. Therefore, methane blue hydrogen provides a middle ground for the fast implementation of SAF as this still lowers the emissions compared to the conventional process of producing jet fuel. Moreover, it provides a market value of SAF that is much cheaper at around 1655 $/t than green hydrogen, which produces SAF at 2496 $/t for WCIQ feedstock. By providing subsidies to OPEX or CAPEX, the process will then be capable of competing with conventional A1 jet fuel. Additionally, the analysis indicates that the uncertainty surrounding OPEX would exert a greater influence on SAF costs than biomass uncertainty. However, it's essential to note that other factors, such as market instability and supply chain disruptions, could also affect the SAF cost.

Nomenclature

TEA	Techno-economic analysis
FT	Fischer Tropsch
BTL	Biomass to liquid
PBTL	Power biomass to liquid
ASU	Air separation unit
RME	Rapeseed methyl ester
AGR	Acid gas removal
Mpa	Megapascal
REquil	Equilibrium reactor
ASF	Anderson-Schulz-Flory
ER	Equivalence ration
α	Chain growth probability
HI	Heat integration
RWGS	Reverse water gas shift
HMBTL	Hydrogen methane – Biomass to Liquid
HCBTL	Hydrogen coal – Biomass to Liquid

CHAPTER 6

Chapter 6. Biomass to SAF – Methanol to Jet Pathway

6.1 Overview

This chapter delves into the simulation process of converting biomass into jet fuel through the methanol pathway using Aspen Plus. Similar to the previous FT chapter, the influence of biomass characteristics and their uncertainties on the yield of SAF are analyzed. Moreover, the results obtained from the process and the Monte Carlo simulations are utilized to conduct techno-economic analysis. The chapter aims to determine the most cost-effective configuration for SAF production by assessing the MTJ pathway's economic viability in reducing the aviation sector's carbon footprint and comparing its efficiency with the different technologies.

Based on:

Shehab, M.; Moshammer, K; Zondervan, E. Techno-economic analysis of the production of sustainable aviation fuel from biomass via Fischer Tropsch and Methanol pathways (*Ongoing manuscript*)

6.2 Introduction

The methanol-to-jet process (MTJ) holds immense potential as a sustainable pathway to traditional fossil-based jet fuels as it offers the chance to reduce greenhouse gas emissions and mitigate aviation's environmental footprint. The process could be integrated with syngas produced through biomass or renewable energies, which makes it a flexible option, as shown in figure 6.1.

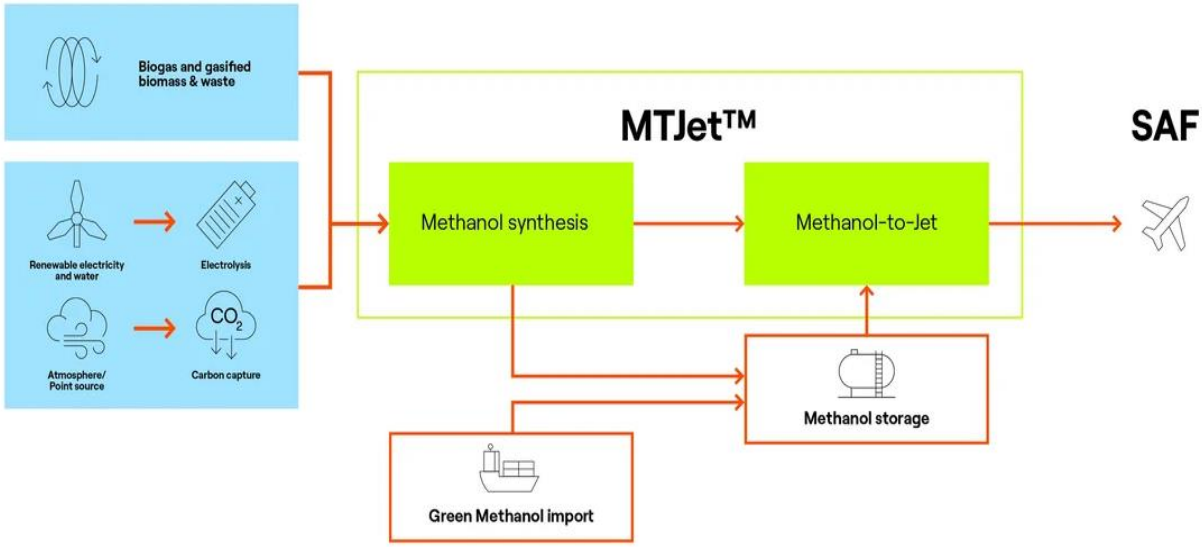

Figure 6.1. *Methanol to Jet pathway flexibility [142].*

Methanol as an intermediate product allows the process to be implemented in different regions by increasing cooperation between different industrial facilities without necessarily having the whole MTJ process assembled in one location. This is because methanol can be easily shipped and sold separately since it's a valuable and stable product. However, despite its advantages, the process of MTJ is not yet approved by the ASTM D7566 standard as it has not yet been tested at a large commercial scale, nor has its economic viability been confirmed. Several projects are currently taking place across the EU to establish demo plants to test the full potential of the process and economic competitiveness. The MTJ and FT processes are similar regarding their need for high-quality syngas with an H_2/CO ratio of 2 – 2.1 [143]. The main deviation starts in the methanol synthesis. Currently, the most widely used technology for methanol synthesis involves $Cu/ZnO/Al_2O_3$ (CZA) catalysts in either multi-tube reactors cooled by boiling water, known as isothermal reactors such as Lurgi and Linde processes, or adiabatic reactors operate with intermittent cold syngas quenching such as ICI and Casale, Haldor Topsoe processes [144]. Methanol can be synthesized from either CO or CO_2, with the simultaneous occurrence of the reverse water-gas shift reaction. When the feed gas comprises both CO and

CO_2, the prevailing belief is that the direct hydrogenation of CO to produce methanol on Cu/Zn-based catalysts is considerably slower than the hydrogenation of CO_2 [143]. Typical operating conditions range from 200 to 300°C and 50 to 100 bar [145]. Figure 6.2 shows the influence of pressure and temperature on methanol yield.

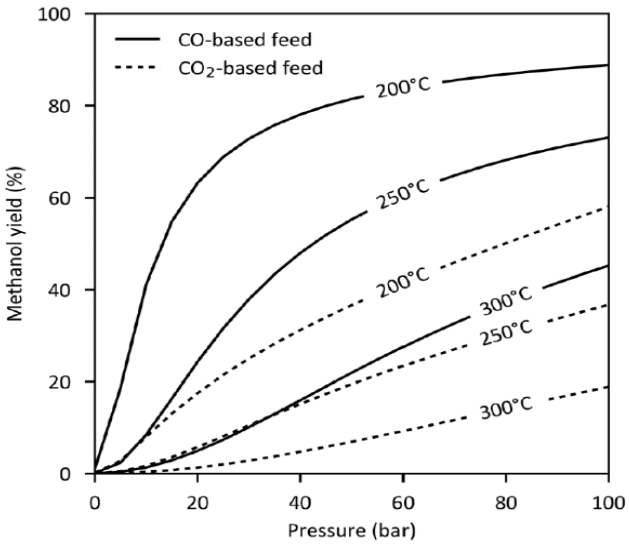

Figure 6.2. *Methanol yield vs temperature and pressure* [143].

Methanol formation is thermodynamically favored at lower temperatures and higher pressures. The hydrogenation of carbon monoxide is exothermic to a greater extent than the hydrogenation of carbon dioxide, necessitating more extensive cooling to maintain the desired reaction temperature [146]. Methanol is considered the primary building block for the upgrading section, which consists of several other steps, such as converting methanol into olefins, oligomerization, and hydrogenation. There are various approaches to produce short-chain olefins from methanol, such as methanol to propylene (MTP), dimethyl ether to olefins (DMTO), and Mobil process [147]. One of the main differences is in the nature of the catalyst used, which directs the selectivity of the process. For instance, the DMTO process favors ethylene and propylene production with traces of higher hydrocarbons. In contrast, the Mobil MTO process primarily produces propylene, butene, and pentene with smaller amounts of ethylene and other higher hydrocarbons [147]. The Mobil process exhibits higher thermal efficiency, while the DMTO process boosts higher olefin yields [148].

The Mobil MTO process is highly established, employing a ZSM-5 catalyst, converts methanol into short-chain olefins (C_3-C_6), along with light paraffins, naphthenes, and aromatics, as shown in figure 6.3 [149]. ZSM-5 is a zeolite catalyst known for its shape selectivity, allowing it to selectively produce molecules with a specific pore size. This shape selectivity helps prevent the formation of larger molecules, such as durene ($C_{10}H_{10}$), by restricting their access to the active sites on the catalyst [150].

	MTO[a] Product
C_1	1.4
C_2	0.3
C_3	2.3
C_4	3.9
$C_2^=$	5.0
$C_3^=$	31.8
$C_4^=$	19.6
Gasoline C_5–C_{11}	35.7
Diesel C_{12}–C_{18}	–
Heavy product C_8^+	–
Water soluble oxygenate	0.3
	100
Total light saturates (C_1–C_3)	4.0
Total light olefins ($C_2^=$-$C_4^=$)	56.3

***Figure 6.3**. The typical hydrocarbon yield of the Mobil MTO process [149].*

Figure 6.3 shows the olefins yield obtained from the Mobil MTO process. The produced olefins then undergo oligomerization to convert the short olefins into longer-chain molecules. Oligomerization has several established processes like Conversion of Olefins to Distillate (COD) and Mobil Olefin to Gasoline and Distillate (MOGD). These processes produce different outputs as they utilize different catalysts and operate at different conditions. However, MOGD has more literature data and is widely considered a promising option for biodiesel and SAF production as proposed by [85,151]. The MOGD process has two operation modes, either for the production of gasoline or distillate. As the thesis focuses on SAF production, the MOGD process with the distillate mode is considered. The next step in the upgrading section is to utilize the longer alkenes produced from the MTO-MOGD process to produce long-chain paraffins. When the double bonds between carbon atoms interact with hydrogen gas under the influence of various metallic catalysts such as palladium and platinum, the double bond is broken, and each carbon atom forms a single bond with a hydrogen atom. This process is known as hydrogenation or catalytic hydrogenation, where olefins are saturated to produce paraffins. The produced liquid paraffins must be separated in distillation columns to produce SAF. It is

essential to highlight that this chapter will focus on the MTO-MOGD process, which is well-established and has a high TRL value.

6.3 Methodology

The methodology of this chapter is identical to what was previously explained in chapter 4. Moreover, the configurations, the structure of the sections, and the subsections were similar to those presented previously in chapter 5.

6.4 Model description - Biomass to clean syngas

This process section is the same as the one explained in section 5.4 since the methanol pathway requires clean syngas similar to the FT reactor. Therefore, biomass is first gasified, followed by the removal of impurities like ash, tar, NH_3, and sulfur. However, one of the main requirements for upgrading syngas to methanol is the ratio of H_2 to CO. The ratio was set at 2.1 to guarantee enough hydrogen available to initiate the reactions with both CO and CO_2. Moreover, the extra hydrogen improves the space-time yield of the catalyst and avoids by-product formation by hydrogen deficiency [146]. The upgrading section is entirely different from the FT process, which needed to be fully simulated, as shown in figure 6.4.

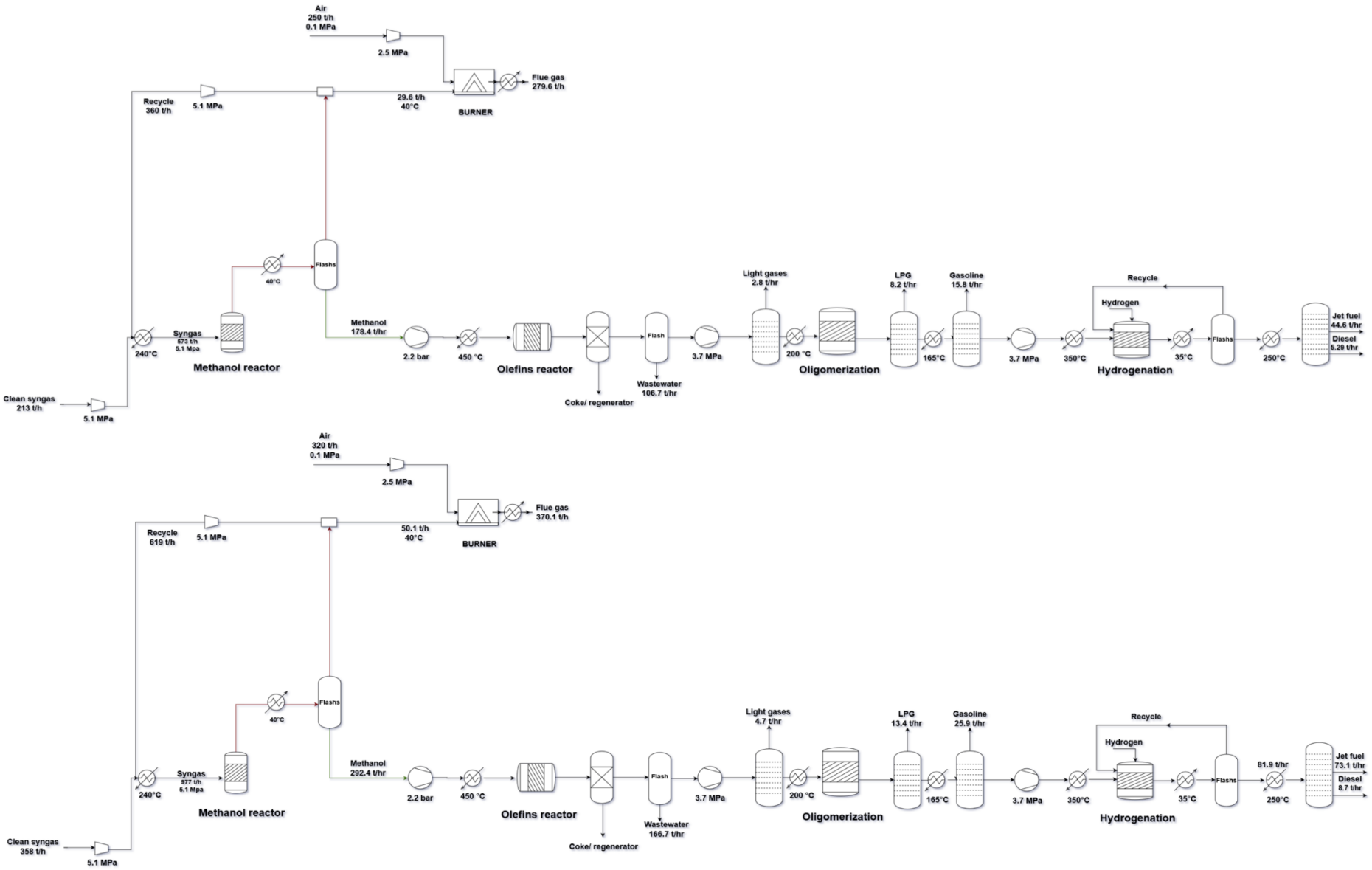

***Figure 6.4**.Process flow diagram of MTJ pathway – BTL configuration (TOP) vs PBTL (BOTTOM)*

6.5 Model description - Upgrading

6.5.1 Methanol synthesis loop (MeOH)

In the industry, the methanol synthesis takes place in a series of plug reactors [152]. However, in the simulation environment, the representation of the methanol reactor is quite flexible and depends on the applied methodology. Therefore, for the Aspen simulation, a stoichiometric reactor was used to simulate the synthesis process of methanol. The stoichiometric reactor operated at temperature and pressure of 240 ℃ and 5.1 MPa, respectively. Several reactions were defined to reflect the chemical reactions that take place in the reactor. Trop et al., simulated the methanol reactor using published experimental data [153]. The fractional conversion of each reaction was provided through the experimental results of the methanol synthesis. Therefore, the methanol reactor was replicated based on the same modeling data. The reactor is set to operate using a Cu/ZnO catalyst. It is essential to highlight the fractional conversion of each reaction would differ if the catalyst or the operating parameters had changed. The utilized reactions and their fractional conversion are summarized in table 6.1.

Table 6.1. *Fractional conversions of reactions inside the methanol reactor [153].*

Number	Reaction	Fractional conversion	Of reactant
6.1	$CO + 2H_2 = CH_3OH$	0.35500	CO
6.2	$CO_2 + 3H_2 = CH_3OH + H_2O$	0.17800	CO_2
6.3	$CO + H_2O = CO_2 + H_2$	0.01800	CO

Both reactions 6.1 and 6.2 are predominant in defining the methanol reactors. However, several side reactions occur, such as the formation of ethanol, propanol, and methyl formate; in this model, they are assumed to be negligible. Moreover, it is noticeable that the fractional conversions are not high, with only around 35% of the CO being converted directly to methanol. Therefore, a recycle stream is typically present in the methanol synthesis to increase the conversion. This is similar to the design loop performed in the Fischer Tropsch process, where the non-reactant syngas is reintroduced to the reactor. This step is performed by cooling the output from the methanol reactor to 30 ℃ to condense the crude methanol. The flashed stream is partially separated where part of the gaseous phase is purged out of the design loop to avoid accumulation in the system [154]. This purged stream could be used to generate heat for the

system. The rest of the non-reactant is sent back to the methanol reactor after recompressing. The crude methanol is then collected and sent to further processing to produce SAF.

6.5.2 Methanol to olefins (MTO)

The upgrading section was adapted entirely from Tufail Kaladia [147]. The first step in producing jet fuel via MTJ pathway involves the synthesis of short-chain olefins. The MOBIL process is selected in this section as it is one of the most established processes for producing olefins [155]. Olefins are the main building block required for the production of SAF. However, there is a large inconsistency regarding the specific reactions occurring within the MTO reactor [147]. The composition of the product stream in the MTO process is highly influenced by the choice of catalyst and the reaction conditions employed during the process. Zeolites are extensively used in the MTO process as they exhibit high selectivity towards short-chain olefin production. Therefore, ZSM-5 was selected as a catalyst. The ZSM-5 catalyst's shape selectivity prevents the production of molecules larger than durene $C_{10}H_{14}$. Durene represents the coke that is being formed within the reactor. In the simulation, methanol initially undergoes a transformation into dimethyl ether (DME), serving as an intermediate chemical species. Subsequently, DME undergoes further reactions to produce light olefins and water. All the reactions associated with the upgrading of methanol to olefins are performed in a stoichiometric reactor for simplification. The methanol enters the process under atmospheric conditions and is then pumped and heated to the MTO reactor conditions of 2 bar and 450 °C. After producing the light olefins, the stream is directed to flash drums to separate the water. Moreover, the formed light olefins contain non-condensable light hydrocarbon gases like methane. Those light gases are separated via distillation and used for heat generation. On the other hand, the catalyst is assumed to be regenerated by burning the formed coke on the catalyst and then recycling the catalyst back to the reactor [155,156]. The reactions in the MTO process are shown in table 6.2.

Table 6.2. *The reactions in the MTO process [151].*

Reaction step	Reaction	Fractional conversion for this reaction	Fractional conversion of component	The overall conversion of the same component until this step
1	2 Methanol ⟶ DME + Water	99%	Methanol	99%
2	DME ⟶ Ethene + Water	30%	DME	30%
3	3 DME ⟶ 2 Propene + 3 Water	100%	DME	100%
4	2 Ethene ⟶ Butene	80%	Ethene	80%
5	2 Propene ⟶ Hexene	45%	Propene	45%
6	Ethene + Propene ⟶ Pentene	45%	Ethene	89%
7	Hexene ⟶ Benzene + 3 Hydrogen	50%	Hexene	50%
8	Benzene + 4 Methanol ⟶ Durene + 4 Water	100%	Methanol	100%
9	2 Butene + 2 Hydrogen ⟶ n-butane + i-butane	15%	Butene	15%
10	Propene + Hydrogen ⟶ Propane	7.5%	Propene	---
11	Ethene + Hydrogen ⟶ Ethane	15%	Ethene	90.65%
12	Ethene + 2 Hydrogen ⟶ 2 Methane	50%	Ethene	95.325%
13	Benzene + 3 Hydrogen ⟶ Cyclohexane	100%	Hydrogen	100%
14	Pentene ⟶ Cyclopentane	50%	Pentene	50%

It is assumed that these reactions occur in series. Each percentage is deducted from the previous component. In the first reaction, 99% of Methanol is converted, while in step 8, the 100% from methanol represents the complete 1% remaining from the first step. The same rule applies to the other components.

6.5.3 Oligomerization (MOGD)

In this part of the upgrading section, the mix of olefins produced in the MTO process was upgraded into longer chain olefins in the range of $C_1 – C_{20}$ over an HZSM – 5 catalyst. This catalyst is widely cited in the literature and is used to produce gasoline and other compounds [147]. The oligomerization reactions produce olefins along with other compounds, such as aromatics and slight fractions of paraffins. A stoichiometric reactor was used to simulate this process. The reactor is set to operate under a pressure of 40 bars and a temperature of 200 °C. It is worth noting that the outcomes from this model could change significantly depending on the catalyst used, which consequently influences the reactions in the reactor. Therefore, across the whole model of MTJ, the focus is on established catalysts that are commercially available. The reactions in the MOGD reactor are provided in Appendix C - Table C1.

6.5.4 Hydrogenation

The alkenes produced from the MOGD process do not represent the real jet fuel composition. Therefore, hydrogenation is needed to saturate the alkenes with hydrogen to produce alkanes (Paraffins). The reactor operates at a temperature and pressure of 350 °C and 3.7 MPa, respectively. The molar ratio of hydrogen to hydrocarbons was set to 3:1 to ensure the presence of enough hydrogen to saturate the olefins [157]. Co-Mo/Al_2O_3 was selected as a catalyst since it is relatively cheap compared to other catalysts like palladium or platinum [158]. The outlet stream from the reactor goes to a flash drum where the unused hydrogen is recycled back to the reactor to reutilize it. The produced liquid hydrocarbons go to distillation columns to separate the different components. Around 89% of the liquid hydrocarbons is jet fuel regardless of the configuration. This percentage depends upon the setup of the upgrading section. Therefore, it does not change in the BTL or PBTL process.

6.6 Model optimization and validation

A sensitivity analysis was performed to study the effect of temperature and pressure on the methanol yield and validate the values that were selected from the literature, as shown in figure 6.5.

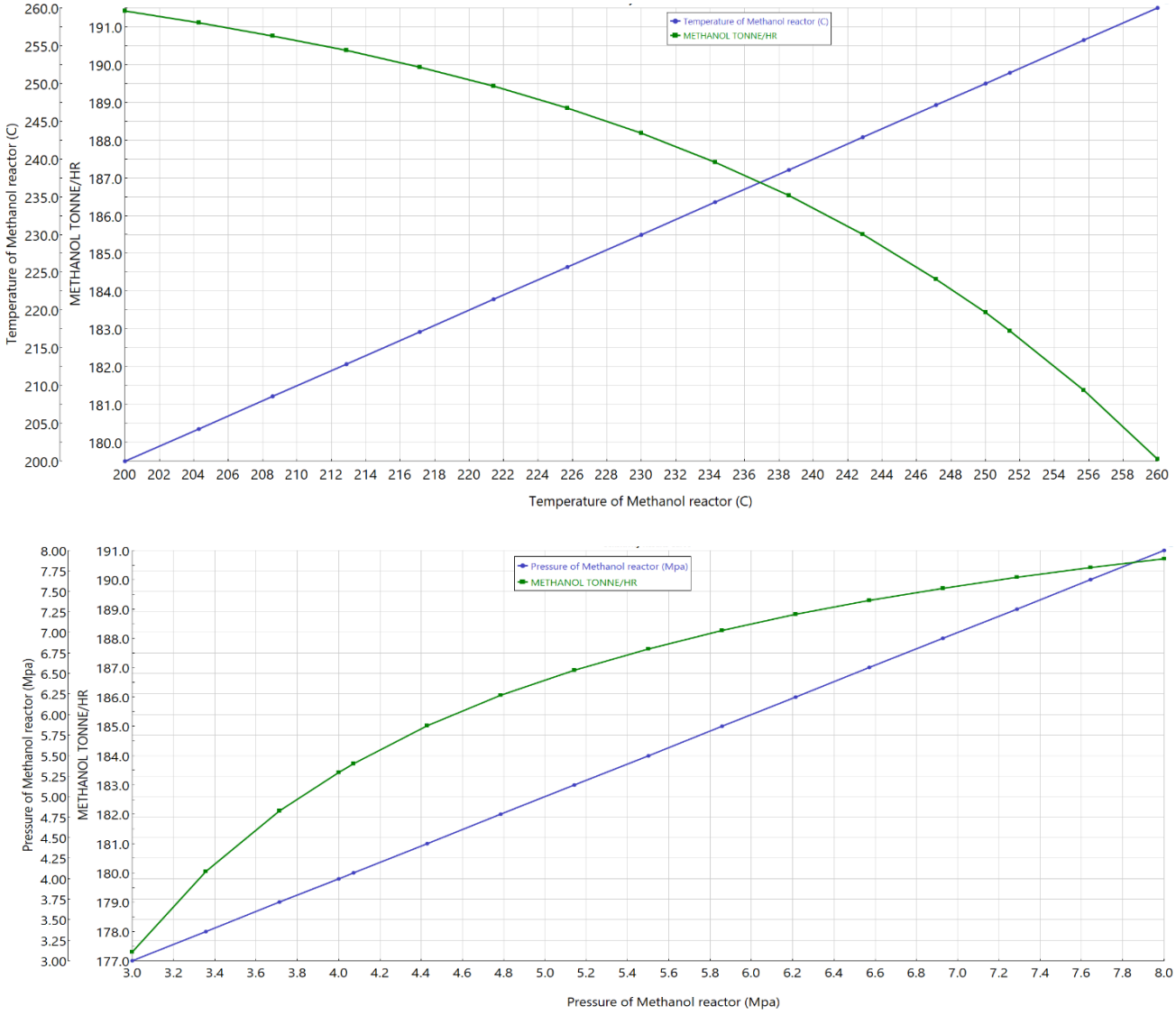

***Figure 6.5**. Sensitivity analysis of temperature (TOP) and pressure (Bottom) vs yield of Methanol*

Figure 6.5 shows that the methanol yield is sensitive to changes in temperature and pressure. In the top figure, the higher the temperature, the lower the methanol yield. This phenomenon is because the methanol reaction is an equilibrium reaction. At higher temperatures, the equilibrium shifts towards the reverse reaction, which produces the reactants (carbon monoxide and hydrogen) from the products (methanol and water). This results in a decrease in the methanol yield. Moreover, it is an exothermic reaction that generates heat. Therefore, methanol formation favors the use of low temperatures and elevated pressures. This can also be observed

in the bottom of figure 6.5, where the methanol yield is higher when higher pressures are applied. However, there is an optimum threshold; if the temperature and pressure exceed it, the process becomes economically unfavorable since methanol production starts to slow down. Moreover, more energy will be needed to increase the pressure. Therefore, a temperature of 240 °C and pressure of 5.2 MPa that were selected for this process are considered optimum values. This is because these operating conditions strike a balance between achieving a high methanol yield and minimizing energy consumption. Lower temperatures might require longer residence times or higher pressures, which can affect the overall efficiency and economics of the process. While lower temperatures can be used, they may result in slower reaction rates and potentially require more expensive or less stable catalysts. Operating at 240 °C is a compromise offering reasonable catalyst stability and good methanol production rates.

Heat integration is important to minimize the need for external utilities. The result of the heat integration for the conversion of biomass to SAF through methanol for the wood pellet sample is shown in figure 6.6.

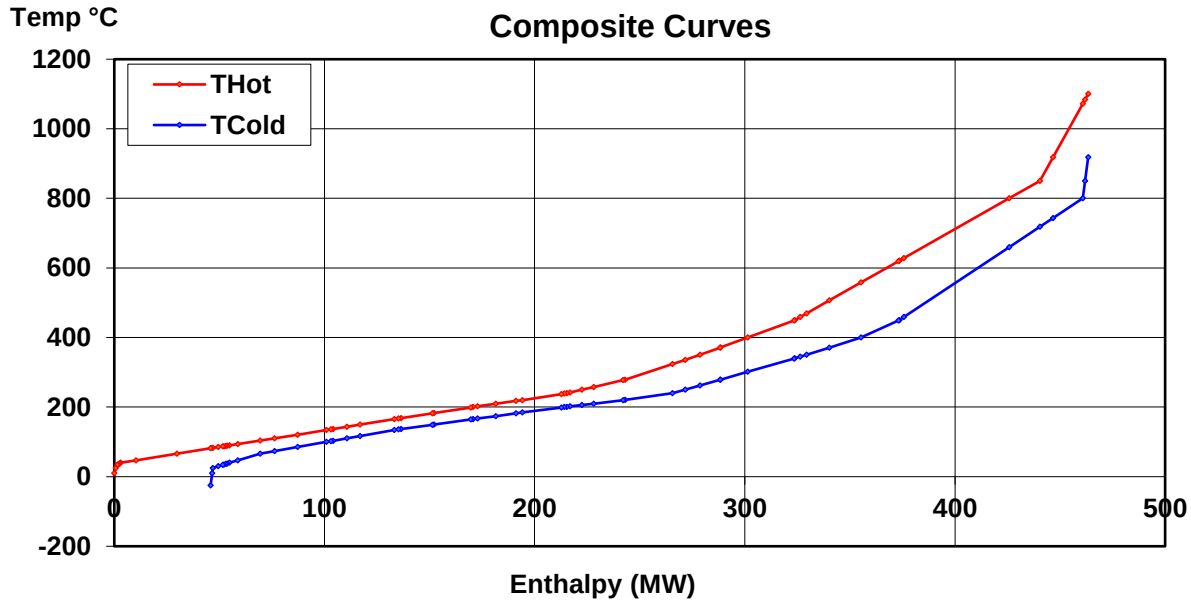

***Figure 6.6**. Heat integration for WP – BTL-MTJ*

The figure shows a need for cooling utilities, while there is no need for heating utilities, similar to the FT pathway. The total cooling utilities required for BTL and PBTL were 45.8 MW and 66.3 MW, respectively. This variation is because the configuration is different, and the number of heating and cooling streams are slightly different, requiring distinct heat exchanger networks. This means that the hot streams are enough to heat up all the cooled streams, while extra external

cooling water is needed to cool down the rest of the hot streams. Compared to FT configurations, which require cooling utilities of 240 MW and 363 MW for BTL and PBTL, respectively, this indicates that MTJ has a great potential to recycle energy from the streams back into the system more effectively than the FT process.

6.7 Simulation results

6.7.1 Methanol yield

Methanol is the first building block in the MTJ process for producing SAF. Therefore, the ratio of methanol yield produced through biomass should be validated against the literature data to ensure that the outcomes from the model are sensible. The yield values were cross-referenced against the literature values obtained from experimental work and other simulation results, as shown in table 6.3.

Table 6.3*. Comparison between the yields of methanol.*

Reference	Gasification type	Yield value (kg methanol/ Kg biomass) %
Yang et al. [159]	Fluidized bed	50-51
Trop et al. [153]	Entrained flow	64
Xiang et al. [160]	Entrained flow	63
Hannula et al. [161]	Fluidized bed	51.1
Anetjärvi et al [162] - BTL	Fluidized bed	51
Anetjärvi et al [162] - PBTL	Fluidized bed	70 – 101%
This study – BTL WCHQ/WCIQ	Fluidized bed	50.8 – 52.3
This study – PBTL WCHQ/WCIQ	Fluidized bed	79 - 81
This study – BTL - WP	Fluidized bed	59.5
This study – PBTL - WP	Fluidized bed	97

Table 6.3 confirms that the yield value (kg methanol /kg biomass) changes depending on several factors, including the type of gasification technology used to produce syngas and the feedstock used in the process. Moreover, the configuration, whether BTL or PBTL, influences the results.

In this study, the yield values for BTL were scattered across the range of 50.8%, 52.3%, and 59.5% for WCHQ, WCIQ, and WP, respectively. Meanwhile, the other literature values have differed in the 50 – 63% range. On the other hand, the PBTL setup produces the highest methanol yield at around 97% when wood pellets are used. Like the PBTL-FT process, the PBTL-MTJ tends to produce more hydrocarbons because there is no loss of carbon thanks to the external hydrogen that replaced the need for a WGS reactor. It was noticeable that there was a lack of literature data that evaluates the PBTL-MTJ configuration for SAF production. However, newly published papers like Anetjärvi et al. have confirmed the potential of such a configuration, which could be a game changer [159]. Anetjärvi *et al*. evaluated different scenarios for PBTL, where the yield varied from 70% to 101%. He assumed that hydrogen was increased to higher ratios to guarantee the conversion of both CO and CO_2 into methanol, where a yield of 101% of methanol per kg of biomass was obtained (the ratio does not sum the external hydrogen added). However, these results will still require further experimental validation.

Other factors, along with the difference in the gasification technology, can explain the deviation in the results mentioned in the literature, starting from the different moisture content of the utilized feedstocks in the literature data and the wood pellet and chips feedstocks used in this chapter. Moreover, the gasifying medium plays a role in providing high or low-quality syngas. Consequently, the syngas quality will affect the yield of methanol. On the other hand, the operational parameters selected for the synthesis also influence the final yield. Furthermore, recycling streams in the process configuration is another aspect to consider. Generally speaking, it is difficult to pinpoint a specific reason due to the differences in technologies, assumptions, and system boundaries. Overall, it can be concluded that when a high-quality syngas is associated with a recycle loop, the process will provide the highest yield of methanol. Consequently, the high yield of methanol will lead to achieve the highest yield of SAF.

6.7.2 SAF characteristics vs conventional jet fuel

Comparing the final product with the characteristics of a jet fuel A-1, which was given in the ASTM standard D7566, is needed to ensure the suitability of this process to produce SAF with the proper quality. Table 6.4 shows the results of the comparison.

Table 6.4. *Properties of conventional jet fuel vs SAF from biomass.*

Properties	**Conventional jet fuel A-1**	**MTJ BTL/PBTL SAF**	**Fischer Tropsch PBTL - SAF**	**Fischer Tropsch BTL - SAF**
Density kg/m_3	775-840	741.1	757.2	757.4
Net heating value MJ/kg	> 42.8	43.5	44.1	44.1
Average boiling point ºC	150 - 300	201.6	233.9	234.5
Flash point ºC	> 38	46.3	64	60.1
Freezing point ºC	Max. -47	-70	-53	-52.8

The table shows several similarities between SAF from MTJ, FT, and conventional jet fuel, where they have relatively similar net heating values and are within similar ranges when it comes to density. However, the flash point and average boiling point deviate significantly compared to each other. The reason behind the deviation is that in the MTJ process, the upgrading takes place in multiple stages to produce long-chain hydrocarbons, contrary to the FT process, which directly generates liquid hydrocarbons within its reactor. Moreover, the catalysts' nature and selectivity play a role in shaping the final product. Unlike the FT process, MTJ does not produce a significant amount of waxes or very long-chain hydrocarbons. This can be explained by looking at the diesel yield, which represents only around 7% of the total fuels, as shown in figure 6.4. All these factors contribute to the difference in the characteristics. Therefore, it can be noticed that the flash point is lower than FT due to the lack of longer-chain hydrocarbons. On the other hand, it is noticeable that the characteristics of both configurations of MTJ-BTL and MTJ-PBTL are the same, while for FT, there is a relatively small difference between them. This is because the upgrading section in the MTJ process does not have a recycle stream, and the process is linear. On the contrary, the FT process includes a recycle stream after the flash separators, as shown in the previous chapter in figure 5.3. Therefore, this influences

the hydrocarbon generation and flow in the system and causes slight variations in SAF properties.

6.7.3 SAF yield

After validating the methanol yield, the SAF yield was evaluated for both cases of BTL and PBTL for the different feedstocks, as shown in figure 6.7.

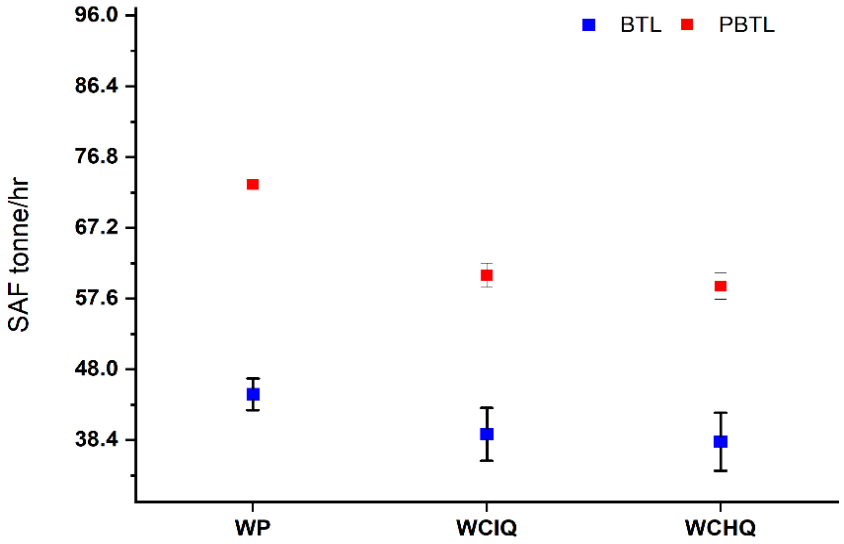

Figure 6.7. *SAF yield of different feedstocks in the BTL and PBTL configurations.*

The results reveal that WP's SAF yield is higher than WCIQ and WCHQ. Meanwhile, the PBTL outperforms the BTL as expected. This is because the methanol flow rate for the upgrading process was higher in the PBTL case compared to its counterpart in the BTL case. It should be mentioned that the error bars represent the uncertainty or variation of yield caused by the uncertainty of biomass characteristics. The overall yield uncertainty was higher for WCIQ and WCHQ than WP, as will be explained in detail in section 6.7.4. On the other hand, regardless of the configuration, the FT process yielded more SAF compared to the MTJ case. For example, for WP, the PBTL-FT case yielded approximately 96.1 t/h compared to 73.1 t/h from the PBTL-MTJ case. This is because the MTJ process does not only produce SAF but also diesel, gasoline, and LPG. Therefore, the selectivity to produce SAF is lower compared to FT. The carbon flow diagrams were drawn to understand the results better, as shown in figure 6.8.

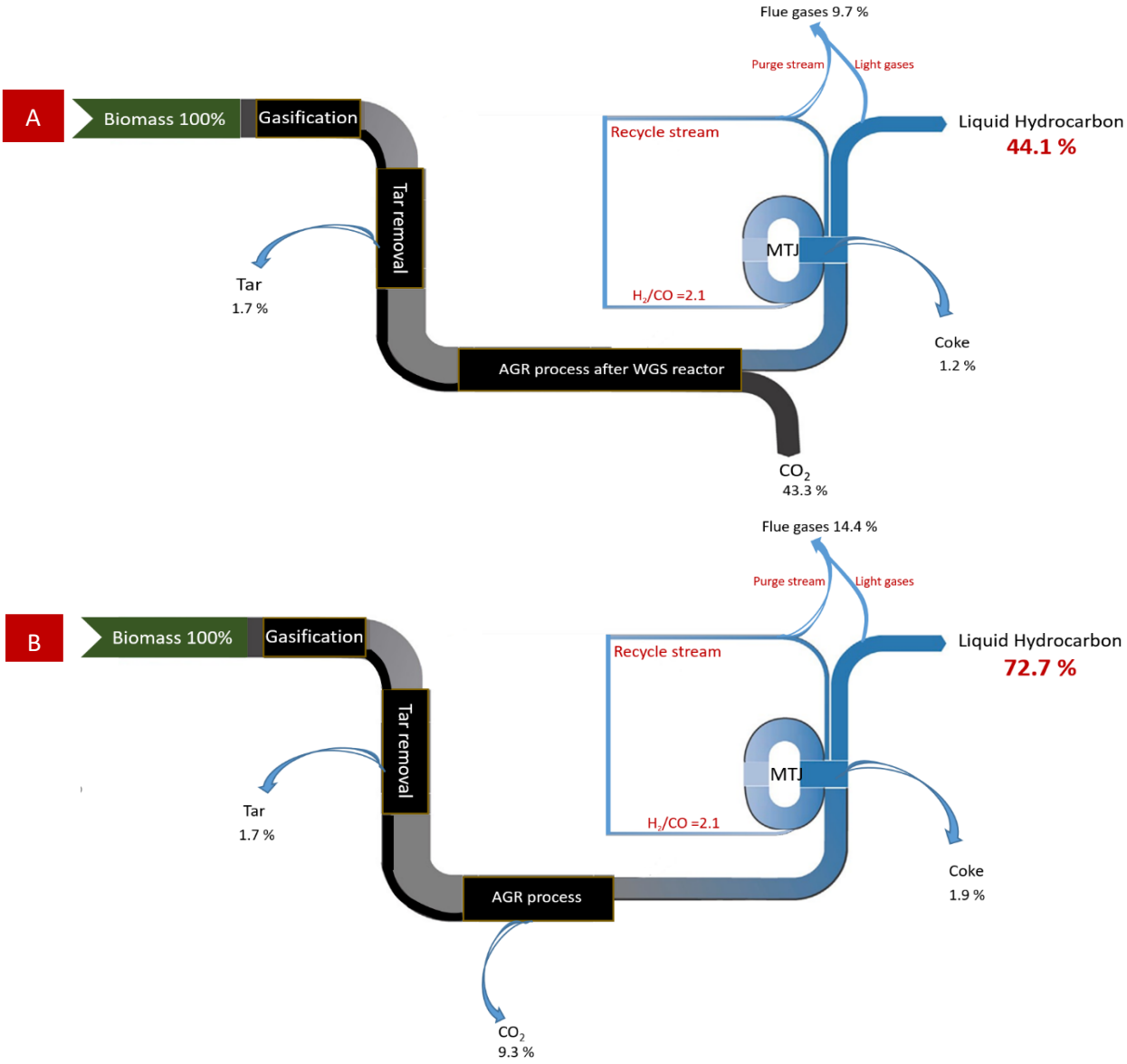

***Figure 6.8**. Carbon flow diagram of BTL (A) and PBTL (B) – WP feedstock. (The graph template is taken and adopted from Dossow et al. [129]).*

The carbon efficiency was evaluated for the WP as well as the other WCIQ and WCHQ. However, the figure only reflects the values for the WP as a case study, while the results of WCIQ and WCHQ followed an identical trend; therefore, they are not displayed here. The difference in carbon utilization between WP and other samples was around 2-3%. This conclusion is expected since WP produces more hydrocarbons than the other samples. One the other hand, when examining the overall carbon utilization, the MTJ process achieves higher efficiency than the FT process. This can be explained by the fact that there are several side streams associated with this process, such as diesel, gasoline, and LPG. The difference in carbon

efficiency for WP between the FT and MTJ processes was around 5.4% and 5.9% for the BTL and the PBTL setup, respectively.

6.7.4 Monte Carlo simulation – Uncertainty assessment

The Monte Carlo simulation was used to assess the variation in the yield caused by the uncertainty in the feedstock. Following the methodology explained in Chapter 4, the uncertainty was evaluated for the different cases. The Monte Carlo simulation has shown that output results followed normal distribution, while the distribution of the uncertainty parameters of biomass characteristics were the assumed the same as previously discussed in section 5.7.4. The results for the WP are shown in table 6.5.

Table 6.5. *Results of Monte Carlo simulation –MTJ*

WP Feedstock – Methanol – BTL-MTJ				
Value	Moisture content (MC) ± 5 %	Carbon (C) ± 0.30 %	Hydrogen (H) ± 0.047%	CH + Moisture (Overall uncertainty)
Average SAF yield (t/h)	44.59	44.60	44.59	44.60
SD (t/h)	0.15	0.25	0.004	0.48
Expanded uncertainty of SAF % (K=2) 95%	0.68	1.11	0.016	2.14
Relative value = Biomass parameter uncertainty /expanded uncertainty	0.14	3.70	0.34	
WP Feedstock – Methanol- PBTL-MTJ				
Average SAF yield (t/h)	73.10	73.10	73.10	73.10
SD (t/h)	0.25	0.20	0.006	0.36
Expanded uncertainty of SAF % (K=2) 95%	0.68	0.55	0.018	0.97
Relative value = Biomass parameter uncertainty /expanded uncertainty	0.14	1.83	0.38	

Similar to the FT pathway, the BTL-MTJ case has shown a higher uncertainty as the process setup clearly influences the uncertainty by increasing the deviation compared to the PBTL-MTJ. This is because of the accumulative effect caused by the presence of the WGS reactor and the sacrifice of carbon monoxide to produce more hydrogen, similar to the FT case. However,

the uncertainties in the FT configurations for the WP (2.5% - 1.02%) were slightly higher than those for the MTJ (2.14% – 0.97%). This outcome implies that the upgrading section has a minimum effect on the yield uncertainty compared to the H_2/CO ratio, the syngas production, cleaning, and purification part of the process. Results of WCIQ and WCHQ are shown in Appendix C in tables C2 and C3.

6.7.5 Techno-economic analysis

The procedure of techno-economic analysis was based on the information explained in section 4.6 for calculating the net production cost of SAF measured in dollars per tonne. Therefore, CAPEX, OPEX, and the annual fuel production were calculated. The applied scenarios, the utility cost, the CEPCI, and the equipment related to auxiliary (e.g., pumps), biomass gasification, and syngas production are the same as the ones mentioned in Chapter 5. Furthermore, the purchased costs for the equipment are calculated using equation 6.1, previously highlighted in Chapter 4. The reference cost, capacity, year, and unit of scale for the MTJ configurations were taken from the literature data, as summarized below in table 6.6.

Table 6.6. *Equipment cost for the MTJ process.*

Equipment	**EC_{ref}**	**Unit**	**S_{ref}**	**Design variable**	**Unit**	**D**	**Reference year**	**Reference**
Methanol reactor	8.22	MUSD	35.77	Feed input	kg/s	0.65	2009	[163]
Olefin's reactor	3.48	MUSD	10.6	Feed input	kg/s	0.65	2009	
Oligomerization	3.48	MUSD	10.6	Feed input	kg/s	0.65	2009	
DME reactor	0.609	MUSD	39.8	Feed input	kg/s	0.57	2009	[164]

The equipment costs were calculated as part of the fixed cost followed by the indirect cost calculation, relying on the assumptions provided in Appendix B in table B3. The breakdown ratios of the capital cost are not shown here since the assumptions were the same as the FT reactor. However, the total values of the total capital cost (TCI) differ from those of the FT process and on a configuration basis. The TCI values for the BTL-MTJ and PBTL-MTJ configurations were 2050.73 and 2017.2, M$, respectively. These values reflect that the PBTL

has a lower CAPEX than the BTL setup. However, it might sound illogical since an external hydrogen source was coupled with the process. However, the electrolyzer's cost has not been considered since the NPC of hydrogen was added to the utilities as part of OPEX. Moreover, WGS and ASU reactors were not needed in the process; therefore, their costs were excluded. Therefore, this observation reveals that the upgrading section in the MTJ process is less influential on the overall process than the part of biomass processing and syngas production and purification. To further validate this claim, a look at the CAPEX of the cases HMBTL and HCBTL can confirm this fact since an ASU is needed to supply oxygen where the TCI is 2279.9 M$ for both cases. Figure 6.9 shows the annualized capital cost (ACC) for MTJ compared side by side with FT pathway.

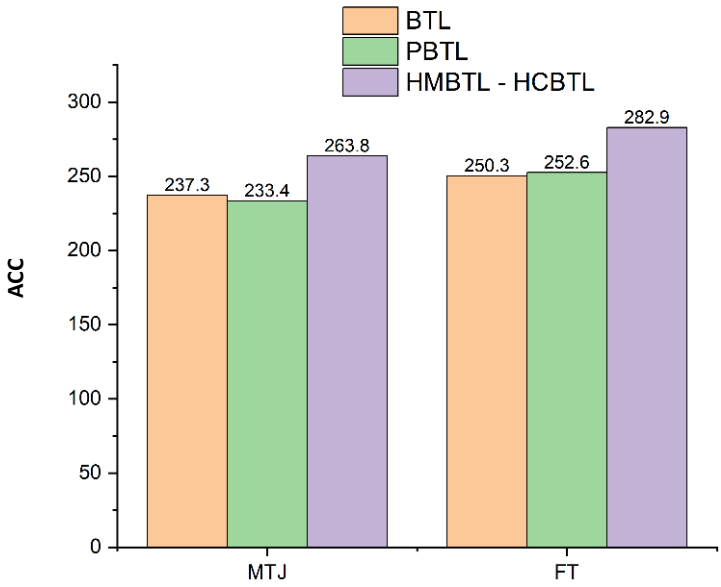

***Figure 6.9**. Annualized capital cost (ACC) for MTJ vs FT.*

PBTL and HMBTL/HCBTL have the same upgrading section with the same scale; however, the capital cost is significantly different. This is because HMBTL/HCBTL requires an ASU, which makes them have the highest ACC. As ASU is needed to provide oxygen for the gasifier, it causes the part of the syngas production process to have a stronger effect on the overall ACC than the upgrading section in the MTJ process. On the other hand, the ACC of MTJ is always lower than the FT when using the same mass flow rate of feedstock. However, for the MTJ plant to produce the same quantity of SAF as the FT, it will require a bigger feed of biomass and larger capital investment, which causes the ACC of the MTJ process to surpass FT. This was confirmed when compared with the results presented by Gonzalez et al., who recorded an increase in annual investment by 24% for the MTJ process compared to the FT when designed to produce the same quantity of SAF [165].

Contrary to the MTJ, the ACC cost of the PBTL-FT process is relatively more costly than BTL-FT, even though no cost for electrolyzer or ASU is assumed. This shows that the upgrading cost in the FT process is more influential on the ACC than the MTJ process due to the need for much larger equipment to accommodate the recycle streams in the FT reactor and the hydrocracker. Figure 6.10 shows the breakdown of the equipment costs in the BTL and PBTL setup.

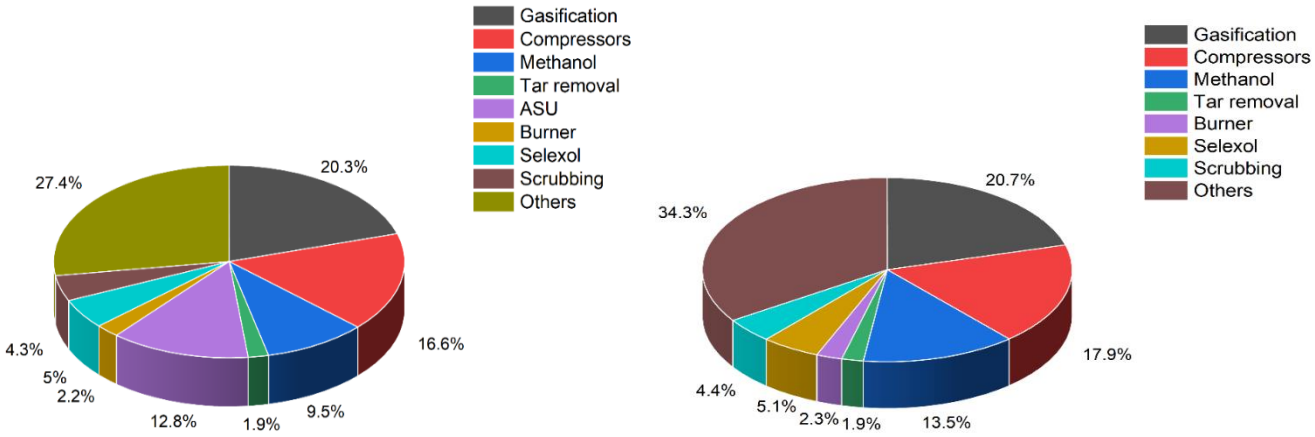

***Figure 6.10**. Breakdown of equipment costs for BTL (Left) and PBTL (Right) – MTJ -WP.*

In the breakdown of the BTL setup, gasification, compressors, and ASU make up most of the total equipment costs. In the PBTL cost, a similar pattern was noticed; however, no ASU is included when green hydrogen is used. Therefore, the methanol reactor comes third as the largest contributor. On the other hand, the term "others" represents multiple equipment, such as pumps, heat exchangers, flash drums, and other auxiliary equipment. These breakdown percentages can change depending on the initial reference data, unit of scale, and assumptions used to estimate the cost of each equipment. OPEX was evaluated for the different cases of MTJ, while only the results of the BTL case are shown in figure 6.11.

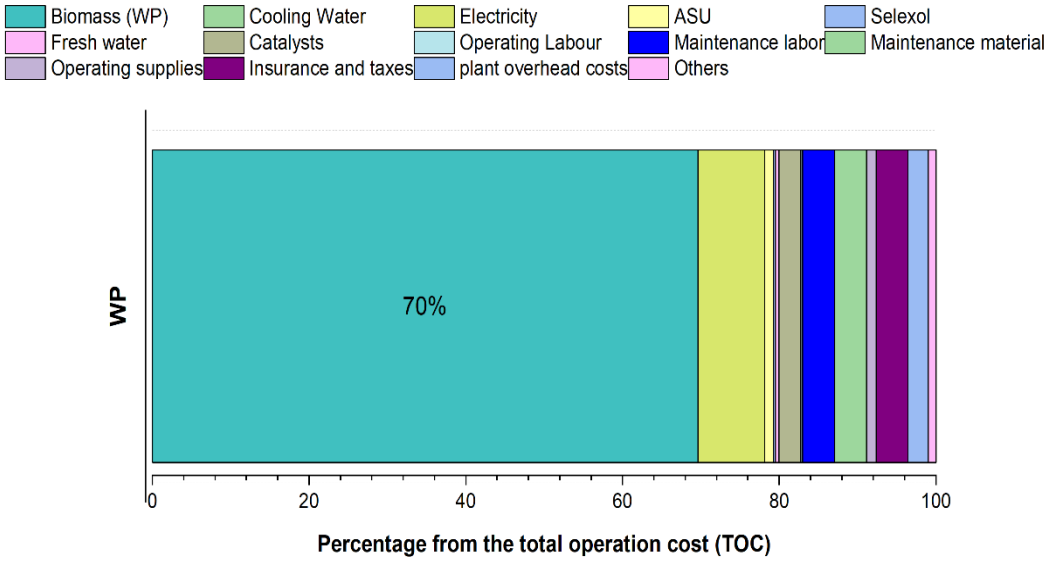

***Figure 6.11**. Breakdown of total operating cost (TOC) for BTL – MTJ -WP.*

For the BTL-MTJ case, the breakdown was relatively similar to the one obtained from the FT pathway in figure 5.13. The total value of OPEX for the BTL-MTJ was around 902 M$/a compared to 894.5 M$/a for BTL-FT. The increase in MTJ's OPEX compared to the FT process comes from the slight increase in utility consumption. The biomass cost in the BTL-MTJ still represents the majority of OPEX with around 70% of the total OPEX compared to 71% for the BTL-FT case. For the PBTL-MTJ case, which was not displayed in figure 6.11, a similar pattern was noticeable to the PBTL-FT, where green hydrogen represented the majority of OPEX, followed by biomass with a share of 60% and 28%, respectively. The total OPEX for PBTL-MTJ and PBTL-FT was 2241 and 2216.2 MUSD, respectively. For all OPEX and CAPEX for the remaining cases of HMBTL-MTJ and HCBTL-MTJ and the results of WCIQ and WCHQ, see Appendix C, table C4. After estimating both CAPEX and OPEX, the NPC results for the different cases and samples were computed, as shown in figure 6.12.

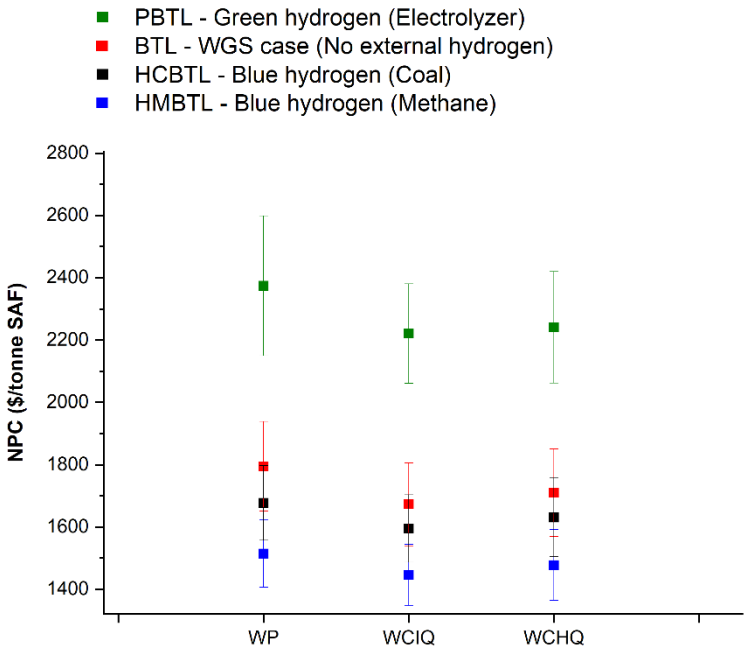

***Figure 6.12**. NPC results for different wood types and hydrogen sources – MTJ.*

Figure 6.12 confirms that WP feedstock produces more expensive SAF than its counterpart from wood chips. The most expensive form of SAF from WP as feedstock comes from the PBTL configuration at an NPC of 2375 USD per tonne. On the contrary, the WCIQ was the most suitable type of wood for SAF production across all configurations with the cheapest possible at 1446.3 USD per tonne when using methane blue hydrogen (HMBTL). On the other hand, MTJ produces cheaper SAF than FT, with around 8% to 13% depending on the configuration. Overall, using blue hydrogen rather than green hydrogen stands out as the most economical configuration in the FT and MTJ pathways.

Moreover, the results of HMBTL configuration are relatively close to the conventional jet fuel, which was priced at around 925 $/t estimated at the beginning of December 2023 [166]. Therefore, it can be concluded that the cheapest form of SAF is around 1.56 times more expensive than conventional jet fuel. It is worth noting that the error bars in the graph represent the accumulative uncertainty caused by the influence of the uncertainty of the feedstock characteristics on SAF cost, plus the uncertainty caused by the variation in the operating parameters, which is explained in detail in the next section.

6.7.6 Uncertainty analysis

Before the Monte Carlo simulation, a sensitivity analysis is typically needed to determine the parameters that influence the cost the strongest. However, since the process inputs and the syngas production section are the same as the FT process, there was no need to include such an analysis. Moreover, the upgrading section in the MTJ process does not require special additional feedstocks/materials that could exponentially increase the OPEX. The costs associated with the upgrading part of the MTJ process are mainly related to the equipment costs and the electricity needed to run the process. Therefore, the Monte Carlo simulation followed the methodology explained in section 4.6, where the SAF yield, electricity, biomass, and hydrogen costs were varied. It should be clarified that the random values generated for the SAF yield resulted from the uncertainty of biomass characteristics. The results of the cost uncertainty caused by biomass characteristics and OPEX are summarized in table 6.7.

Table 6.7. *Summary of the uncertainty of SAF cost for methanol configurations.*

Factor (NPC)	BTL -MTJ	PBTL -MTJ	HMBTL - MTJ	HCBTL-MTJ
Wood Pellet (WP)				
Cost uncertainty (U) due to Biomass characteristics uncertainty - WP	1.29	0.587	0.585	0.585
Cost uncertainty (U) due to OPEX uncertainty K=2, 95% - WP	6.73	7.28	6.75	6.79
Overall Cost Uncertainty (WP)	8.02	7.87	7.05	7.09
Wood chips industrial quality (WCIQ)				
Cost uncertainty (U) due to Biomass characteristics uncertainty - WCIQ	2.17	0.99	0.99	0.99
Cost uncertainty (U) due to OPEX uncertainty K=2, 95% - WCIQ	5.79	6.02	5.68	5.71
Overall Cost Uncertainty (WCIQ)	7.96	7.01	6.67	6.7
Wood chips high quality (WCHQ)				
Cost uncertainty (U) due to Biomass characteristics uncertainty - WCHQ	2.37	1.09	1.09	1.09
Cost uncertainty (U) due to OPEX uncertainty K=2, 95% - WCHQ	5.85	6.70	6.53	6.52
Overall Cost Uncertainty (WCHQ)	8.2	7.8	7.62	7.61

Regardless of the feedstock, the results reveal that the cost uncertainty in the BTL configuration is higher than in all other configurations, whether using green or blue hydrogen as in the PBTL and HMBTL/HCBTL, respectively. However, when these results are compared side by side with the results of FT previously shown in tables 5.5 and 5.8, it is noticeable that the cost uncertainty associated with the FT pathway is higher in all feedstocks and configurations. This leads to the conclusion that the nature of the configurations and the equipment arrangement could maximize or minimize the uncertainty, especially considering that FT has more recycle streams and separators.

6.7.7 Efficiency evaluation

Following the procedure explained in section 4.7, the key performance indicators for the processes were evaluated and compared with the literature data. The values of flow rates and LHV were taken from the model and the experimental results. Table 6.8 shows this comparison adopted from Astonios, et al [85].

Table 6.8. *Comparison between the process performance and the literature [85,118,140].*

Study	**Technology**	**Y_{SAF}**	***f_{SAF}***	**EJFE**	**η_{tot}**	**$\eta_{tot\text{-}fuels}$**
Ruokonen et al	rWGS MeOH	7.6%	21.8%	21.8%	21.8%	77.4%
Astonios et al	CO_2 - MeOH	22%	85.8%	45.5%	45.5%	52.9%
This study	BTL-MTJ	14.9%	60.2%	29.1%	28.8%	51.0%
This study	PBTL-MTJ	24.4%	60.3%	47.8%	47.0%	83.6%

The table shows how the PBTL-MTJ configuration outperforms all other configurations, where more SAF is produced with a yield of 24.4%, followed by the conventional PTL with 22%. In the case of Ruokonen et al, the simulation was not optimized to maximize the production of SAF but instead to produce a mix of transportation hydrocarbons [151]. However, this proves the sensitivity of configuration optimization since most catalysts used in this process have a broad selectivity. Moreover, it was highly noticeable that there is a lack in the literature evaluating different configurations and scenarios for the MTJ pathway utilizing biomass, as it was difficult to validate these outcomes based on commercial or experimental results.

6.8 Conclusions

The analysis reveals that wood chips of industrial quality, despite their relatively high moisture and ash content, stand out as the most economical feedstock for sustainable aviation fuel production in both Fischer-Tropsch and Methanol-to-Jet pathways. In comparison, MTJ demonstrates a lower net production cost than the FT process, yet both pathways are more expensive than conventional jet fuel, with ratios ranging from 1.56 to 2.57 for MTJ and 1.79 to 2.8 for FT. Applying a carbon fee to conventional jet fuel or providing subsidies to SAF's CAPEX and OPEX would narrow the cost gap. These subsidies would make SAF a competitive solution for decarbonizing the aviation sector. Similar to the FT process, OPEX's uncertainty is more influential on the overall SAF cost than the uncertainty in biomass characteristics. On the other hand, the analysis reveals that PBTL-MTJ has the highest overall efficiency and yield of 47% and 24.4% compared to BTL-MTJ of 28.8% and 14.9%, and PTL of 45.5% and 22%, respectively. Additionally, further analysis is essential to investigate operational challenges linked to using a feedstock with high uncertainty or a mix of feedstocks with different qualities, which necessitates testing in experimental facilities.

Nomenclature

MeOH	Methanol
MTJ	Methanol to Jet
MTO	Methanol to olefins
MOGD	Mobil olefins to gasoline and distillate
ZSM	Zeolite Socony Mobil
HZSM	High-Silica Zeolite Socony Mobil
DME	Dimethyl ether
LPG	Liquified petroleum gas
SMR	Steam methane reformer

CHAPTER 7

Chapter 7. Conclusions and Outlook

7.1 Conclusions

Focusing on minimizing financial losses caused by unreliable biomass measurements, this research focused on improving the existing metrological procedures to overcome the challenges of characterizing biomass. Moreover, the thesis evaluated the impact of biomass characteristics and its uncertainty on process yield, efficiency, and cost. The work progressed through three distinct phases:

Firstly, an experimental phase where three different types of woody biomass (wood chips industrial quality, high quality, and wood pellets) were analyzed. The results led to the proposal of a modified experimental practice and provided several solutions to avoid the typical mistakes during measurements. Moreover, a detailed uncertainty budget was introduced for the measurements of energy content, where the uncertainty sources were specified and quantified. This uncertainty budget was eventually conveyed to the ISO committee, hoping to be introduced in the next version of the standard. Following the newly recommended experimental practice, the repeatability has been improved by around 50–80%, while the final relative expanded uncertainty was enhanced by 10–30%. The maximum relative expanded uncertainty was approximately ±1%, representing a substantial reduction compared to the typical uncertainty range available in the literature of 5%. This improved practice helps the biomass providers and end-users to ensure comparable results and avoid a potential financial loss.

On the other hand, elemental analysis was used to determine the biomass composition as it served as an alternative method to measure the energy content; however, it faced several challenges since sulfur content was barely detectable and required other technologies for determination, which added unnecessary complexity to the determination of energy content. On the contrary, elemental analysis is a decisive tool when simulating sustainable aviation production from biomass, as it is the main building block for the model.

Secondly, a comprehensive analysis of sustainable aviation fuel policies, technologies, and pathways was performed, covering technical and non-technical aspects where the most promising SAF pathway for process simulation was decided. The Fischer Tropsch process coupled with gasification was selected as it is the most flexible pathway in terms of its suitability to utilize different feedstocks and its high sustainability credentials with a substantial emissions

reduction of approximately 7.7 to 12.2 gCO_{2e}/MJ compared to the conventional jet fuel baseline of 89 gCO_{2e}/MJ. Moreover, this pathway uses locally available feedstocks, which makes the EU capable of sustaining itself without relying on imports and without compromising the aviation sector in the case of any disruption in the supply chain caused by natural phenomena or due to geopolitical storms. On the other hand, this comprehensive analysis proved that the EU is indeed capable of meeting its SAF uptake targets in 2030 by using the available feedstocks and technologies. However, by 2050, a deficit of 1.35 Mt of SAF was estimated due to the EU's lack of available bio-based feedstocks. This deficit corresponds to the need for an extra 2.4 Mt of waste fats, oils, and grains (FOGs) or approximately 10.8 Mt of agricultural residuals and cover crops in 2050. This requires the EU to introduce additional policy frameworks to redirect more biomass towards SAF production to ensure meeting the long-term SAF demand or alternatively importing these feedstocks from the neighboring Balkan states where the bio-waste is largely unused. This deficit revealed that the existing technologies are still inefficient enough to meet all SAF targets; therefore, non-approved ASTM pathways such as Methanol to Jet must be studied to evaluate their performance and economic viability.

Thirdly, the Fischer Tropsch coupled with gasification as an approved ASTM pathway along with the Methanol to Jet as a non-approved ASTM pathway were simulated using the experimental data for the three different types of woody biomass that were measured in the first phase. Each pathway was modeled twice for two configurations, with and without an external hydrogen source, PBTL and BTL, respectively. The results revealed that the uncertainty of biomass characteristics influences the SAF yield and cost, depending on the pathway. For the FT process, the influence of biomass characteristics and its uncertainty on the SAF yield ranged from 1.03% to 4.81%. At the same time, the impact on cost varied from 0.89%-4.2%, depending on which sample and configuration was used. For the MTJ process, the influence was relatively less, ranging from 0.97% to 3.95% for the yield while ranging from 0.587%-2.37% on SAF cost. However, when assessing the uncertainty on SAF cost caused by OPEX's uncertainty, it was found that it causes a more considerable influence compared to the biomass characteristics ranging from 5.42% to 7.26% and 5.68% to 7.28% for the FT and MTJ process, respectively. However, OPEX uncertainty combined multiple factors; therefore, it is logical that it had a higher impact than biomass characteristics. In addition to the fact that any uncertainty in biomass characteristics would potentially correspond to operational challenges in the plant, which requires experimental validation to assess its actual impact, which was not available within the scope of this thesis.

On the other hand, the wood pellet produced more sustainable aviation fuel in both pathways due to its higher carbon and hydrogen content by 3.14% and 0.23%, respectively, compared to the wood chips. Therefore, this led to the production of more high-quality syngas, which was suitable for upgrading to SAF. However, configuration-wise, the PBTL setup produced more SAF as it had a higher carbon conversion efficiency than the BTL setup. The PBTL efficiency was around 67.3% and 72.7% for the FT and MTJ processes, respectively. MTJ had a higher carbon conversion as it could produce different types of fuels, unlike the FT process, where the product was primarily SAF. From an economic perspective and regardless of which feedstock was used, the HMBTL setup (methane blue hydrogen) was more economical than using green hydrogen (PBTL), coal blue hydrogen (HCBTL), or the BTL, where it costs for WCIQ, 1655 $/t and 1446.3 $/t for the FT and MTJ process, respectively. While using blue hydrogen would indeed increase the environmental footprint of the process, it remains a fair compromise to achieve the EU's SAF uptake targets while significantly cutting emissions. Moreover, the analysis revealed that wood chips of industrial quality stand out as the most economical wood feedstock for sustainable aviation fuel production in Fischer-Tropsch and Methanol pathways despite their lower quality compared to wood pellets.

In comparison, Methanol to Jet demonstrated a lower net production cost than the Fischer Tropsch process, yet both pathways are more expensive than conventional jet fuel, with ratios ranging from 1.56-2.57 and 1.79-2.8 for Methanol to Jet and Fischer Tropsch pathways, respectively. With conventional jet fuel sitting at 925 $ per tonne, two policy options can bridge the cost gap with SAF and accelerate aviation decarbonization: a carbon tax or direct subsidies for SAF production (CAPEX and OPEX). Both strategies would eventually make SAF a more competitive option and boost its utilization across the EU.

7.2 Outlook

New techniques are needed for biomass characterization, focusing on online measurements that could take place in real-time to be installed on the production line since the current technologies are based on wet chemistry techniques, which are typically slow and time-consuming. Therefore, the new techniques should aim to provide faster and more efficient results with low uncertainty.

Besides the experimental techniques and simulation results, experimental validation in a pilot plant is necessary to enhance the results and facilitate the identification of key areas for improvement in the process. Additionally, the pilot facility would reveal the operational difficulties caused when mixing different feedstocks with different qualities simultaneously, which would not be possible through simulation work alone. Moreover, the analysis was focused on the uncertainty of biomass characteristics and OPEX. In reality, several sources of uncertainty are associated with equipment dimensioning, sensor draft, seasonal fluctuation, and supply chain that would need to be assessed in future work in detail.

This analysis focused on two different configurations, BTL and PBTL; however, superstructure optimization could be used to widen the scope by analyzing all the potential configurations and combinations of technologies to specify the most efficient and cost-effective routes. Testing the economic viability of utilizing a combination of steam and O_2 for gasification or a completely different technology like chemical loop gasification would be necessary before drawing any concrete conclusion about the best setup for SAF production.

Ultimately, it is noted that Methanol to Jet, as a non-approved ASTM pathway, was investigated, but it is only one technology among others that await approval. Hence, future research should explore other novel SAF pathways like waste pyrolysis and algae to validate their potential for SAF production. These alternatives may offer more appealing solutions than current SAF technologies [167–169].

Appendix A

1- Information on additional tests performed - Attempts to combust 1 g of the samples

Several trials were performed by testing several factors to check the combustion of 1 g of the sample as follows:

Several oxygen pressures were tested: 28, 30, 31, and 33 bar. In all these cases, incomplete combustion was observed, but when the pressure exceeded 33 bars, the sample tended to explode extremely inside the bomb. In case of lower oxygen pressure of around 28 bars, the sample still didn't give complete combustion, but only tiny parts of the sample exploded. Different bombs with different volumes of 350 and 250 mL were used, and the bomb head (cover) was replaced three times by older and newer ones. No complete combustion was observed.

Multiple crucibles have been used: 2 platinum crucibles weighing 10 and 12 g, fused silica crucibles weighing 12 and 14 g, and a platinum crucible weighing 5 g. No complete combustion was observed, but the combustion showed a slightly different pattern from one crucible to another. The sample combustion in the crucibles made of platinum exploded, and parts jumped out of the crucible to drop to the bottom of the bomb. In the case of the crucibles made of fused silica, which is relatively thicker with less heat conductivity, the combustion seemed to be slower, and therefore, it didn't severally explode. For the crucible that weighed 5 g, the sample exploded and scattered all over the bomb.

Different fuse setups with different samples were tested to check the combustion. A wire of platinum, a wire of platinum with a cotton thread, a wire of nickel, and a wire of nickel with a cotton thread were tested. In all these cases, no complete combustion was recorded.

Based on these findings, the applied pressure to form the pellet was evaluated as the last possible cause behind the incomplete combustion, which is clarified in the main text.

Table A1. *The moisture content of different samples in cycle 1 and cycle 2.*

Parameter	**PTB**		**TUBITAK**		**BRML**	
Cycle	Cycle 1	Cycle 2	Cycle 1	Cycle 2	Cycle 1	Cycle 2
MC % WC-HQ	10.5	10.86	11.83	11.77	6.2	11.1
MC % WC-IQ	10.2	10.59	11.63	11.51	7	10.2
MC % WP	5.6	5.68	6.05	5.72	5.9	6.4
Mass range	0.30-0.45	0.26-0.59	0.41-0.51	0.42-0.59	1.40-1.43	0.50-0.53

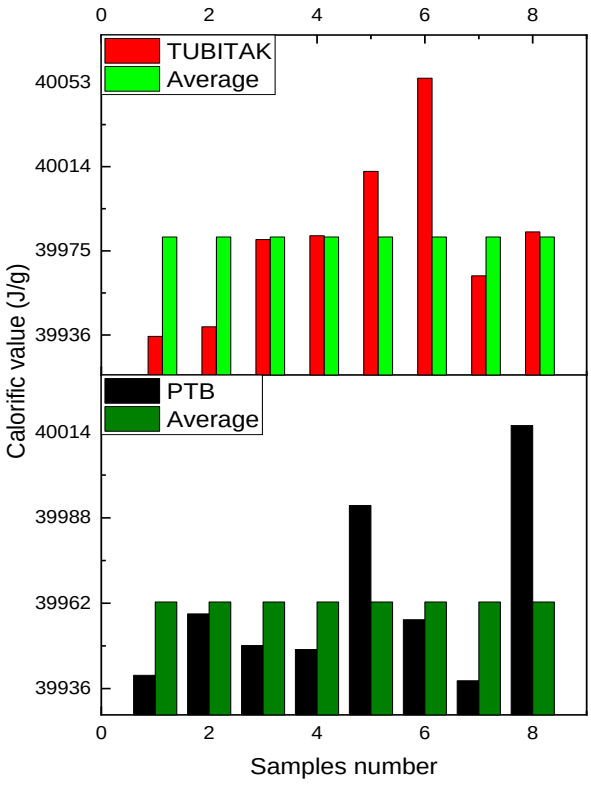

Figure A1*. Comparison between the calorific value of biodiesel between TUBITAK and PTB.*

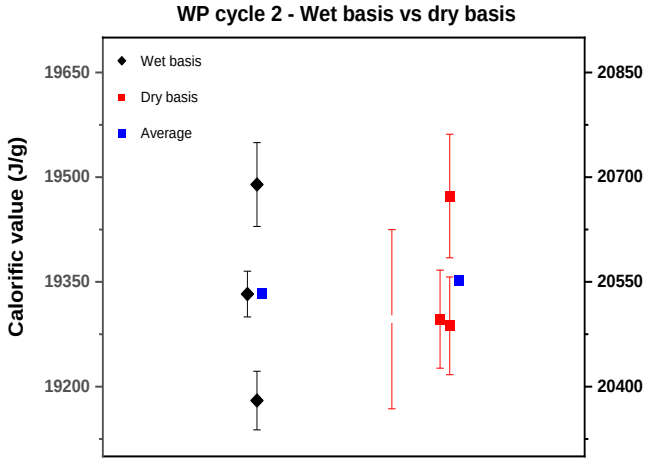

Figure A2. *Uncertainty of WP at PTB with and without the heterogeneity factor.*

The figure shows the difference in the uncertainty (error bar) in the case of adding the uncertainty caused by the heterogeneity/reproducibility to the final total uncertainty. If this factor is not added, all three institutes and their values won't overlap at any point. To have a well-representing uncertainty, this factor should be added. With this factor, the uncertainty now extends to overlap with the other institutes.

Appendix B

Section 4.6: the following code was used for the Monte Carlo simulation to generate random values that follow normal and rectangular distributions.

The code generates random values that cover the upper and lower limits of the uncertainty. The code has 99.7% coverage to ensure that the random values represent the whole uncertainty range. The code was generated with the aid of ChatGPT.

1- Normal Distribution code

```
import random

# Define the range of the uncertainty

lower_bound =

upper_bound =

# Define the mean and standard deviation for the normal distribution

mean = (lower_bound + upper_bound) / 2

std_dev = (upper_bound - lower_bound) / (2 * 3.29)  # 3.29 corresponds to
99.7% confidence interval

# Generate 1000 random values from a normal distribution within the range of
-- and --

random_values = []

while len(random_values) < 1000:

    value = random.gauss(mean, std_dev)

    if lower_bound <= value <= upper_bound:

        random_values.append(value)

# Print the generated random values

for value in random_values:

    print(value)
```

2- Rectangular distribution code

```
import random
# Define the range of the uniform distribution
min_value = ---
```

```
max_value = ---

# Generate 1000 random values from the rectangular distribution
random_values = [random.uniform(min_value, max_value) for _ in range(100)]

# Print the generated random values
for value in random_values:
    print(value)
```

Section 5.6: The thesis does not focus on how the different types of gasifiers and gasifying mediums affect the final yield or performance of the gasification. However, a single case based on the BTL setup for WP feedstock was analyzed to compute the possible influence of another gasifying medium on the final cost of SAF. It was noticeable that when a mix of steam and oxygen was utilized, the final SAF cost varied in the range of 2-4%. This is because a small ASU unit was needed, and less electricity for it. Consequently, this has contributed, along with the change in the yield, in varying the final cost. Therefore, further study is needed to map and test all the different scenarios and feedstocks to determine the optimum gasification setup and operating conditions that achieve the lowest cost of SAF. On the other hand, the thesis focused on replicating an existing pilot plant for gasification for simplification, as the aim of the thesis goes beyond a specific unit of operation.

Section 5.7.4: the following code was used for the Monte Carlo simulation to couple Aspen Plus and excel with python:

The code is intended to utilize the previously generated random data that was introduced to an excel file. The code then introduces each parameter value to Aspen Plus while ensuring that the total composition of biomass is 100%. The code was generated with the aid of ChatGPT.

```
import win32com.client as win32

import openpyxl

# Set the file path to the Aspen Plus simulation

aspen_path                                                                    =
r'C:\Users\ShehabM\Desktop\1672023\Differentcatalyst\WCHQvfcat.bkp'

# Set the file path to the Excel sheet

excel_path = r'C:\Users\ShehabMGAM\Desktop\values.xlsx'

# Connect to Aspen Plus

aspen = win32.Dispatch('Apwn.Document')

aspen.InitFromArchive2(aspen_path)
```

```
# Specify the column names in the Excel sheet
moisture_column = 'A'
carbon_column = 'B'
hydrogen_column = 'C'
oxygen_column = 'D'
# Specify the path to change moisture, carbon, hydrogen, and oxygen
moisture_path = r"\Data\Streams\BIOMASS\Input\ELEM\NC\BIOMASS\PROXANAL\#0"
carbon_path = r"\Data\Streams\BIOMASS\Input\ELEM\NC\BIOMASS\ULTANAL\#1"
hydrogen_path = r"\Data\Streams\BIOMASS\Input\ELEM\NC\BIOMASS\ULTANAL\#2"
Oxygen_path = r"\Data\Streams\BIOMASS\Input\ELEM\NC\BIOMASS\ULTANAL\#6"
# Specify the path to record output value
output_path = r"\Data\Streams\JETFUEL\Output\MASSFLMX_LIQ"
# Load the Excel sheet
workbook = openpyxl.load_workbook(excel_path)
sheet = workbook.active
# Get the number of rows in the sheet
num_rows = sheet.max_row
# Loop through each row in the Excel sheet
for row in range(2, num_rows + 1):
    # Get the moisture, carbon, hydrogen, and oxygen values from the Excel
sheet
    moisture = sheet[f'{moisture_column}{row}'].value
    carbon = sheet[f'{carbon_column}{row}'].value
    hydrogen = sheet[f'{hydrogen_column}{row}'].value
    oxygen = sheet[f'{oxygen_column}{row}'].value
    # Set the moisture, carbon, hydrogen, and oxygen in Aspen Plus
    aspen.Tree.FindNode(moisture_path).Value = moisture
    aspen.Tree.FindNode(carbon_path).Value = carbon
```

```
    aspen.Tree.FindNode(hydrogen_path).Value = hydrogen
    aspen.Tree.FindNode(Oxygen_path).Value = oxygen
    # Run the Aspen Plus simulation
    aspen.Engine.Run2()
    # Get the output node
    output_node = aspen.Tree.FindNode(output_path)
    # Check if the output node has a value
    if output_node is not None and output_node.Value is not None:
        # Print the output value
        print(f"Moisture: {moisture} | Carbon: {carbon} | Hydrogen: {hydrogen} | Oxygen: {oxygen} | Output Value: {output_node.Value}")
    else:
        print(f"Output Path has no value for Moisture: {moisture} | Carbon: {carbon} | Hydrogen: {hydrogen} | Oxygen: {oxygen}")
# Close Aspen Plus
aspen.Close()
```

1- The results of Monte Carlo for WCIQ and WCHQ in the Fischer Tropsch process are shown below:

Table B1. *Monte Carlo results of WCIQ – FT.*

	Moisture content (MC) ± 5 %	Carbon (C) ± 0.30 %	Hydrogen (H) ± 0.047%	CH + Moisture (Overall uncertainty)
WCIQ Feedstock – BTL				
Average SAF yield (t/h)	47.68	47.68	47.68	47.68
SD (t/h)	0.89	0.42	0.007	1.04
Expanded uncertainty of SAF % (K=2) 95%	3.74	1.76	0.003	4.38
Relative value = Biomass parameter uncertainty /expanded uncertainty	0.75	5.18	0.02	--
WCIQ Feedstock – PBTL				
Average SAF yield (t/h)	79.09	79.09	79.09	79.14
SD (t/h)	0.59	0.31	0.047	0.70
Expanded uncertainty of SAF % (K=2) 95%	1.49	0.78	0.12	1.76
Relative value = Biomass parameter uncertainty /expanded uncertainty	0.29	2.29	0.86	--

Table B2. *Monte Carlo results of WCHQ – FT.*

WCHQ Feedstock – BTL				
	Moisture content (MC) ± 5 %	Carbon (C) ± 0.30 %	Hydrogen (H) ± 0.047%	CH + Moisture (Overall uncertainty)
Average SAF yield (t/h)	46.38	46.38	46.38	46.38
SD (t/h)	0.91	0.44	0.0012	1.12
Expanded uncertainty of SAF % (K=2) 95%	3.93	1.88	0.005	4.81
Relative value = Biomass parameter uncertainty /expanded uncertainty	0.79	5.08	0.03	--
WCHQ Feedstock – PBTL				
Average SAF yield (t/h)	76.99	76.99	76.99	77
SD (t/h)	0.59	0.32	0.073	0.75
Expanded uncertainty of SAF % (K=2) 95%	1.55	0.83	0.19	1.95
Relative value = Biomass parameter uncertainty /expanded uncertainty	0.31	2.24	0.91	--

Table B3. *Factors of direct and indirect FCI cost and OPEX were copied from Albrecht et al.[83].*

Factor	j	Basis	value
Total direct plant costs (D)			
Equipment installation	1	EC	0.39
Instrumentation and control	2	EC	0.26
Piping (installed)	3	EC	0.31
Electrical (installed)	4	EC	0.10
Buildings including services	5	EC	0.29
Yard improvements	6	EC	0.12
Service facilities (installed)	7	EC	0.55
Total indirect plant costs (I)			
Engineering and supervision	8	EC	0.32
Construction expenses	9	EC	0.34
Legal expenses	10	EC	0.04
As function of total direct and indirect costs (D + I)			
Contractor's fee	11	D + I	0.05
Contingency	12	D + I	0.1

Opex Estimation	j	Basis	Value
Operating supervision	1	OL[a]	0.15
Maintenance labor	2	FCI	0.01
Maintenance material	3	FCI	0.01
Operating supplies	4	M[b]	0.15
Laboratory charges	5	OL[a]	0.2
Insurance and taxes	6	FCI	0.02
Plant overhead costs	7	TLC[c]	0.6
Administrative costs	8	PO	0.25

[a)] OL = Operating labor
[b)] M = Maintenance labor & maintenance material
[c)] TLC = total labor costs consisting of operating labor, operating supervision, and maintenance labor
[d)] PO = Plant overhead costs

***Table B4**. Detailed results of TEA for WP, WCIQ, and WCHQ – Fischer Tropsch process.*

Sample	SAF NPC $ per tonne	OPEX (MUSD)	ACC (MUSD)	CAPEX (MUSD)
WP – BTL	2130.29	894.59	250.31	1946.89
WP – PBTL	2588.12	2216.16	252.58	1964.54
WP – HMBTL	1669.08	1309.10	282.98	2201.02
WP - HCBTL	1848.38	1480.14	282.98	2201.02
WCIQ - BTL	1985.62	688.4	246.86	1920.03
WCIQ – PBTL	2496.18	1691.99	247.35	1923.82
WCIQ – HMBTL	1655.26	1010.25	275.76	2144.82
WCIQ - HCBTL	1821.55	1139.44	275.76	2144.82
WCHQ - BTL	2041.88	687.93	246.86	1920.02
WCHQ – PBTL	2518.78	1662.07	242.69	1887.64
WCHQ – HMBTL	1678.88	998.89	270.72	2105.62
WCHQ - HCBTL	1845.13	1124.62	270.72	2105.62

Appendix C

Table C1. *The reactions of the MOGD process were taken from Tufail Ahmed* ***[147].***

	Reaction	Fraction conversion	Overall conversion
Propene	5 Propene → 3 Pentene	0.18%	90%
	2 Propene → Hexene	2.43%	
	7 Propene → 3 Heptene	1.71%	
	8 Propene → 3 Octene	3.06%	
	3 Propene → Nonene	30.78%	
	10 Propene → 3 Decene	3.78%	
	11 Propene → 3 Undecene	4.59%	
	4 Propene → Dodecene	27.9%	
	13 Propene → 3 Tridecene	1.98%	
	14 Propene → 3 Tetradecene	3.78%	
	5 Propene → Pentadecene	8.19%	
	16 Propene → 3 Hexadecene	1.62%	
Butene	3 Butene → 2 Hexene	6.65%	95%
	2 Butene → Octene	21.85%	
	3 Butene → Dodecene	20.9%	
	4 Butene → Hexadecene	19%	
	5 Butene → Eicosene	12.35%	
	6 Butene → Tetracosene	14.25%	
Pentene	2 Pentene → Decene	27%	90%
	12 Pentene → 5 Dodecene	19.8%	
	3 Pentene → Pentadecene	43.2%	
Hexene	3 Hexene → 2 Nonene	14.875%	85%
	2 Hexene → Dodecene	62.05%	
	3 Hexene → Octadecene	8.075%	
Heptene	2 Heptene → Tetradecene	67%	67%
Octene	3 Octene → 2 Dodecene	10%	50%
	2 Octene → Hexadecene	40%	

***Table C2**. Results of Monte Carlo simulation of WCIQ – MTJ.*

	Moisture content (MC) ± 5 %	Carbon (C) ± 0.30 %	Hydrogen (H) ± 0.047%	CH + Moisture (Overall uncertainty)
WCIQ Feedstock – BTL				
Average SAF yield (t/h)	39.18	39.31	39.18	39.18
SD (t/h)	0.60	0.29	0.014	0.71
Expanded uncertainty of SAF % (K=2) 95%	3.10	1.46	0.07	3.60
Relative value = Biomass parameter uncertainty /expanded uncertainty	0.62	4.29	0.5	--
WCIQ Feedstock – PBTL				
Average SAF yield (t/h)	60.77	60.76	60.76	60.76
SD (t/h)	0.44	0.23	0.037	0.50
Expanded uncertainty of SAF % (K=2) 95%	1.45	0.75	0.12	1.64
Relative value = Biomass parameter uncertainty /expanded uncertainty	0.29	2.21	0.86	--

Table C3. *Results of Monte Carlo simulation of WCHQ-MTJ.*

	Moisture content (MC) ± 5 %	Carbon (C) ± 0.30 %	Hydrogen (H) ± 0.047%	CH + Moisture (Overall uncertainty)
WCHQ Feedstock – BTL				
Average SAF yield (t/h)	38.14	38.18	38.16	38.16
SD (t/h)	0.61	0.30	0.04	0.75
Expanded uncertainty of SAF % (K=2) 95%	3.20	1.56	0.22	3.95
Relative value = Biomass parameter uncertainty /expanded uncertainty	0.64	4.22	1.05	--
WCHQ Feedstock – PBTL				
Average SAF yield (t/h)	59.27	59.29	59.28	59.29
SD (t/h)	0.43	0.23	0.05	0.54
Expanded uncertainty of SAF % (K=2) 95%	1.44	0.78	0.18	1.81
Relative value = Biomass parameter uncertainty /expanded uncertainty	0.29	2.11	0.86	--

***Table C4**. Detailed results of TEA for WP, WCIQ, and WCHQ – Methanol to Jet process.*

Sample	SAF NPC $ per tonne	OPEX (MUSD)	ACC (MUSD)	CAPEX (MUSD)
WP – BTL	1792.33	901.86	237.29	1845.66
WP – PBTL	2374.53	2241.03	233.42	1815.47
WP – HMBTL	1514.89	1314.81	263.81	2051.89
WP - HCBTL	1679.02	1485.85	263.81	2051.89
WCIQ - BTL	1673.06	697.06	237.49	1847.16
WCIQ – PBTL	2221.21	1697.57	226.54	1761.95
WCIQ – HMBTL	1446.33	997.92	254.95	1982.93
WCIQ - HCBTL	1595.47	1127.12	254.95	1982.93
WCHQ - BTL	1710.43	695.33	235.13	1828.78
WCHQ – PBTL	2241.06	1668.98	225.09	1750.78
WCHQ – HMBTL	1478.34	996.33	253.12	1968.73
WCHQ - HCBTL	1631.19	1125.53	253.12	1968.73

References

[1] M.A. Hasan, A.A. Mamun, S.M. Rahman, K. Malik, Al Amran, Md. Iqram Uddin, A.N. Khondaker, O. Reshi, S.P. Tiwari, F.S. Alismail, Climate Change Mitigation Pathways for the Aviation Sector, Sustainability 13 (2021) 3656. https://doi.org/10.3390/su13073656.

[2] C. Bergero, G. Gosnell, D. Gielen, S. Kang, M. Bazilian, S.J. Davis, Pathways to net-zero emissions from aviation, Nat Sustain (2023) 1–11. https://doi.org/10.1038/s41893-022-01046-9.

[3] McKinsey, Climate math: What a 1.5-degree pathway would take: Decarbonizing global business at scale is achievable, but the math is daunting., 2020. https://www.mckinsey.com/capabilities/sustainability/our-insights/climate-math-what-a-1-point-5-degree-pathway-would-take.

[4] International Civil Aviation Organization, Report on the updated long term traffic forecasts. A40-WP/20., 2019. www.icao.int/Meetings/a40/Documents/WP/wp_020_en.pdf.

[5] Air Transport Action Group, Balancing growth in connectivity with a comprehensive global air transport response to the climate emergency, 2020. https://aviationbenefits.org/media/167187/w2050_full.pdf (accessed 1 March 2023).

[6] V. Undavalli, O.B. Gbadamosi Olatunde, R. Boylu, C. Wei, J. Haeker, J. Hamilton, B. Khandelwal, Recent advancements in sustainable aviation fuels, Progress in Aerospace Sciences 136 (2023) 100876. https://doi.org/10.1016/j.paerosci.2022.100876.

[7] P. Kurzawska, Overview of Sustainable Aviation Fuels including emission of particulate matter and harmful gaseous exhaust gas compounds, Transportation Research Procedia 59 (2021) 38–45. https://doi.org/10.1016/j.trpro.2021.11.095.

[8] Maryam Raeisi, SUSTAINABLE PRODUCTION PATHWAYS FOR ADDED-VALUE PRODUCTS FROM MICROALGAE APPROACH: A SUPERSTRUCTURE OPTIMIZATION APPROACH. PhD thesis, Enschede, Netherlands, 2023. https://research.utwente.nl/en/publications/sustainable-production-pathways-for-added-value-products-from-mic.

[9] Jan Nielsen, Presentation "Introduction to the BIOFMET project and the concept of metrological traceability", Braunschweig, 2023.

[10] Wonders of the world, Dimensions of the Egyptian pyramids. https://www.wonders-of-the-world.net/Pyramids-of-Egypt/Dimensions-of-the-pyramids-of-Egypt.php.

[11] Collezioni.museoegizio, Royal cubit rod inscribed with the name of pharaoh Amenhotep II.

[12] I. García-Maroto, F. Muñoz-Leiva, Adoption of Biomass Heating Systems, pp. 177–206.

[13] N. Pedišius, M. Praspaliauskas, J. Pedišius, E.F. Dzenajavičienė, Analysis of Wood Chip Characteristics for Energy Production in Lithuania, Energies 14 (2021) 3931. https://doi.org/10.3390/en14133931.

[14] M. Jewiarz, M. Wróbel, K. Mudryk, S. Szufa, Impact of the Drying Temperature and Grinding Technique on Biomass Grindability, Energies 13 (2020) 3392. https://doi.org/10.3390/en13133392.

[15] G. Cavalaglio, F. Cotana, A. Nicolini, V. Coccia, A. Petrozzi, A. Formica, A. Bertini, Characterization of Various Biomass Feedstock Suitable for Small-Scale Energy Plants as Preliminary Activity of Biocheaper Project, Sustainability 12 (2020) 6678. https://doi.org/10.3390/su12166678.

[16] F. Lind, S. Heyne, F. Johnsson, What is the efficiency of a biorefinery, 2012. https://publications.lib.chalmers.se/records/fulltext/local_162671.pdf (accessed 2012).

[17] Atkins M. J., Walmsley T. G., Ong B. H. Y., Walmsley M. R. W., Neale J. R., Application of p-graph techniques for efficient use of wood processing residues in biorefineries, Chemical Engineering Transactions 52 (2016) 499–504. https://doi.org/10.3303/CET1652084.

[18] S. Perisanu, A. Neacsu, D. Gheorghe, Classification of calorimeters, Chemical Thermodynamics and Thermal Analysis 13 (2024) 100124. https://doi.org/10.1016/j.ctta.2023.100124.

[19] S.V. Meschel, A brief history of heat measurements by calorimetry with emphasis on the thermochemistry of metallic and metal-nonmetal compounds, Calphad 68 (2020) 101714. https://doi.org/10.1016/j.calphad.2019.101714.
[20] 19ENG09 BIOFMET, D1: Report on required parameters and metrological methodologies for measuring calorific value of biofuels and qualifying impurities, moisture, and ash content: BIOFMET-D1. http://www.biofmet.eu/documents/.
[21] M. Shehab, C. Stratulat, K. Ozcan, A. Boztepe, A. Isleyen, E. Zondervan, K. Moshammer, A Comprehensive Analysis of the Risks Associated with the Determination of Biofuels' Calorific Value by Bomb Calorimetry, Energies 15 (2022) 2771. https://doi.org/10.3390/en15082771.
[22] E. Anerud, D. Bergström, J. Routa, L. Eliasson, Fuel quality and dry matter losses of stored wood chips - Influence of cover material, Biomass and Bioenergy 150 (2021) 106109. https://doi.org/10.1016/j.biombioe.2021.106109.
[23] Hailong He, Miles F. Dyck, Robert Horton, Min Li, Huijun Jin, Bingcheng Si, Chapter Five - Distributed Temperature Sensing for Soil Physical Measurements and Its Similarity to Heat Pulse Method 148, pp. 173–230. https://www.sciencedirect.com/science/article/pii/S0065211317300883.
[24] R.T. Muehleisen, Understanding the concepts of uncertainty, reproducibility, and repeatability and the application to acoustic testing, The Journal of the Acoustical Society of America 137 (2015) 2215. https://doi.org/10.1121/1.4920068.
[25] J.H. Williams, Guide to the Expression of Uncertainty in Measurement (the GUM) 6-1 to 6-9. https://doi.org/10.1088/978-1-6817-4433-9ch6.
[26] A.S. Lister, 7 Validation of HPLC methods in pharmaceutical analysis 6, pp. 191–217. 10.1016/S0149-6395(05)80051-0.
[27] British Standards Institution, Solid biofuels — Determination of calorific value, 2017. www.iso.org/standard/61517.html.
[28] K. Lukas, J. Tomas, D. Martin, A. Mehmet, The Effect of Moisture on the Particle Size Characteristics of Knife-milled Beech Chips, Chemical Engineering Transactions 88 (2021) 739–744. https://doi.org/10.3303/CET2188123.
[29] European standard DIN ISO 14780, Solid biofuels — Sample preparation. www.iso.org/standard/66480.html.
[30] BSI Standards Publication, Solid biofuels — Determination of moisture content — Oven dry method: Moisture in general analysis sample. https://www.iso.org/standard/61637.html.
[31] M. Feidt, From Thermostatics to Non-equilibrium Thermodynamics 1–41. https://doi.org/10.1016/B978-1-78548-232-8.50001-7.
[32] P. Basu, Analytical Techniques, in: Biomass Gasification, Pyrolysis and Torrefaction, Elsevier, 2018, pp. 479–495.
[33] Ralph S. Jessup, Precise Measurement of Heat of Combustion with a Bomb Calorimeter, in: P.K. Sarangi, S. Nanda, P. Mohanty (Eds.), Recent Advancements in Biofuels and Bioenergy Utilization, Springer Singapore, Singapore, 2018.
[34] I. Teodorescu, R. Erbaşu, J.M. Branco, D. Tăpuşi, Study in the changes of the moisture content in wood, IOP Conf. Ser.: Earth Environ. Sci. 664 (2021) 12017. https://doi.org/10.1088/1755-1315/664/1/012017.
[35] D. Kuptz, K. Schreiber, F. Schulmeyer, S. Lesche, T. Zeng, F. Ahrens, V. Zelinski, C. Schön, A. Pollex, H. Borchert, V. Lenz, A. Loewen, M. Nelles, H. Hartmann, Evaluation of combined screening and drying steps for the improvement of the fuel quality of forest residue wood chips—results from six case studies, Biomass Conv. Bioref. 9 (2019) 83–98. https://doi.org/10.1007/s13399-019-00389-2.

[36] J.M. Craven, J. Swithenbank, V.N. Sharifi, D. Peralta-Solorio, G. Kelsall, P. Sage, Hydrophobic coatings for moisture stable wood pellets, Biomass and Bioenergy 80 (2015) 278–285. https://doi.org/10.1016/j.biombioe.2015.06.004.
[37] J.S. Tumuluru, D.J. Heikkila, Biomass Grinding Process Optimization Using Response Surface Methodology and a Hybrid Genetic Algorithm, Bioengineering (Basel) 6 (2019). https://doi.org/10.3390/bioengineering6010012.
[38] Parr instrument company, Pellet press: 2811, Illionois - USA, 2018. https://www.parrinst.com/es/files/downloads/2015/07/2811MB_Parr_2811-Pellet-Press-Literature.pdf.
[39] SIB64 Report, Metrology for Moisture in Materials: METefnet project, May/2016. https://www.euramet.org/research-innovation/search-research-projects/details/project/metrology-for-moisture-in-materials.
[40] P. Hoffmeyer, E.T. Engelund, L.G. Thygesen, Equilibrium moisture content (EMC) in Norway spruce during the first and second desorptions, Holzforschung 65 (2011) 875–882. https://doi.org/10.1515/HF.2011.112.
[41] V.R. Meyer, Measurement uncertainty, J. Chromatogr. A 1158 (2007) 15–24. https://doi.org/10.1016/j.chroma.2007.02.082.
[42] H.M.D. Kabir, A. Khosravi, M.A. Hosen, S. Nahavandi, Neural Network-Based Uncertainty Quantification: A Survey of Methodologies and Applications, IEEE Access 6 (2018) 36218–36234. https://doi.org/10.1109/ACCESS.2018.2836917.
[43] A. Hashad, Investigation of non-rotating piston gauges as primary and secondary standards for the intermediate vaccum pressure range from 0 to 15 Kpa. Dissertation, Braunschweig, Germany., 2021.
[44] M.F. Llorente, J.C. García, Suitability of thermo-chemical corrections for determining gross calorific value in biomass, Thermochimica Acta 468 (2008) 101–107. https://doi.org/10.1016/j.tca.2007.12.003.
[45] J. Larsson, A. Elofsson, T. Sterner, J. Åkerman, International and national climate policies for aviation: a review, Climate Policy 19 (2019) 787–799. https://doi.org/10.1080/14693062.2018.1562871.
[46] X. Fageda, J.J. Teixidó, Pricing carbon in the aviation sector: Evidence from the European emissions trading system, Journal of Environmental Economics and Management 111 (2022) 102591. https://doi.org/10.1016/j.jeem.2021.102591.
[47] Department for Transport, Sustainable aviation fuels mandate: Summary of consultation responses and government response, 2022. https://assets.publishing.service.gov.uk/government/uploads/system/uploads/attachment_data/file/1060601/sustainable-aviation-fuels-mandate-consultation-summary-of-responses.pdf.
[48] European Commission, ReFuelEU Aviation initiative: Sustainable aviation fuels and the 'fit for 55' package, 2022. https://www.easa.europa.eu/en/light/topics/fit-55-and-refueleu-aviation.
[49] European Union, DIRECTIVE (EU) 2018/2001 OF THE EUROPEAN PARLIAMENT AND OF THE COUNCIL: on the promotion of the use of energy from renewable sources, 2018.
[50] International Civil Aviation Organization, CORSIA Sustainability criteria for corsia eligible fuels, 2022. https://www.icao.int/environmental-protection/CORSIA/Documents/CORSIA_Eligible_Fuels/ICAO%20document%2005%20-%20Sustainability%20Criteria%20-%20November%202022.pdf.
[51] US Department of Agriculture, und USDA Foreign Agricultural Service., Consumption of vegetable oils worldwide from 2013/14 to 2022/2023, by oil type (in million metric tons). https://www.statista.com/statistics/263937/vegetable-oils-global-consumption/ (accessed 21 May 2023).

[52] S.K. Karan, L. Hamelin, Towards local bioeconomy: A stepwise framework for high-resolution spatial quantification of forestry residues, Renewable and Sustainable Energy Reviews 134 (2020) 110350. https://doi.org/10.1016/j.rser.2020.110350.
[53] B.D. Titus, K. Brown, H.-S. Helmisaari, E. Vanguelova, I. Stupak, A. Evans, N. Clarke, C. Guidi, V.J. Bruckman, I. Varnagiryte-Kabasinskiene, K. Armolaitis, W. de Vries, K. Hirai, L. Kaarakka, K. Hogg, P. Reece, Sustainable forest biomass: a review of current residue harvesting guidelines, Energ Sustain Soc 11 (2021) 1–32. https://doi.org/10.1186/s13705-021-00281-w.
[54] C.Panoutsou, K. Maniatis, Sustainable biomass availability in the EU, to 2050, 2021. https://www.concawe.eu/wp-content/uploads/Sustainable-Biomass-Availability-in-the-EU-Part-I-and-II-final-version.pdf.
[55] M. Prussi, C. Panoutsou, D. Chiaramonti, Assessment of the Feedstock Availability for Covering EU Alternative Fuels Demand, Applied Sciences 12 (2022) 740. https://doi.org/10.3390/app12020740.
[56] C. Carraro, S. Searle, C. Baldino, Waste and residue availability for advanced biofuel production in the European Union and the United Kingdom, 202100. https://trid.trb.org/view/1894362.
[57] J. O'Malley, N. Pavlenko, S. Searle, Estimating sustainable aviation fuel feedstock availability to meet growing European Union demand, in: Working Paper, 2021.
[58] EU, Directive (EU) 2018/851 of the European Parliament and of the Council of 30 May 2018 amending Directive 2008/98/EC on waste, 2018. https://www.eea.europa.eu/publications/reaching-2030s-residual-municipal-waste.
[59] IEA Bioenergy, Progress in Commercialization of Biojet /Sustainable Aviation Fuels (SAF): Technologies, potential and challenges, 2021 (accessed https://www.ieabioenergy.com/blog/publications/progress-in-the-commercialization-of-biojet-sustainable-aviation-fuels-technologies-potential-and-challenges/).
[60] M. Prussi, U. Lee, M. Wang, R. Malina, H. Valin, F. Taheripour, C. Velarde, M.D. Staples, L. Lonza, J.I. Hileman, CORSIA: The first internationally adopted approach to calculate life-cycle GHG emissions for aviation fuels, Renewable and Sustainable Energy Reviews 150 (2021) 111398. https://doi.org/10.1016/j.rser.2021.111398.
[61] World economic forum - McKinsey & Company, Clean Skies for Tomorrow Sustainable Aviation Fuels as a Pathway to Net-Zero Aviation, 2020. https://www.weforum.org/publications/clean-skies-for-tomorrow-sustainable-aviation-fuels-as-a-pathway-to-net-zero-aviation/.
[62] N. Pavlenko, An assessment of the policy options for driving sustainable aviation fuels in the European Union, 2021. https://theicct.org/publication/an-assessment-of-the-policy-options-for-driving-sustainable-aviation-fuels-in-the-european-union/.
[63] É. Yáñez, H. Meerman, A. Ramírez, É. Castillo, A. Faaij, Assessing bio-oil co-processing routes as CO 2 mitigation strategies in oil refineries, Biofuels, Bioprod. Bioref. 15 (2021) 305–333. https://doi.org/10.1002/bbb.2163.
[64] J. Breuer, J. Scholten, J. Koj, F. Schorn, M. Fiebrandt, R. Samsun, R. Albus, K. Görner, D. Stolten, R. Peters, An Overview of Promising Alternative Fuels for Road, Rail, Air, and Inland Waterway Transport in Germany, Energies 15 (2022) 1443. https://doi.org/10.3390/en15041443.
[65] ktalley, Implementing NATO's Strategic Concept on China, Atlantic Council, 2023. https://www.atlanticcouncil.org/in-depth-research-reports/report/implementing-natos-strategic-concept-on-china/ (accessed 22 April 2023).
[66] Transport&environment, Briefing - 10 years of EU fuels policy increased EU's reliance on unsustainable biofuel, 2021. https://www.transportenvironment.org/wp-content/uploads/2021/08/Biofuels-briefing-072021.pdf.
[67] Transport&environment, Briefing - Food not fuel: Part Two: Vegetable oils are being burned in cars despite empty supermarket shelves and skyrocketing prices, 2022.

https://www.transportenvironment.org/wp-content/uploads/2022/06/Food-vs-Fuel_-Part-2_Vegetable-oils-in-biofuels.pdf.
[68] S.K. Gupta (Ed.), Breeding oilseed crops for sustainable production: Opportunities and constraints / edited by Surinder Kumar Gupta, Academic Press, Amsterdam, 2015.
[69] V. Havrysh, A. Kalinichenko, P. Pysarenko, M. Samojlik, Sunflower Residues-Based Biorefinery: Circular Economy Indicators, Processes 11 (2023) 630. https://doi.org/10.3390/pr11020630.
[70] Z. Shams Esfandabadi, M. Ranjbari, S.D. Scagnelli, The imbalance of food and biofuel markets amid Ukraine-Russia crisis: A systems thinking perspective, Biofuel Res. J. 9 (2022) 1640–1647. https://doi.org/10.18331/BRJ2022.9.2.5.
[71] N.Pavlenko, S.Searle, Fueling flight: Assessing the sustainability implications of alternative aviation fuels, 2021. https://theicct.org/sites/default/files/publications/Alternative-aviation-fuel-sustainability-mar2021.pdf.
[72] European union aviation safety agency, European aviation environmental report, 2022. https://www.easa.europa.eu/eco/sites/default/files/2023-02/230217_EASA%20EAER%202022.pdf.
[73] European enviornmental agency, Municipal waste management in the Western Balkan countries, 2022. https://www.eea.europa.eu/publications/municipal-waste-management-in-western (accessed 21 May 2023).
[74] D. Chiaramonti, Sustainable Aviation Fuels: the challenge of decarbonization, Energy Procedia 158 (2019) 1202–1207. https://doi.org/10.1016/j.egypro.2019.01.308.
[75] U.S. Department of Energy, Sustainable Aviation Fuel: Review of Technical Pathways, 2020. https://www.energy.gov/sites/prod/files/2020/09/f78/beto-sust-aviation-fuel-sep-2020.pdf.
[76] E. Cabrera, J.M.M. de Sousa, Use of Sustainable Fuels in Aviation—A Review, Energies 15 (2022) 2440. https://doi.org/10.3390/en15072440.
[77] L. Testa, D. Chiaramonti, M. Prussi, S. Bensaid, Challenges and opportunities of process modelling renewable advanced fuels, Biomass Conv. Bioref. (2022) 1–36. https://doi.org/10.1007/s13399-022-03057-0.
[78] M.M. El-Halwagi, Sustainable Design Through Process Integration: Fundamentals and Applications to Industrial Pollution Prevention, Resource Conservation, and Profitability Enhancement, secondnd ed, Amsterdam, 2017.
[79] Aspen Energy Analyzer, Aspen Technology, 2019. https://www.aspentech.com/en/products/pages/aspen-energy-analyzer.
[80] Diego Mauricio Freire Ordóñez, SUSTAINABLE PRODUCTION OF SYNTHETIC FUELS FROM RENEWABLE ENERGY, London - UK, 2023.
[81] R.K. Sinnott, G. Towler, Chemical engineering design, Butterworth-Heinemann, an imprint of Elsevier, Oxford, 2020. https://www.sciencedirect.com/science/book/9780081025994.
[82] Aspen Process Economic Analyzer, Aspen Technology, 2019. https://www.aspentech.com/en/products/pages/aspen-process-economic-analyzer.
[83] F.G. Albrecht, D.H. König, N. Baucks, R.-U. Dietrich, A standardized methodology for the techno-economic evaluation of alternative fuels – A case study, Fuel 194 (2017) 511–526. https://doi.org/10.1016/j.fuel.2016.12.003.
[84] I. Farrance, R. Frenkel, Uncertainty in measurement: a review of monte carlo simulation using microsoft excel for the calculation of uncertainties through functional relationships, including uncertainties in empirically derived constants, The Clinical biochemist. Reviews 35 (2014) 37–61.
[85] K. Atsonios, J. Li, V.J. Inglezakis, Process analysis and comparative assessment of advanced thermochemical pathways for e-kerosene production, Energy 278 (2023) 127868. https://doi.org/10.1016/j.energy.2023.127868.

[86] R. Rauch, J. Hrbek, H. Hofbauer, Biomass gasification for synthesis gas production and applications of the syngas, Wiley Interdisciplinary Reviews: Energy and Environment 3 (2014) 343–362. https://doi.org/10.1002/wene.97.
[87] T. Bhaskar, B. Balagurumurthy, R. Singh, M.K. Poddar, Chapter 12 - Thermochemical Route for Biohydrogen Production, in: A. P, A. Pandey (Eds.), Biohydrogen, Elsevier, Amsterdam, 2014, pp. 285–316.
[88] EA Bioenergy, Gasification of Biomass and Waste: Task 33. https://task33.ieabioenergy.com/ (accessed Jan 2024).
[89] V.S. Sikarwar, M. Zhao, Biomass Gasification 205–216. https://doi.org/10.1016/B978-0-12-409548-9.10533-0.
[90] R. Kaur, P. Gera, M.K. Jha, T. Bhaskar, Chapter 8 - Thermochemical Route for Biohydrogen Production, in: A. Pandey, S.V. Mohan, J.-S. Chang, P.C. Hallenbeck, C. Larroche (Eds.), Biohydrogen, Second edition, Elsevier, Amsterdam Netherlands, Cambridge MA United States, 2019, pp. 187–218.
[91] Matevz Mencigar, Process design and simulation of gasification and Fischer-Tropsch process for biofuels production from lignocellulosic biomass. Master thesis, 2020. https://projekter.aau.dk/projekter/files/335444248/K10_K_10_F20.pdf (accessed Jan 2024).
[92] D.F. Barbosa Lima, F. Ademar, M. Kaminski, P. Matar, Modeling and Simulation of Water Gas Shift Reactor: An Industrial Case, in: V. Patel (Ed.), Petrochemicals, InTech, 2012.
[93] D.A. Bell, B.F. Towler, M. Fan, Chapter 7 - Hydrogen Production and Integrated Gasification Combined Cycle (IGCC), in: D.A. Bell, B.F. Towler, M. Fan (Eds.), Coal gasification and its applications, firstst ed., William Andrew/Elsevier, Oxford U.K., Burlington MA, 2011, pp. 137–156.
[94] D.E. Sparks, G. Jacobs, M.K. Gnanamani, V.R.R. Pendyala, W. Ma, J. Kang, W.D. Shafer, R.A. Keogh, U.M. Graham, P. Gao, B.H. Davis, Poisoning of cobalt catalyst used for Fischer–Tropsch synthesis, Catalysis Today 215 (2013) 67–72. https://doi.org/10.1016/j.cattod.2013.01.011.
[95] D. Freire Ordóñez, T. Halfdanarson, C. Ganzer, N. Shah, N.M. Dowell, G. Guillén-Gosálbez, Evaluation of the potential use of e-fuels in the European aviation sector: a comprehensive economic and environmental assessment including externalities, Sustain. Energy Fuels 6 (2022) 4749–4764. https://doi.org/10.1039/d2se00757f.
[96] V.S. Sikarwar, M. Zhao, P.S. Fennell, N. Shah, E.J. Anthony, Progress in biofuel production from gasification, Progress in Energy and Combustion Science 61 (2017) 189–248. https://doi.org/10.1016/j.pecs.2017.04.001.
[97] V. Subramanian, K. Cheng, Y. Wang, Fundamentally Understanding Fischer–Tropsch Synthesis, pp. 107–114. https://www.sciencedirect.com/science/article/pii/B9780124095472135309.
[98] M. Samavati, Design and analysis of solid oxide electrolysis-based systems for synthetic liquid fuels production, 2018. http://kth.diva-portal.org/smash/record.jsf?pid=diva2%3A1206127&dswid=3144.
[99] B. Viswanathan, Chapter 2 - Petroleum, pp. 29–57. https://www.sciencedirect.com/science/article/pii/B9780444563538000022.
[100] J. Lee, S. Hwang, J.G. Seo, U.G. Hong, J.C. Jung, I.K. Song, Pd catalyst supported on SiO2–Al2O3 xerogel for hydrocracking of paraffin wax to middle distillate, Journal of Industrial and Engineering Chemistry 17 (2011) 310–315. https://doi.org/10.1016/j.jiec.2011.02.029.
[101] J. Lee, S. Hwang, J.G. Seo, S.-B. Lee, J.C. Jung, I.K. Song, Production of middle distillate through hydrocracking of paraffin wax over Pd/SiO2–Al2O3 catalysts, Journal of Industrial and Engineering Chemistry 16 (2010) 790–794. https://doi.org/10.1016/j.jiec.2010.05.011.

[102] C. Bouchy, G. Hastoy, E. Guillon, J.A. Martens, Fischer-Tropsch Waxes Upgrading via Hydrocracking and Selective Hydroisomerization, Oil & Gas Science and Technology - Rev. IFP 64 (2009) 91–112. https://doi.org/10.2516/ogst/2008047.
[103] P. Shah, G. Sturtevant, J. Gregor, M. Humbach, F. Padrta, K. Steigleder, Fischer-Tropsch wax characterization and upgrading: Final report Allied-Signal, Inc., Des Plaines, IL (USA). Engineered Materials Research Center, 1988. https://www.osti.gov/biblio/6632526.
[104] V. Calemma, C. Gambaro, W.O. Parker, R. Carbone, R. Giardino, P. Scorletti, Middle distillates from hydrocracking of FT waxes: Composition, characteristics and emission properties, Catalysis Today 149 (2010) 40–46. https://doi.org/10.1016/j.cattod.2009.03.018.
[105] S. Mishra, R.K. Upadhyay, Review on biomass gasification: Gasifiers, gasifying mediums, and operational parameters, Materials Science for Energy Technologies 4 (2021) 329–340. https://doi.org/10.1016/j.mset.2021.08.009.
[106] A. Almena, P. Thornley, K. Chong, M. Röder, Carbon dioxide removal potential from decentralised bioenergy with carbon capture and storage (BECCS) and the relevance of operational choices, Biomass and Bioenergy 159 (2022) 106406. https://doi.org/10.1016/j.biombioe.2022.106406.
[107] M. Pilar González-Vázquez, F. Rubiera, C. Pevida, D.T. Pio, L.A. Tarelho, Thermodynamic Analysis of Biomass Gasification Using Aspen Plus: Comparison of Stoichiometric and Non-Stoichiometric Models, Energies 14 (2021) 189. https://doi.org/10.3390/en14010189.
[108] M. Paiva, A. Vieira, H.T. Gomes, P. Brito, Simulation of a Downdraft Gasifier for Production of Syngas from Different Biomass Feedstocks, ChemEngineering 5 (2021) 20. https://doi.org/10.3390/chemengineering5020020.
[109] D.S. Upadhyay, A.K. Sakhiya, K. Panchal, A.H. Patel, R.N. Patel, Effect of equivalence ratio on the performance of the downdraft gasifier – An experimental and modelling approach, Energy 168 (2019) 833–846. https://doi.org/10.1016/j.energy.2018.11.133.
[110] A.A. Susastriawan, H. Saptoadi, Effect of Air Supply Location and Equivalence Ratio on Thermal Performance of Downdraft Gasifier Fed by Wood Sawdust, [Journal of Sustainable Development of Energy, Water and Environment Systems] [11] (2023) [1]-[10].
[111] N.A. Jamin, S. Saleh, Abdul Samad, Noor Asma Fazli, Influences of Gasification Temperature and Equivalence Ratio on Fluidized Bed Gasification of Raw and Torrefied Wood Wastes, Chemical Engineering Transactions 80 (2020) 127–132. https://doi.org/10.3303/CET2080022.
[112] H.A. Choudhury, S. Chakma, V.S. Moholkar, Chapter 14 - Biomass Gasification Integrated Fischer-Tropsch Synthesis: Perspectives, Opportunities and Challenges, in: A. Pandey, T. Bhaskar, M. Stöcker, R. Sukumaran (Eds.), Recent advances in thermochemical conversion of biomass, Elsevier, Amsterdam, 2015, pp. 383–435.
[113] M. Ostadi, E. Rytter, M. Hillestad, Boosting carbon efficiency of the biomass to liquid process with hydrogen from power: The effect of H2/CO ratio to the Fischer-Tropsch reactors on the production and power consumption, Biomass and Bioenergy 127 (2019) 105282. https://doi.org/10.1016/j.biombioe.2019.105282.
[114] M. Arvidsson, M. Morandin, S. Harvey, Biomass Gasification-Based Syngas Production for a Conventional Oxo Synthesis Plant—Process Modeling, Integration Opportunities, and Thermodynamic Performance, Energy Fuels 28 (2014) 4075–4087. https://doi.org/10.1021/ef500366p.
[115] D. Fiaschi, L. Lombardi, Integrated Gasifier Combined Cycle Plant with Integrated CO2 – H2S Removal: Performance Analysis, Life Cycle Assessment and Exergetic Life Cycle Assessment, International Journal of Thermodynamics (2002).
[116] A. Helf, S. Cloete, F. Keller, J. Hendrik Cloete, A. Zaabout, Carbon-negative hydrogen from biomass using gas switching integrated gasification: Techno-economic assessment, Energy

Conversion and Management 270 (2022) 116248. https://doi.org/10.1016/j.enconman.2022.116248.
[117] F. Habermeyer, E. Kurkela, S. Maier, R.-U. Dietrich, Techno-Economic Analysis of a Flexible Process Concept for the Production of Transport Fuels and Heat from Biomass and Renewable Electricity, Front. Energy Res. 9 (2021) 723774. https://doi.org/10.3389/fenrg.2021.723774.
[118] D.H. König, N. Baucks, R.-U. Dietrich, A. Wörner, Simulation and evaluation of a process concept for the generation of synthetic fuel from CO2 and H2, Energy 91 (2015) 833–841. https://doi.org/10.1016/j.energy.2015.08.099.
[119] V.S. Sikarwar, M. Zhao, P. Clough, J. Yao, X. Zhong, M.Z. Memon, N. Shah, E.J. Anthony, P.S. Fennell, An overview of advances in biomass gasification, Energy Environ. Sci. 9 (2016) 2939–2977. https://doi.org/10.1039/C6EE00935B.
[120] M. Hillestad, Modeling the Fischer–Tropsch Product Distribution and Model Implementation, Chemical Product and Process Modeling 10 (2015) 147–159. https://doi.org/10.1515/cppm-2014-0031.
[121] A.A. Adeleke, X. Liu, X. Lu, M. Moyo, D. Hildebrandt, Cobalt hybrid catalysts in Fischer-Tropsch synthesis, Reviews in Chemical Engineering 36 (2020) 437–457. https://doi.org/10.1515/revce-2018-0012.
[122] Kluh Daniel, Gaderer Matthias, Integrating a Fischer-Tropsch Fuel Production Process into Pulp Mills, Chemical Engineering Transactions 94 (2022) 13–18. https://doi.org/10.3303/CET2294002.
[123] C. Bouchy, Gaelle Hastoy, E. Guillon, J. Martens, Fischer-Tropsch Waxes Upgrading via Hydrocracking and Selective Hydroisomerization, Oil & Gas Science and Technology-revue De L Institut Francais Du Petrole (2009).
[124] P.T. Benavides, D.C. Cronauer, F. Adom, Z. Wang, J.B. Dunn, The influence of catalysts on biofuel life cycle analysis (LCA), Sustainable Materials and Technologies 11 (2017) 53–59. https://doi.org/10.1016/j.susmat.2017.01.002.
[125] A. Curcio, S. Rodat, V. Vuillerme, S. Abanades, Experimental assessment of woody biomass gasification in a hybridized solar powered reactor featuring direct and indirect heating modes, International Journal of Hydrogen Energy 46 (2021) 37192–37207. https://doi.org/10.1016/j.ijhydene.2021.09.008.
[126] D. Venugopal, L. Thangavelu, N. Elumalai, Air and oxygen gasification simulation analysis of sawdust, Therm sci 23 (2019) 1043–1053. https://doi.org/10.2298/TSCI170613102V.
[127] N. Couto, A. Rouboa, V. Silva, E. Monteiro, K. Bouziane, Influence of the Biomass Gasification Processes on the Final Composition of Syngas, Energy Procedia 36 (2013) 596–606. https://doi.org/10.1016/j.egypro.2013.07.068.
[128] Review of Technologies for Gasification of Biomass and Wastes: Final report, 2009. http://wiki.gekgasifier.com/f/Review+of+Biomass+Gasification+Technologies.NNFCC.Jun09.pdf.
[129] M. Dossow, V. Dieterich, A. Hanel, H. Spliethoff, S. Fendt, Improving carbon efficiency for an advanced Biomass-to-Liquid process using hydrogen and oxygen from electrolysis, Renewable and Sustainable Energy Reviews 152 (2021) 111670. https://doi.org/10.1016/j.rser.2021.111670.
[130] R.-U. Dietrich, F.G. Albrecht, S. Maier, D.H. König, S. Estelmann, S. Adelung, Z. Bealu, A. Seitz, Cost calculations for three different approaches of biofuel production using biomass, electricity and CO 2, Biomass and Bioenergy 111 (2018) 165–173. https://doi.org/10.1016/j.biombioe.2017.07.006.
[131] C. Markowitsch, M. Lehner, M. Maly, Evaluation of process structures and reactor technologies of an integrated power-to-liquid plant at a cement factory, Journal of CO2 Utilization 70 (2023) 102449. https://doi.org/10.1016/j.jcou.2023.102449.

[132] International energy agency, Energy technology perspectives: Special Report on Carbon Capture Utilisation and Storage. CCUS in clean energy transitions, 2020. https://www.iea.org/data-and-statistics/charts/global-average-levelised-cost-of-hydrogen-production-by-energy-source-and-technology-2019-and-2050.
[133] Statista, Average monthly electricity wholesale price in Germany from January 2019 to December 2023, 2023. https://www.statista.com/statistics/1267541/germany-monthly-wholesale-electricity-price/.
[134] Carmen-ev.de, Marktpreise Hackschnitzel: Preisentwicklung bei Waldhackschnitzeln. https://www.carmen-ev.de/service/marktueberblick/marktpreise-energieholz/marktpreise-hackschnitzel/.
[135] O. Emenike, S. Michailos, K.J. Hughes, D. Ingham, M. Pourkashanian, Techno-economic and environmental assessment of BECCS in fuel generation for FT-fuel, bioSNG and OME x, Sustainable Energy Fuels 5 (2021) 3382–3402. https://doi.org/10.1039/D1SE00123J.
[136] I. Hannula, Hydrogen enhancement potential of synthetic biofuels manufacture in the European context: A techno-economic assessment, Energy 104 (2016) 199–212. https://doi.org/10.1016/j.energy.2016.03.119.
[137] S. Maier, S. Tuomi, J. Kihlman, E. Kurkela, R.-U. Dietrich, Techno-economically-driven identification of ideal plant configurations for a new biomass-to-liquid process – A case study for Central-Europe, Energy Conversion and Management 247 (2021) 114651. https://doi.org/10.1016/j.enconman.2021.114651.
[138] Eric D. Larson, Haiming Jin, Fuat E. Celik, Gasification-Based Fuels and Electricity Production from Biomass, without and with Carbon Capture and Storage, 2005.
[139] I.S. Tagomori, P.R. Rochedo, A. Szklo, Techno-economic and georeferenced analysis of forestry residues-based Fischer-Tropsch diesel with carbon capture in Brazil, Biomass and Bioenergy 123 (2019) 134–148. https://doi.org/10.1016/j.biombioe.2019.02.018.
[140] G. Zang, P. Sun, A.A. Elgowainy, A. Bafana, M. Wang, Performance and cost analysis of liquid fuel production from H2 and CO2 based on the Fischer-Tropsch process, Journal of CO2 Utilization 46 (2021) 101459. https://doi.org/10.1016/j.jcou.2021.101459.
[141] J.S. Lee, Clarifying the terms of heating values, 2017. https://open.library.ubc.ca/soa/cIRcle/collections/graduateresearch/42591/items/1.0343474.
[142] TOPSOE, The MTJet™ process pathway. https://www.topsoe.com/our-resources/knowledge/our-products/process-licensing/mtjet-process.
[143] Lacerda de Oliveira Campos, Bruno, K. John, P. Beeskow, K. Herrera Delgado, S. Pitter, N. Dahmen, J. Sauer, A Detailed Process and Techno-Economic Analysis of Methanol Synthesis from H2 and CO2 with Intermediate Condensation Steps, Processes 10 (2022) 1535. https://doi.org/10.3390/pr10081535.
[144] G. Bozzano, F. Manenti, Efficient methanol synthesis: Perspectives, technologies and optimization strategies, Progress in Energy and Combustion Science 56 (2016) 71–105. https://doi.org/10.1016/j.pecs.2016.06.001.
[145] J. Ott, V. Gronemann, F. Pontzen, E. Fiedler, G. Grossmann, D.B. Kersebohm, G. Weiss, C. Witte, Methanol, Ullmann's Encyclopedia of Industrial Chemistry (2012). https://doi.org/10.1002/14356007.a16_465.pub3.
[146] V. Dieterich, A. Buttler, A. Hanel, H. Spliethoff, S. Fendt, Power-to-liquid via synthesis of methanol, DME or Fischer–Tropsch-fuels: a review, Energy Environ. Sci. 13 (2020) 3207–3252. https://doi.org/10.1039/D0EE01187H.
[147] TUFAIL KALADIA, PRODUCTION OF SUSTAINABLE AVIATION FUEL FROM RENEWABLE CO2. Master, Netherlands, 2023.

[148] A.A. Avidan, Gasoline and Distillate Fuels From Methanol, in: D.M. Bibby, C.D. Chang, R.F. Howe, S. Yurchak (Eds.), Studies in Surface Science and Catalysis Methane Conversion, Elsevier, 1988, pp. 307–323.
[149] T. Mokrani, M. Scurrell, Gas Conversion to Liquid Fuels and Chemicals: The Methanol Route-Catalysis and Processes Development, Catalysis Reviews 51 (2009) 1–145. https://doi.org/10.1080/01614940802477524.
[150] S.A. Tabak, S. Yurchak, Conversion of methanol over ZSM-5 to fuels and chemicals, Catalysis Today 6 (1990) 307–327. https://doi.org/10.1016/0920-5861(90)85007-B.
[151] J. Ruokonen, H. Nieminen, A.R. Dahiru, A. Laari, T. Koiranen, P. Laaksonen, A. Vuokila, M. Huuhtanen, Modelling and Cost Estimation for Conversion of Green Methanol to Renewable Liquid Transport Fuels via Olefin Oligomerisation, Processes 9 (2021) 1046. https://doi.org/10.3390/pr9061046.
[152] B.N. Pamphile, N.J. Ndjibu, E. Vanshok, E.N. Gédéon, Modeling and simulation of reactors in plug flow reactor (PFR) and Packed Bed Reactor (PBR) series for the conversion of methanol into hydrocarbons, AJEST 16 (2022) 286–294. https://doi.org/10.5897/AJEST2022.3091.
[153] P. Trop, B. Anicic, D. Goricanec, Production of methanol from a mixture of torrefied biomass and coal, Energy 77 (2014) 125–132. https://doi.org/10.1016/j.energy.2014.05.045.
[154] J.D. Medrano-García, R. Ruiz-Femenia, J.A. Caballero, Revisiting Classic Acetic Acid Synthesis: Optimal Hydrogen Consumption and Carbon Dioxide Utilization, in: A.C. Kokossis, M.C. Georgiadis, E. Pistikopoulos (Eds.), Computer Aided Chemical Engineering 33 European Symposium on Computer Aided Process Engineering, Elsevier, 2023, pp. 145–150.
[155] P. Tian, Y. Wei, M. Ye, Z. Liu, Methanol to Olefins (MTO): From Fundamentals to Commercialization, ACS Catal. 5 (2015) 1922–1938. https://doi.org/10.1021/acscatal.5b00007.
[156] N. Zhang, R. Zhu, S.-L. Chen, N. Chen, Y. Cao, L. Ma, T. Wu, W. Sun, Insight into the Coke Precursor in the Process of the Methanol-to-Olefins Reaction, Energy Fuels 34 (2020) 742–748. https://doi.org/10.1021/acs.energyfuels.9b02861.
[157] S. Geleynse, K. Brandt, M. Garcia-Perez, M. Wolcott, X. Zhang, The Alcohol-to-Jet Conversion Pathway for Drop-In Biofuels: Techno-Economic Evaluation, ChemSusChem 11 (2018) 3728–3741. https://doi.org/10.1002/cssc.201801690.
[158] L. Tao, J.N. Markham, Z. Haq, M.J. Biddy, Techno-economic analysis for upgrading the biomass-derived ethanol-to-jet blendstocks, Green Chem. 19 (2017) 1082–1101. https://doi.org/10.1039/C6GC02800D.
[159] S. Yang, B. Li, J. Zheng, R.K. Kankala, Biomass-to-Methanol by dual-stage entrained flow gasification: Design and techno-economic analysis based on system modeling, Journal of Cleaner Production 205 (2018) 364–374. https://doi.org/10.1016/j.jclepro.2018.09.043.
[160] Y. Xiang, J. Zhou, B. Lin, X. Xue, X. Tian, Z. Luo, Exergetic evaluation of renewable light olefins production from biomass via synthetic methanol, Applied Energy 157 (2015) 499–507. https://doi.org/10.1016/j.apenergy.2015.05.039.
[161] I. Hannula, V. Arpiainen, Light olefins and transport fuels from biomass residues via synthetic methanol: performance and cost analysis, Biomass Conv. Bioref. 5 (2014) 63–74. https://doi.org/10.1007/s13399-014-0123-9.
[162] E. Anetjärvi, E. Vakkilainen, K. Melin, Benefits of hybrid production of e-methanol in connection with biomass gasification, Energy 276 (2023) 127202. https://doi.org/10.1016/j.energy.2023.127202.
[163] R.C. Baliban, J.A. Elia, V. Weekman, C.A. Floudas, Process synthesis of hybrid coal, biomass, and natural gas to liquids via Fischer–Tropsch synthesis, ZSM-5 catalytic conversion, methanol synthesis, methanol-to-gasoline, and methanol-to-olefins/distillate technologies, Computers & Chemical Engineering 47 (2012) 29–56. https://doi.org/10.1016/j.compchemeng.2012.06.032.

[164] M. Hennig, M. Haase, Techno-economic analysis of hydrogen enhanced methanol to gasoline process from biomass-derived synthesis gas, Fuel Processing Technology 216 (2021) 106776. https://doi.org/10.1016/j.fuproc.2021.106776.
[165] A. Gonzalez-Garay, C. Heuberger-Austin, X. Fu, M. Klokkenburg, Di Zhang, A. van der Made, N. Shah, Unravelling the potential of sustainable aviation fuels to decarbonise the aviation sector, Energy Environ. Sci. 15 (2022) 3291–3309. https://doi.org/10.1039/D1EE03437E.
[166] International Air Transport Association, Jet Fuel Price Monitor, 2023. https://www.iata.org/en/publications/economics/fuel-monitor/ (accessed 4 December 2023).
[167] M.N. Saeed, M. Shahrivar, G.D. Surywanshi, T.R. Kumar, T. Mattisson, A.H. Soleimanisalim, Production of aviation fuel with negative emissions via chemical looping gasification of biogenic residues: Full chain process modelling and techno-economic analysis, Fuel Processing Technology 241 (2023) 107585. https://doi.org/10.1016/j.fuproc.2022.107585.
[168] Z.I. Rony, M. Mofijur, M.M. Hasan, S.F. Ahmed, F. Almomani, M.G. Rasul, M.I. Jahirul, P. Loke Show, M.A. Kalam, T. Mahlia, Unanswered issues on decarbonizing the aviation industry through the development of sustainable aviation fuel from microalgae, Fuel 334 (2023) 126553. https://doi.org/10.1016/j.fuel.2022.126553.
[169] I. Hussain, S.A. Ganiyu, H. Alasiri, K. Alhooshani, A state-of-the-art review on waste plastics-derived aviation fuel: Unveiling the heterogeneous catalytic systems and techno-economy feasibility of catalytic pyrolysis, Energy Conversion and Management 274 (2022) 116433. https://doi.org/10.1016/j.enconman.2022.116433.